Università degli Studi di Napoli *Federico II*

Università di Camerino

DOTTORATO DI RICERCA IN QUANTUM TECHNOLOGIES

Ciclo XXXIV

Coordinatore: prof. Francesco Tafuri

Tripartite coupled hybrid cavity optomechanics

Settore Scientifico Disciplinare FIS/02

Dottorando
Ahmad Shafiei Aporvari

Tutore
Prof. David Vitali

Anni 2018/2022

TABLE OF CONTENTS

LIST OF FIGURES

FIGURE

LIST OF TABLES

TABLE

ABSTRACT

This thesis theoretically studies a full coupling quantum system which is a mixing of quantum electrodynamics and optomechanics. To this end, we consider a generic cavity optomechanics scheme involving a tripartite system consisting of a Fabry-Perot cavity, a qubit, and a mechanical resonator where the three components are mutually interacting. The first three chapters provide the necessary theoretical tools for the understanding of the models and concepts as are used throughout this work. The last three chapters present the main results obtained during this Ph.D. project.

In this study, the coupling between a cavity mode and an atom has been explored within the field of QED, while for the optomechanical part, the interaction between the cavity and the mechanical resonator has been described in terms of usual radiation-pressure coupling. However, the dispersive, radiation–pressure interaction between the mechanical and the electromagnetic modes is typically very weak, harnessing up to now the demonstration of interesting nonlinear dynamics and quantum control at the single-photon level. It has been shown both theoretically and experimentally that if the interaction is mediated by a nonlinear element (such as qubit), one can have effective dynamics corresponding to a huge enhancement of the single-photon optomechanical coupling.

We first study the Hamiltonian for the closed system considering that its Hamiltonian is in Rabi form, and we investigate its spectrum as a function of the coupling strength. We analyzed the eigenvalues using various mathematical techniques. We particularly exploit the Bloch-Siegert approach to rewrite the Hamiltonian in the form of the quantum Rabi model, which has analytical solutions. In comparison with rotating wave approximation, the Bloch-Siegert approach leads to an effective Hamiltonian for non-zero detuning; moreover, this method leads to relatively accurate solutions even for the large coupling strength.

Next, we investigate the dynamics of the tripartite system when the cavity mode and the mechanical mode interact via an off-resonant qubit in the presence of damping and losses. We determine the condition under which the qubit can be adiabatically eliminated, and the system dynamics can be considered as an effective optomechanical system operating in the strong coupling regime, where the effective optomechanical coupling rate is of the order of the frequency. We use the Schrieffer–Wolff treatment to construct an effective optomechanical Hamiltonian.

Finally, we verify the results by investigating the stationary cavity photon number and the stationary mean phonon number in the low excitation regime.

CHAPTER 1

Introduction

Cavity optomechanics studies the mutual interactions between mechanical and optical modes. It spans over a wide range of applications, including fundamental physics and technological research, with motivations as extended as gravitational wave detection, quantum manipulation of light, and realization of high precision sensors.

While cavity optomechanics was initially investigated under the context of very large-scale interferometers, the strength of the optomechanical interactions actually tends to be inversely proportional to the resonator dimensions. For this reason, the recent research has been focused mainly on the miniaturization of optomechanical configurations, and many fundamental quantum phenomena were explained for the first time in micro and nano-optomechanical implementations.

The aim of achieving large optomechanical strength at the single-photon level is the underlying motivation of this thesis.

Historical introduction

The origin of light-matter interaction dates backed to 1619 when Keppler explained why the tail of comets points away from the sun and postulated that the light could exert forces on the mechanical objects, see Fig. (1.1). More than two centuries later, in 1873, Maxwell predicted the optical force, also known as radiation pressure, based on his new theory of electromagnetic waves. Later, around the turn of the century, in 1901, the first experimental observation of this force was demonstrated by Nicolas and Hull [1] and Lebedew [2].

In 1970s, Braginsky investigated the effects of the radiation pressure force in the context of astronomical gravitational wave interferometers exhibiting a harmonically suspended mirror. It is in this context that the researcher understood a dynamic backaction effect of the optical force that could lead to either damping or anti-damping of mechanical motion, and Braginsky and colleagues demonstrated these effects in the microwaves domain [3]. He also studied the so-called "*Standard Quantum Limit*" (SQL) on the accuracy at which the position of a free test mass can be measured by an interferometer as a result of the quantum fluctuations of radiation pressure and shot noise [4].

Since then, the cavity optomechanics concepts have been extended to the quantum realm. It was theoretically suggested to use the quantum properties of radiation pressure to create non-classical states of the light, to observe non-classical entangled states of mechanics and light [6, 7], and to understand quantum non-demolition measurements [8] and also cooling with feedback schemes [9, 10].

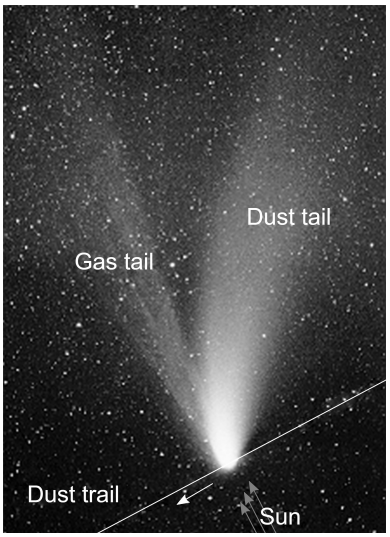

Figure 1.1: Diagram of a comet shows that the Sun's radiation pressure causes the tail to point away from the Sun. The gas tail (also known ion tail) is mainly affected by the magnetic field of the solar wind. The image is taken from NASA website [5].

At the same time to the discussion about radiation pressure in optical cavities, Ashkin examined the possibility of manipulating small dielectric particles using radiation-pressure forces. In 1970, he demonstrated the possibility to accelerate and trap small dielectric particles utilizing radiation pressure and optical gradient forces [11]. In 1978, he achieved laser cooling of the atomic motion of micro particles [12]. His work laid the foundations for optical tweezers, whose applications are now widely used to control biological particles in a non-destructive way, and of laser cooling, resulting in creation one of the major subfields of atomic, molecular and optical physics [13].

In the early 2000s, these two seemingly different concepts of the somehow same field were brought together when it was realized that radiation pressure and optical gradient forces could be used to couple mechanical and optical modes of toroid microcavities [14, 15]. By achieving more compact scales at the micro and nano-scale, cavity optomechanics was rapidly expanded to various setups such as nanomembranes [16], photonic crystals [17], or cantilevers [18]. Over the past years, the ever going developments in micro and nano fabrications techniques have enabled to increase the optical and mechanical quality factors of resonators and to reduce the volumes down to a regime in which optical forces are routinely dominant over other phenomena.

Today, most research groups working in the field of optomechanics mainly focus on micro or nano-scale resonators. Although there is a large diversity of setups, they can all be compared to a miniaturized form of a Fabry-Perot cavity with a moving end-mirror, which constitutes the typical optomechanical cavity.

Standard cavity optomechanics

The typical optomechanical setup is a Fabry-Perot cavity with one end mirror fixed and the other allowed to oscillate, as illustrated in Fig. (1.2). The cavity is illuminated by means of a laser,

through a motionless input mirror and the intracavity light field gives rise to the radiation pressure that leads to a mechanical displacement of the mirror.

From the mechanical perspective, radiation pressure on the oscillating mirror leads to mechanical displacement and changes the cavity length. From the optical perspective, when the driving laser is slightly detuned with respect to the cavity mode frequency, any shift of the cavity length will strongly alter the intra-cavity light field intensity. Now, as radiation pressure force corresponds to a transfer of momentum between phonons and photons, its strength is proportional to the energy stored within the cavity and thereby modulated by mechanical motion. Hence, the optical field depends very sensitively on the position of the mirror, and in turn, the position of the mirror depends on the circulating intensity; the two resonators are dynamically coupled to each other.

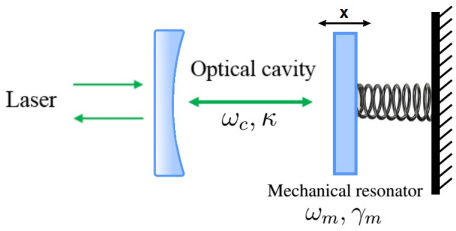

Figure 1.2: Schematic of a driven Fabry-Perot cavity with a movable mirror. The optical cavity mode with frequency ω_c is coupled to the mechanical oscillator with frequency ω_m.

The Fabry-Perot constitutes a good starting point when discussing optomechanical systems, as most of them can be described in analogy to the Fabry-Perot cavity with a moving mirror. At the first look, although the optomechanical setup presented here may seem rather special, it could be considered as a very generic model representing optomechanical interaction. It has been realized in a variety of physical systems, including ultracold atoms [19] and superconducting microwave circuits [20].

Before proceeding with further theoretical discussions, we briefly present the essential parameters of optomechanical systems and present some selected applications of them.

Desired optomechanical parameters

It is very important to introduce several important parameters, which enable us to quantify some different properties of the optomechanical system. The most practical parameters are as follows:

The mechanical mass. Through this thesis, in some points, we refer to the mass of mechanical resonator as effective mass, particularly when the mechanical system support multimodes. The effective mass can vary by many orders of magnitude, depending on the systems, from grams to picograms, and for decreasing masses one has typically increasing frequencies. .

The mechanical -angular- frequency ω_m . In optomechanical systems, higher resonance frequency is desirable, as it provides larger bandwidth and allows isolation from thermal noise [21].

The mechanical damping rate γ_m. Often, lower mechanical dissipation rate is desirable, as it characterizes a system with higher mechanical quality factor $Q_m = \omega_m/\gamma_m$. It is inversely proportional to the phonon life time, that is $\gamma_m = 1/\tau$.

The optical damping rate κ. This quantity manifests the cavity mode decay rate. Similarly, this quantity is linked to the optical quality factor $Q_c = \omega_c/\kappa$ where ω_c is cavity resonant frequency. In optomechanical systems, high quality factor is desirable to enhance the light-matter coupling.

Single-photon optomechanical coupling rate g_{cm}. This parameter quantifies the interaction between a single phonon and a single photon. It is also known as "vacuum optomechanical rate".

The optomechanical coupling strength, g **(in Hz)**. This quantity depends on the laser intensity, also known as "light-enhanced optomechanical coupling" which is defined for the linearized regime (this regime will be discussed later).

Operating optomechanical regime

In optomechanics there are different operating regimes defined according to the relationship between optomechanical parameters:

Weak coupling regime $g \ll \{\gamma_m, \kappa\}$. Energy tends to be lost by the system before it can be exchanged between the resonator and the optical mode. However, one can still observe some quantum bahavior in this regime. Mainly, the system operating in this regime, can be readily investigated under usual approximation methods such as rotating wave approximation (RWA).

Strong coupling regime, $g \gg \{\gamma_m, \kappa\}$. An important feature of the strong coupling regime is that the mechanical and the optical modes can be hybridised and form normal modes, so-called polaritons. In the strong coupling regime an oscillatory exchange of energy, takes place between the resonator and optical field [22].

Ultra-strong coupling regime, $g > \omega_m$. It is a new regime of quantum light-matter interaction, that goes beyond weak and strong coupling, and in the past decade switched from a theoretical realm to the experimental realization. Achieving the ultra-strong coupling opens new route to study light-matter systems and describe new quantum phenomena occurring in this regime.

Single-photon strong coupling regime, $g_{cm} > \{\kappa, \gamma_m\}$. In this optomechanical regime, adding a new photon to the cavity can shift the cavity resonance frequency by more than its linewidth. In general, in this regime the fundamental nonlinear nature leads to neoclassical behaviour such as strong photon blockade, non-classical interfaces between modes, and hybridisation of the mechanical and optical modes [23]. As we will see later, on expects that in this regime nonlinearity effects play important role and it is not possible to completely describe the system with the linearized approach. Experimentally, the single-photon strong coupling has been observed with cold atom clouds [24].

Experimental optomechanical platforms:

The optomechanical interaction is very general so it can be implemented in different experimental platforms with diverse optomechanical interaction schemes and radiation pressure forces. In the following we briefly present several different geometries of the optomechanical system. A more comprehensive discussion can be found in a review by Aspelmeyer et al. [25].

Suspended mirrors

The straightforward way to realize a Fabry-Perot cavity with one movable mirror can be implemented using suspended mirrors. This scheme was originally realized in gravitational wave detectors, with large optical cavities and mirrors. With the progress in miniaturization of optomechanical systems, this scheme is now represented at smaller scales with resonators such as micropillars [26] and microlevers [27], as shown in Fig. (1.3).

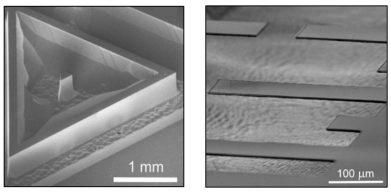

Figure 1.3: Two examples of suspended mirrors with micro-scale resonators. Left micropillar [26] , right: cantilever [28].

The high optical quality factor is the main positive attribute of suspended mirrors. However, as a downside, in order to achieve efficient optomechanical coupling the size of the resonator must be larger than the wavelength of the optical field which in turn leads to practical limitation of the mechanical properties compared to other optomechanical setups.

Suspended microcavities:

The Fabry-Perot model can be created in a monolithic and integrated setup, where the radiation pressure forces excite the structural vibration modes of a micro-sized optical cavity. The optomechanical coupling is increased by the small size of the microcavity and by the presence of additional optical forces and coupling mechanisms, as a result of optical propagation in a dielectric structure.

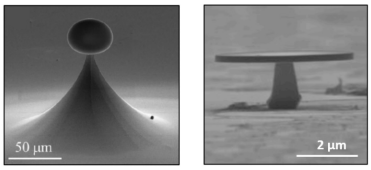

Figure 1.4: Suspended optical microcavities. Left: microsphere [29], right: microdisk [30].

Suspended optical microcavites have several distinct properties that make them fascinating systems regarding to cavity optomechanics. They have extremely small sizes with high optical/mechanical quality factor. These structures have small masses down to the nanogram scale, operating with mechanical frequencies up to GHz. More importantly, optical microcavites are compatible with micro-fabrication techniques. The major challenge is their large nonlinear effects

due to the strong light confinement, which leads to complicated system behavior.

Two kinds of optical resonators are illustrated in Fig. (1.4): microspheres [29], microdisks [30].

Mechanical resonator in the middle of an optical cavity:

Instead of having the back-end mirror of the Fabry-Perot cavity vibrating, one can also place a mechanical resonator (a membrane) in the middle of the cavity. Physically speaking, the cavity is divided into right and left sub-cavity. The cavity's effective length is changed by the phase shift arising from the motion of the membrane. It also leads to a dissipative optomechanical coupling, in which the absorption rate of the cavity is modulated. The primary motivation behind this configuration originates from the separation between the optical and mechanical degrees of freedom. Consequently, most limitations imposed on the size and mass of the mechanical oscillator in the case of suspended mirrors are relaxed. In this situation, the optical and mechanical parts can be optimized separately, without impacting each other, and high optical and mechanical quality factors can be achieved, with almost no constraint on the mechanical frequency and mass. This scheme has been realized with nanomembranes of sub-wavelength thickness [16] and nanorods [31]. It, however, remains challenging to realize and manipulate, as it critically depends on the experimental positioning and alignment of the mechanical resonator and cavity mirrors.

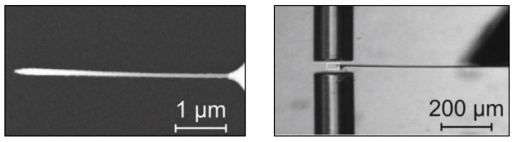

Figure 1.5: Left: SEM image of the nanoresonator. Right: fiber based Fabry-Perot cavity with a nanonoresonator in the middle. Figures are taken from [25].

Optomechanical crystals:

In a one dimensional dielectric structure, a photonic bandgap can be created by nano-patterning of a periodic structure. By introducing a defect in the lattice, wavelength-scale confinement of the optical field is achieved, which is known as photonic crystals. As for the mechanical perspective, the same concepts allow to create phononic crystals. In optomechanical crystals, the two approaches are combined into the same entity [17].

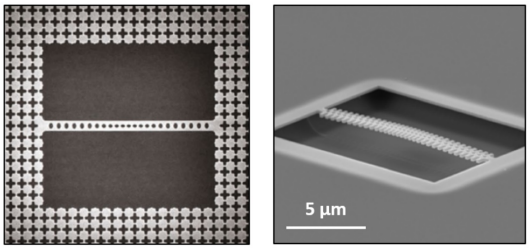

Figure 1.6: Optomechanical crystals [25, 17].

Optomechanical crystals provide promising perspectives for the development of cavity optomechanics due to their high mechanical frequencies, low masses, and small optical and mechanical localization volumes, and some of the best optomechanical coupling rates to date have been achieved with these schemes [32]. Moreover, optomechanical crystals can be included on-chip, with integrated photonic architectures, and are compatible with classical CMOS fabrication processes.

To summarize this section, a comparison of optomechanical parameters of selected experimental are listed on table (1.1).

Table 1.1: Comparison between the experimental parameters for three optomechanical setups.

	$g_{cm}/2\pi$	$\kappa/2\pi$	$\omega_m/2\pi$	$\gamma_m/2\pi$	g_{cm}/κ
Optomechanical crystals [32]	1.1 MHz	160 MHz	5.1 GHz	1.2kHz	0.007
Microdisk [33]	200 Hz	200 kHz	10.5MHz	32 Hz	0.001
Cold atom clouds [19]	600 kHz	660 kHz	42 kHz	1 kHz	0.9

Overview of the thesis

This thesis aimed to study a generic hybrid optomechanical system when the optical and mechanical modes interact via an off-resonant two-level atom.

The structure of this work is as follows.

Chapter 2 provides the necessary theoretical elements for understanding the primary language and notation of quantum optics, which forms the basis of our work. In this chapter, the quantization of electromagnetism filed inside a single optical mode cavity is briefly explained, and it ends with a discussion of quantized field-atom interactions.

Chapter 3 discusses the basic standard optomechanical theory. Then it studies it as an open system by taking into account the effect of the environment on the dynamics of the system using both the Schroedinger and Heisenberg approaches. Next, we will use a linearized form of equation of motion to describe different quantum effects such as optical spring effect and optomechanical damping. Finally, moving to the nonlinear regime, the single-photon coupling regime is discussed, enabling us to understand some pure quantum effects such as the photon blockade effect.

Chapter 4 introduces the hybrid optomechanical system and studies the Hamiltonian of the system in order to find its eigenvalues and eigenvectors. To this end, we apply different approximates approaches such as the generalized RWA and a variational method called the Bloch-Siegert (BS) method. We then rewrite the Hamiltonian in the form of Generalized Rabi model and then compared the accuracy of the eigenenergies for these approximation methods.

Chapter 5 studies the dynamics of the model in the presence of decay and dissipation. It shows that under proper conditions and for a specific range of frequencies, the tripartite system can be described using an effective standard optomechanical Hamiltonian in which the magnitude of the effective coupling rate is of the order of mechanical frequencies. Therefore, the hybrid tripartite optomechanical system operates in single-photon coupling regime.

Finally, Chapter 6 summarises the key research results presented in this thesis.

CHAPTER 2

Theoretical background

This chapter provides the necessary theoretical tools for understanding of models and concepts as are used throughout the subsequent chapters.

The chapter starts with the classical and quantum description of harmonic oscillators; the classical Hamiltonian is obtained using Lagrangian formalism and generalizes to the quantum description using the canonical quantization method. In the next steps, we briefly explain the quantization of electromagnetism field inside an optical cavity, followed by a short description of a convenient way of representing the quantum state of the oscillator in phase space, the so-called Wigner function, and then put forward a few important quantum states: coherent, squeezed, and thermal states. Finally, we will explain the power spectral density function, often used in detection. At last, the chapter ends with a brief explanation of quantized field-atom interactions.

2.1 Harmonic Oscillator: Classical and quantum analysis

In this thesis, the formalism of quantum Harmonic oscillators is used to describe optical modes (photons) inside a cavity as well as modes of mechanical motions (phonons). Fig. (2.1) shows a particle of mass, m, subjected to a linear restoring force $F = -kx$, where k defines as spring constant and $x = 0$ is equilibrium position. When it displaced to a new position a, this force acts to bring the mass back to its equilibrium position. Using equation of motion together with initial conditions $x(0) = a$ and $\dot{x}(0) = v$, the particle position is the time dependent function; $x(t) = a\cos(\omega t) + (v/\omega)\sin(\omega t)$, where $\omega = \sqrt{k/m}$ being the *angular frequency*. This particle moves back and forth between positions $x = \pm\sqrt{a^2 + v^2/\omega^2}$ with the time period $2\pi/\omega$, hence this system is known as harmonic oscillator.

The state of the system is given by a set of generalized coordinates $\mathbf{q} = \{q_i\}_{i=1,\ldots,n}$, n being the number of degrees of freedom of the system. The Hamiltonian then is obtained from the Lagrangian $L(\mathbf{q}, \dot{\mathbf{q}}, t)$,

$$H(\mathbf{q}, \mathbf{p}) = \mathbf{p}\dot{\mathbf{q}}(\mathbf{q}, \mathbf{p}) - L[\mathbf{q}, \dot{\mathbf{q}}(\mathbf{q}, \mathbf{p}), t]. \tag{2.1}$$

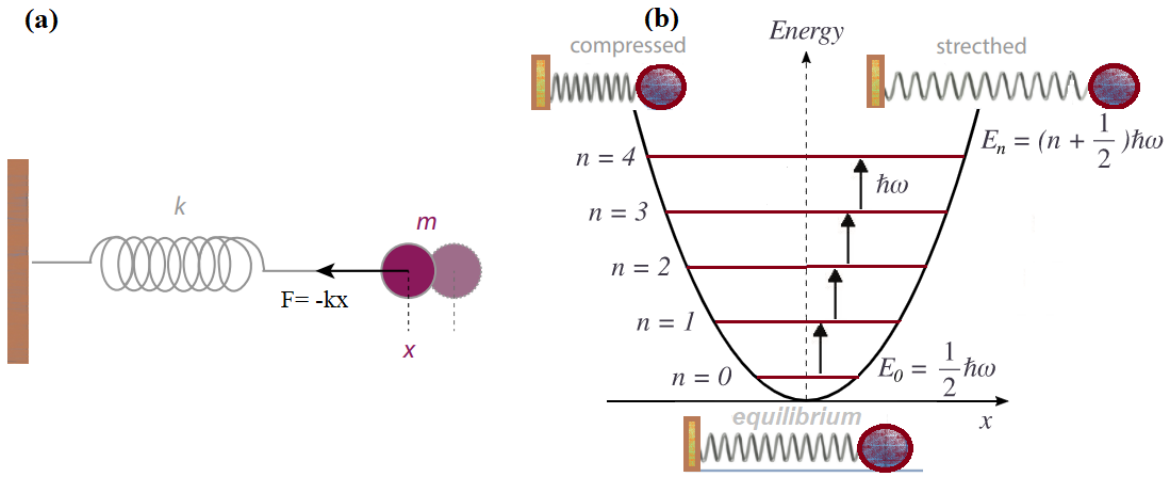

Figure 2.1: Model of harmonic oscillator. (a) a particle of mass m is subjected to a restoring force $F = -kx$. Oscilating mass bouncing back and forth around equilibrium position $x = 0$. (b) The total potential energy is plotted versus position. Despite to the classical case, the energy levels of quantum harmonic oscillator E_n are discreet and evenly separated by $\hbar\omega$.

In this formalism $p_j = \partial L/\partial \dot{q}_j$ is generalized momentum.

Using the Hamiltonian formalism and Euler-Lagrange equations one can arrive to the canonical equations

$$\dot{q}_j = \frac{\partial H}{\partial p_j} \quad \text{and} \quad \dot{p}_j = -\frac{\partial H}{\partial q_j}, \tag{2.2}$$

Having these formalisms in mind, we turn back to one-dimensional harmonic oscillator, the Hamiltonian for one-Dimensional harmonic oscillator reads,

$$H = \frac{p^2}{2m} + \frac{m\omega^2}{2}q^2, \tag{2.3}$$

leading to the canonical equations

$$\dot{q} = \frac{p}{m} \quad \text{and} \quad \dot{p} = -m\omega^2 q, \tag{2.4}$$

The trajectory of the system in the phase space is obtained using conservation of the Hamiltonian $H(t) = H(0)$ and leads directly to $q^2 + p^2/m^2\omega^2 = R^2$, as displayed in Fig. (2.1). The particle evolves periodically on a circular trajectory of radius R returning to its initial point at times $t_n = 2\pi n/\omega$. The trajectory can also be represented by defining the so-called normal variable $v(t) = q(t) + ip(t)/m\omega = R\mathit{exp}[i\varphi(t)]$, which in this case has a constant amplitude $|v| = R$ and a phase that decreases linearly with time, $\varphi(t) = \varphi(0) - \omega t$.

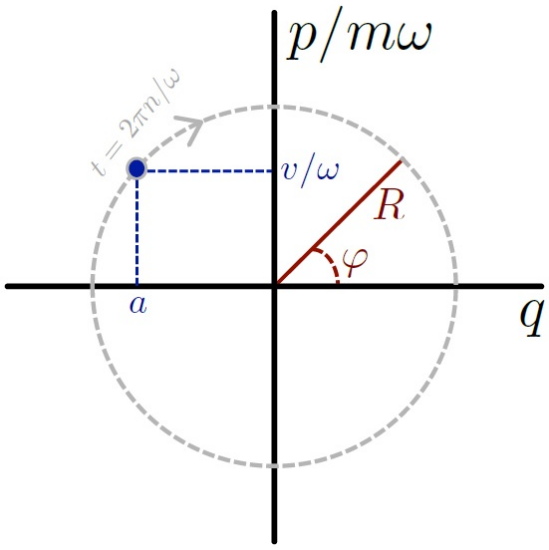

Figure 2.2: Phase space trajectory of the classical harmonic oscillator. It starts at a point $a, v/\omega$ and describes a circular trajectory of radius R coming back to this initial point at times t_n. Defining the amplitude and phase of the oscillator, the motion is described by a fixed amplitude and a phase, which decreases linearly with time.

2.1.1 The quantum harmonic oscillator

We generalize the description of classical Hamiltonian of the system to the quantum case. In this approach, any classical Hamiltonian can be quantized using a process known as *Canonical Quantization*, described by Dirac in 1925 [34]. From the classical point of view, a set of dynamics variables of the system $(q_1, q_2, ...q_j; p_1, p_2, ...p_j)$ are used to describe quantities of the system in the future time. Each pair of q_i and p_i in the classical Hamiltonian is replaced with a pair of operators $\hat{q}_i$ and $\hat{p}_i$ which do not commute. Note that, operators associated to different canonical variables commute with each other. Hence, briefly

$$(q_1, ..., q_i; p_i, ..., p_i) \quad \Longrightarrow \quad [\hat{q}_j, \hat{p}_k] = i\hbar\delta_{jk}, \tag{2.5}$$

where $\hbar \approx 1.054 \times 10^{-34}$ Js is the reduced Planck constant.

Replacing the classical conjugate variables in Eq. (2.3) by the corresponding quantum operators, leads to the quantum Hamiltonian of the system,

$$\hat{H} = \frac{\hat{p}^2}{2m} + \frac{m\omega^2}{2}\hat{q}^2, \tag{2.6}$$

where $\hat{q}$ and $\hat{p}$ obey the canonical commutation relation

$$[\hat{q}, \hat{p}] = i\hbar. \tag{2.7}$$

The nonzero commutation relation Eq. (2.7) leads directly to the well known Heisenberg uncertainty principle

$$\Delta\hat{q}\Delta\hat{p} \geq \frac{1}{2}|\langle[\hat{q}, \hat{p}]\rangle| = \frac{\hbar}{2}, \tag{2.8}$$

where $\Delta(\hat{\mathcal{O}}) = [\langle\hat{\mathcal{O}}^2\rangle - \langle\hat{\mathcal{O}}\rangle^2]$ defines as the standard deviation of operator $\hat{\mathcal{O}}$. This relation links the simultaneous knowledge can be achieved on the position x and momentum p of a quantum object.

Most of the time, we work with dimensionless versions of the position and momentum $\hat{X} = \hat{q}/q_{zpf}$ and $\hat{P} = \hat{p}/p_{zpf}$ quadrature(although we may still addresses them as *position* and *momentum*). The x_{zp} and p_{zp} are, respectively, the standard deviation of the zero-point motion and zero-point momentum of the oscillator, given by

$$x_{zp} = \sqrt{\frac{\hbar}{2m\omega}} \quad \text{and} \quad p_{zp} = \sqrt{\frac{\hbar m\omega}{2}}. \tag{2.9}$$

We can rewrite the Hamiltonian (2.6) based on quadrature operatorsas

$$\hat{H} = \frac{\hbar\omega}{4}\big(\hat{X}^2 + \hat{P}^2\big), \tag{2.10}$$

and these quadratures satisfy the following commutation relation

$$[\hat{X}, \hat{P}] = 2i, \tag{2.11}$$

so that

$$\Delta X\Delta P \geq \frac{1}{2}|\langle[\hat{X}, \hat{P}]\rangle| = 1. \tag{2.12}$$

The existence of zero-point motion and momentum is a direct consequence of the zero-point energy of a harmonic oscillator. Many of the quantum features of harmonic oscillators only becomes evident if it is possible to measure the motion of the oscillator with a precision surpassing the level of the zero-point motion. Even though nowadays mechanical oscillators used in quantum optomechanics experiments vary in size and frequency through many orders of magnitude, a typical micromechanical oscillator possess mass and resonance frequency on the order of $m \sim 1\mu g$ and $\omega/2\pi \sin 1$ MHz, respectively [25]. Hence, Eqs. (2.9) result in typical order-of-magnitude estimates for the zero-point motion of $x_{zp}^{micro} \sim 10^{-17}$ m and $x_{zp}^{micro} \sim 10^{-17}$ m.

Once the quantum Hamiltonian is specified one can obtain all system's quantum properties.

Using the time-independent Schroedinger equation, $\hat{H}\,|\varphi_n\rangle = E_n\,|\varphi_n\rangle$, where E_n are the energy eigenvalues and $|\varphi_n\rangle$ the corresponding eigenvectors. The state of the system at time "t" is obtained by solving the time-dependent Schroedinger equation:

$$i\hbar\frac{d}{dt}\,|\Psi\rangle = \hat{H}\,|\Psi\rangle \tag{2.13}$$

To find the eigenstates of Eq. (2.6), it is extremely useful to define the *annihilation* $\hat{a}$ and *creation operators* $\hat{a}^\dagger$

$$\hat{a} = \sqrt{\frac{m\omega}{2\hbar}}\big(\hat{q} + i\frac{\hat{p}}{m\omega}\big), \tag{2.14}$$

$$\hat{a}^\dagger = \sqrt{\frac{m\omega}{2\hbar}}\big(\hat{q} - i\frac{\hat{p}}{m\omega}\big). \tag{2.15}$$

Then we can decompose the quadratures as

$$\hat{X} = (\hat{a}^\dagger + \hat{a}) \quad \text{and} \quad \hat{P} = i(\hat{a}^\dagger - \hat{a}), \tag{2.16}$$

By construction, it is easy to show that the creation $\hat{a}^\dagger$ and annihilation $\hat{a}$ operators obey the Boson commutation relation

$$[\hat{a}^\dagger, \hat{a}] = 1 \tag{2.17}$$

Thus, the Hamiltonian (2.6) can be written as a function of $\hat{a}$ and $\hat{a}^\dagger$

$$\hat{H} = \hbar\omega(\hat{a}^\dagger\hat{a} + 1/2). \tag{2.18}$$

In term of these operators, finding the eigenstates of the Hamiltonian Eq. (2.18) is straightforward; the problem reduces to find the eigenstates of the *number operator* $\hat{N} = \hat{a}^\dagger\hat{a}$, with $|n\rangle$ as its eigenstate and the corresponding eigenvalue n, so that, $\hat{N}\,|n\rangle = n\,|n\rangle$. The eigenvectors $|n\rangle_{n=0,1,\ldots}$ form an orthogonal sets $\langle n|m\rangle = \delta_{nm}$, and based on the axioms of quantum mechanics, any observable can be expanded using these complete basis, known as the *Fock states*. It is easy to show that Number operator $\hat{N}$ is a positive operator, that is, $n \geqslant 0$. The annihilation and creation operators, $\hat{a}$ and $\hat{a}^\dagger$, allow us to move through this basis;

$$\hat{a}\,|n\rangle = \sqrt{n}\,|n-1\rangle \quad \text{and} \quad \hat{a}^\dagger\,|n+1\rangle = \sqrt{n+1}\,|n+1\rangle\,. \tag{2.19}$$

These operators have a well defined number of excitations, $\Delta N = 0$. Since, the ground state $|0\rangle$ has no quanta, it known as the vacuum state of the oscillator. All of the Fock states can be

generated by repeatedly applying the raising operator on the vacuum state,

$$|n\rangle = \frac{(\hat{a}^\dagger)^n}{\sqrt{n!}} |0\rangle . \tag{2.20}$$

The quanta of a mechanical oscillator are known as *phonons*, and those of the electromagnetic (EM) field known as *photons*. It is worth to mention that, during of this work, we use $\hat{a}$ and $\hat{a}^\dagger$ operators for optical resonators(or photons), while $\hat{b}$ and $\hat{b}^\dagger$, serve as for mechanical resonators(phonon). These operators, also follow bosonic commutation relation, e.g. $[\hat{b}, \hat{b}^\dagger] = 1$.

Let us now explain some physical consequences of the quantum harmonic Hamiltonian. The spectrum of the system is

$$E_n = \hbar\omega(n + 1/2)_{n=0,1,\ldots}, \tag{2.21}$$

where the vectors $|n\rangle_{n=0,1,\ldots}$ are eigenvectors of the energy. The energy levels are displayed in the Fig (2.1).b. This levels are discrete and separated evenly by $\hbar\omega$.

2.1.2 Unitary dynamics in the Heisenberg picture

Generally, when the system is isolated and decoupled from its environment, the dynamics of an arbitrary operator $\hat{\mathcal{O}}$ of a quantum system is determined in the Heisenberg picture via the Heisenberg equation of motion

$$\dot{\hat{\mathcal{O}}}(t) = [\hat{\mathcal{O}}, \hat{H}(t)]/\hbar. \tag{2.22}$$

By considering the canonical Hamiltonian of Eq. (2.18) and Eq. (2.10), the Heisenberg equation then gives the time evolution of the annihilation operator $\hat{a}(t)$, position $\hat{X}$ and momentum $\hat{P}$;

$$\hat{a}(t) = \hat{a}(0)\exp(-i\omega t), \tag{2.23}$$

$$\hat{Q}(t) = \cos(\omega t)\hat{Q}(0) + \sin(\omega t)\hat{P}(0), \tag{2.24}$$

$$\hat{P}(t) = \cos(\omega t)\hat{P}(0) - \sin(\omega t)\hat{Q}(0). \tag{2.25}$$

As expected, the position and momentum oscillate with frequency ω.

2.2 Quantization of the electromagnetic field

We introduced the harmonic oscillator in the context of the mechanical oscillator, and we are now use this model to illustrate an optical field mode. We aim to find an expression for the quantization of the EM field inside an optical cavity with perfect mirrors. We will follow a heuristic, but

physically intuitive approach to examine the correspondence between the e.f mode and a collection of harmonic oscillators.

Let us start with Maxwell's equations formulated as partial differential equations for the electric and magnetic vector fields **E**(r, t) and **B**(r, t), respectively, where **r** is the position where the fields are observed. In free space with no charges or current sources, the four Maxwell equations are written as

$$\nabla.\mathbf{B} = 0 \quad \text{and} \quad \nabla \times \mathbf{E} = -\partial_t \mathbf{B}, \tag{2.26}$$

$$\nabla.\mathbf{E} = 0 \quad \text{and} \quad \nabla \times \mathbf{B} = -\mu_0 \epsilon_0 \partial_t \mathbf{E}, \tag{2.27}$$

where $\nabla = (\partial_x, \partial_y, \partial_z)$. Based of our assumption in the absence of sources charge density function $\rho(\mathbf{r}, t)$ and a current distribution vector $\mathbf{j}(\mathbf{r}, t)$ are equal to zero. The parameters $\epsilon_0 = 8.8 \times 10^{-12}$ F/m and $\mu_0 = 1.3 \times 10^{-6}$ H/m are, respectively, the vacuum electric permittivity and magnetic permeability. These parameters are related to the light speed c by $c = 1/\sqrt{\epsilon_0 \mu_0} \simeq 3 \times 10^8$ m/s.

The most elementary solution of Maxwell equations is a field that oscillate at the well-defined frequency; this elementary solution is known as mode. This oscillation mode can be quantized as a harmonic oscillator. Let us take a travelling plane wave as a freely propagating field

$$\mathbf{E}(\mathbf{r}, t) = \epsilon_l \mathcal{E}_l(t) \exp(i\mathbf{k}_l.\mathbf{r}) + c.c \tag{2.28}$$

where c.c denotes the complex conjugate part. The first Maxwell equation entails perpendicularity the filed polarization vector ϵ_l to the wave propagation vector $\mathbf{k}_l$, that is $\epsilon_l \perp \mathbf{k}_l$. Moreover, the second and third Maxwell equations imply that **E**, **B** and **k** are three mutually orthogonal vectors forming right handed set. Finally, taking the time derivative of the last Maxwell equations and using the second order Maxwell equations, we get a second differential equation for $\mathcal{E}_l(t)$;

$$\frac{d^2 \mathcal{E}_l(t)}{dt^2} = -i\omega_l(t) \mathcal{E}_l(t), \tag{2.29}$$

where the solutions are

$$\mathcal{E}_l = \mathcal{E}_l(0) \exp(-i\omega_l t), \tag{2.30}$$

where $\mathcal{E}_l(t)$ characterizes the state of the field in the mode l. Based on this expression, we have

$$\mathbf{E}(\mathbf{r}, t) = \epsilon_l \mathcal{E}_l(0) \exp i(\mathbf{k}_l.\mathbf{r} - \omega t) + c.c. \tag{2.31}$$

$$\mathbf{B}(\mathbf{r}, t) = \frac{\mathbf{k}_l \times \epsilon_l}{\omega_l} \mathcal{E}_l(0) \exp i(\mathbf{k}_l.\mathbf{r} - \omega t) + c.c. \tag{2.32}$$

Therefore, for a travelling EM field propagating along **k**, the dynamics is completely determined

by Eq. (2.29).

According to the canonical quantization method, we have to identify two dynamical variables of the field that are canonically conjugated to each other. In fact, we can show that the real and imaginary parts of $\mathcal{E}_l$ are canonically conjugated variables. Let us define a dimensionless variable α_l,

$$\mathcal{E}_l(t) = i\mathcal{E}_l^{(1)}\alpha_l(t), \tag{2.33}$$

where $\mathcal{E}_l^{(1)}$ has the same dimension of an electric field and will be defined in the following. The equation $d\alpha_l(t)/dt = -i\omega_l\alpha_l(t)$ fully determines the dynamics evolution of the EM field in the mode l. The real and imaginary parts of α_l are defined as

$$\alpha_l(t) = \frac{1}{\sqrt{2\hbar}}\big(Q_l + iP_l\big), \tag{2.34}$$

thus

$$Q_l = \sqrt{\frac{\hbar}{2}}(\alpha_l(t) + \alpha_l^*(t)), \tag{2.35}$$

$$P_l = -i\sqrt{\frac{\hbar}{2}}(\alpha_l(t) - \alpha_l^*(t)). \tag{2.36}$$

The EM field Hamiltonian of mode l

$$H_l = \frac{\epsilon_0}{2}\int_{V_l} d^3r(\mathbf{E}^2 + c^2\mathbf{B}^2) = 2\epsilon_0 V_l|\mathcal{E}_l(t)|^2 = 2\epsilon_0 V_l\big[\mathcal{E}_l^{(1)}\big]^2|\alpha_l(t)|^2, \tag{2.37}$$

where the volume of integration V_l is not different from quantization volume. It can be a real volume, such as a cavity limited by mirrors, while in the case of radiation field extending to infinity, this V_l is supposed as a large fictitious cubic box with size L, hence $V = L^3$. For the latter case, using *periodic boundary condition* leads to the condition for wave vector $k_{lj} = 2\pi n_{lj}$ ($j = \{x, y, z\}$), here $n_{lj} = 0, \pm1, \pm2, ...$

We make the following choice for $\mathcal{E}_l^{(1)}$

$$\mathcal{E}_l^{(1)} = \sqrt{\frac{\hbar\omega_l}{2\epsilon_0 V_l}}, \tag{2.38}$$

In fact $\mathcal{E}_l^{(1)}$ is the amplitude of the filed with energy $\hbar\omega_l$ in the quantization volume V_l. By substitution, Eq. (2.37) turns to a familiar form

$$H_l = \hbar\omega_l|\alpha_l(t)|^2 = \frac{\omega_l}{2}\big(Q_l^2 + P_l^2\big). \tag{2.39}$$

The variables P_l and Q_l are canonically conjugated variables and, also, obey the canonical com-

mutation relation,

$$[\hat{Q}_l, \hat{P}_l] = i\hbar. \tag{2.40}$$

According to the Dirac notation, Eq. (2.34) turns to

$$\alpha_l(t) \;\rightarrow\; \hat{a}_l = \frac{1}{\sqrt{2\hbar}}(\hat{Q}_l + i\hat{P}_l), \tag{2.41}$$

$$\alpha_l^*(t) \;\rightarrow\; \hat{a}_l^\dagger = \frac{1}{\sqrt{2\hbar}}(\hat{Q}_l - i\hat{P}_l), \tag{2.42}$$

so that the usual harmonic oscillator Hamiltonian is obtained,

$$\hat{H}_l = \hbar\omega_l\Big(\hat{Q}_l^2 + \hat{P}_l^2\Big) = \hbar\omega_l\Big(\hat{a}_l^\dagger\hat{a}_l + \frac{1}{2}\Big). \tag{2.43}$$

Consequently, we are in position to write quantum counterparts of electric and magnetic fields Eq. (2.31) and Eq. (2.32):

$$\hat{\mathbf{E}}(\mathbf{r}) = i\varepsilon_l\mathcal{E}_l^{(1)}\big[\hat{a}_l e^{i\mathbf{k}_l.\mathbf{r}} - \hat{a}_l^\dagger e^{-i\mathbf{k}_l.\mathbf{r}}\big], \tag{2.44}$$

$$\hat{\mathbf{B}}(\mathbf{r}) = i\frac{\mathbf{k}_l \times \varepsilon_l}{\omega_l}\mathcal{E}_l^{(1)}\hat{a}_l \exp\; i\{\mathbf{k}_l.\mathbf{r}\} + h.c. \tag{2.45}$$

Note that the these expressions do not depend on time, as we are in Schroedinger picture.

Using Schroedinger equation one can obtain eigenvalues of the Hamiltonian Eq. (2.43),

$$E_{n_l} = \hbar\omega_l\Big(n_l + \frac{1}{2}\Big) \quad \text{with} \quad n_l = 0, 1, 2, ... \tag{2.46}$$

where these expressions are in the form of Eq. (2.21). It is worth providing some words for the radiation momentum, which for the classical EM field is given by

$$\mathbf{P}_l = \epsilon_0 \int_{V_l} d^3r(\mathbf{E} \times \mathbf{B}) = |\alpha_l|^2\hbar\mathbf{k}_l. \tag{2.47}$$

The corresponding quantum observable for radiation momentum is $\hat{P}_l = \hbar\mathbf{k}\hat{a}^\dagger\hat{a}$. Apparently the eigenstates are $|n_l\rangle$.

A closer look at Eq. (2.2) shows that differently from classical physics, the electric field in the vacuum states($|n_l = 0\rangle$) gives none-zero value

$$\Delta E = \big(\langle 0_l|\,\hat{\mathbf{E}}^2\,|0_l\rangle - |\,\langle 0_l|\,\hat{\mathbf{E}}\,|0_l\rangle\,|^2\big)^{1/2} = \mathcal{E}_l^{(1)}, \tag{2.48}$$

quantifying the vacuum electric field fluctuations. This remarkable consequence of quantum uncertainty leads to many interesting phenomena. For example, the vacuum fluctuations are responsible

for the spontaneous emission [35]. Moreover, vacuum fluctuations modify energy levels of an atom, known as Lamb shift.

So far, the calculations have been done for a single mode but it is straightforward to generalize the Hamiltonian to the multimode case as $\hat{H} = \sum_l \hat{H}_l$, hence

$$\hat{H} \left| n_1, ..., n_l, ... \right\rangle = \left(\sum_l E_{n_l} \right) \left| n_1, ..., n_l, ... \right\rangle , \tag{2.49}$$

Note that in this case, the commutation relation Eq. (2.40) for multi-modes generalizes to

$$[\hat{Q}_l, \hat{P}_m] = i\hbar\delta_{lm}, \tag{2.50}$$

Therefore, operators associated with two different modes do commute and, quantized radiation in the absence of charges can be consider as a set of independent harmonic oscillators.

2.2.1 Density matrix and representations

In a real experiment, the quantum system interacts unavoidably with its environment, thus the state (or wave function) can not be described with a (*pure*) state $|\psi\rangle$. In this case, an ensemble(or mixture) of states $|\psi_1\rangle , |\psi_2\rangle , ...$ is used to statistically describe the state. Any mixed state has an associated hermitian density operator,

$$\hat{\rho} = \sum_i p_i \left| \psi_i \right\rangle \left\langle \psi_i \right| , \tag{2.51}$$

where the factors p_i are interpreted as the probabilities of the system be in *ith* ensemble, implying

$$Tr(\hat{\rho}) = \sum_i p_i = 1, \tag{2.52}$$

where *Tr* is the trace operation. In general, for any arbitrary density state, the expectation of an arbitrary observable $\hat{\mathcal{O}}$ is given by

$$\langle \hat{\mathcal{O}} \rangle = Tr[\hat{\mathcal{O}}\hat{\rho}]. \tag{2.53}$$

If we know the Hamiltonian $\hat{H}$ of the system, in principle, it is straightforward to determine the time evolution of the density matrix using the Schroedinger equation;

$$i\hbar \frac{d\rho}{dt} = [\hat{H}, \hat{\rho}]. \tag{2.54}$$

We recall in the density operator formalism, the state is pure if and only if $\rho^2 = \rho$ that its purity is measured by the quantity $Tr(\rho^2)$.

2.3 Quantum states in phase space: Wigner function

Earlier we mentioned that a state of classical system specified by generalized coordinates $\mathbf{q}(t)$ represents a definite trajectory on the phase space, which in principal enable us to obtain the definite values of the measured quadratures. However, the state of a quantum system is affected by the uncertainty principle, which means, there is not a well define trajectory. In other words, the measurements of the observable do not lead to well defined value as these observable are always affected by *quantum noises*; the position and momentum do not have simultaneous eigenstates. Instead, it is possible to define several equivalent space distributions in quantum mechanics- including P-function [36], Husimi Q-function [37], and Wigner function [38]. These functions, in particular, enable us to visualize statistics that one would obtain by measuring the quadratures, $\langle x| \hat{\rho} |x\rangle$ and $\langle p| \hat{\rho} |p\rangle$, corresponding to measure X and P quadratures.

Among these distribution functions, we select the Wigner function as it provides the closest quantum analogy to the classical phase space probability distribution of position and momentum. It should be thought of as a quasi-probability distribution; quasi, because the uncertainty principle allows localised regions of negative quasi-probabilities. In particular, having negative probabilities, which is obviously against classical probability, reveal that some quantum behaviour is happening.

The state of an oscillator in Q-P plane is visualized on a diagram called *ball and stick* diagram. For example, Wigner functions representation for a displaced thermal state includes a vector from origin to the point $\{\langle \hat{Q} \rangle, \langle \hat{P} \rangle\}$, and an uncertainty contour representing the extent of the state.

The *Wigner distribution* $W_\rho(x, p)$, has the position and momentum probability density functions as its marginals,

$$\langle x| \hat{\rho} |x\rangle = \int_{\mathbb{R}} dp W_\rho(x, p) \quad \text{and} \quad \langle p| \hat{\rho} |p\rangle = \int_{\mathbb{R}} dx W_\rho(x, p), \tag{2.55}$$

and the *Wigner function*, can be uniquely defined by

$$W_\rho(x, p) = \frac{1}{4\pi} \int_{\mathbb{R}} dy \ \exp(-\frac{i}{2} py) \langle x + y/2| \hat{\rho} |x - y/2\rangle , \tag{2.56}$$

It is possible to check the proper normalization, i.e., $\int_{\mathbb{R}^2} dx dp W_\rho(x, p) = 1$. Furthermore, it can be shown that the quantum expectation value of the symmetrically ordered operators $\hat{A}(\hat{X}, \hat{P})$ which

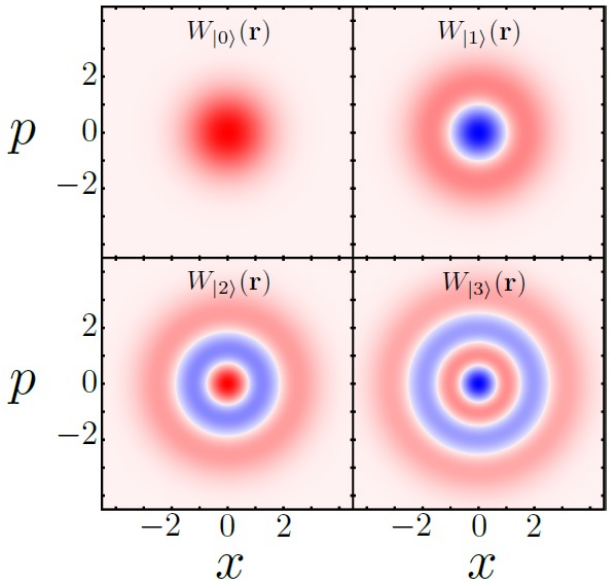

Figure 2.3: Density plot of the Wigner functions corresponding to the first 4 Fock states. Red and blue regions correspond to positive and negative values of the function, respectively. In both cases regions with higher contrast correspond to larger absolute value.

shows by $A^{(s)}$ [1] is obtained as

$$\langle \hat{A} \rangle = \int_{\mathbb{R}^2} dxdp W_\rho(x,p) A^{(s)}. \tag{2.57}$$

In order to determine the behaviour of a system, one can use Wigner function and the covariance formalism. In general, to specify $\hat{\rho}$, one needs to know the statistics of all operators (and their higher moments), and in principle this requires infinite set of moments. One important class of states are *Gaussian states*, whose Wigner distributions are Gaussian function, and more importantly, all higher-order moments are found solely by the first and second moments. The Gaussian states are defined

$$W(\mathbf{r}) = \frac{1}{2\pi\sqrt{\det V}} \exp\Big[-\frac{1}{2}(\mathbf{r}-\bar{r})^T V^{-1} (\mathbf{r}-\bar{r}) \Big], \tag{2.58}$$

where the column-like vector $\mathbf{r} = col(x,p)$ is defined as phase-space vector, the mean vector is defined as $\bar{r} = col(\langle \hat{X} \rangle, \langle \hat{P} \rangle)$. The *covariance matrix* V is given by

$$V = \begin{bmatrix} \langle \Delta \hat{X}^2 \rangle & \frac{1}{2}\langle \{\Delta \hat{X}, \Delta \hat{P}\} \rangle \\ \frac{1}{2}\langle \{\Delta \hat{X}, \Delta \hat{P}\} \rangle & \langle \Delta \hat{P}^2 \rangle \end{bmatrix}, \tag{2.59}$$

where $\Delta \hat{A} = \hat{A} - \langle \hat{A} \rangle$ describes the fluctuations.Therefore, the covariance of any coherent state is

[1] For example symmetrized version when $\hat{A} = \hat{X}^2\hat{P}$, is written as $(\hat{X}^2\hat{P})^{(s)} = (\hat{X}^2\hat{P} + \hat{P}\hat{X}^2 + \hat{X}\hat{P}\hat{X})/3$.

equal to identity matrix. Moreover, the uncertainty principle requires $\det\{V\} \geqslant 1$.

Gaussian states are special in quantum mechanics, since they are completely characterized by mean vector and covariance matrix (first and second order moments), and also, it is easy to generate them in the laboratory since they can be generated using Hamiltonian which are quadratic in the bosonic operators. In the following, we shall introduce some important quantum mechanical states which belong to the Gaussian class.

2.3.1 Coherent states

An important class of states of the harmonic oscillator, in fact the *most classical* states which give rise to a sensible classical limit, are known as coherent states, introduced by Nobel prize winner Roy J. Glauber [36].

Coherent states may be defined as the eigenstates of the annihilation operator, $\hat{a}\,|\alpha\rangle = \alpha\,|a\rangle$ with $\alpha \in \mathbb{C}$. An alternative way involves the displacement of the vacuum

$$|\alpha\rangle = \hat{D}(\alpha)\,|0\rangle \tag{2.60}$$

where the unitary displacement operator is

$$\hat{D}(\alpha) = \exp(\alpha\hat{a}^\dagger - \alpha^*\hat{a}). \tag{2.61}$$

We can see *displacement* when this operator is applied to $\hat{a}$ and $\hat{a}^\dagger$

$$\hat{D}^\dagger(\alpha)\hat{a}\hat{D}(\alpha) = \hat{a} + \alpha \quad \text{and} \quad \hat{D}^\dagger(\alpha)\hat{a}^\dagger\hat{D}(\alpha) = \hat{a}^\dagger + \alpha^*. \tag{2.62}$$

Similarly, for quadratures the displacement transformation reads

$$\hat{D}^\dagger(\alpha)\hat{X}\hat{D}(\alpha) = \hat{X} + 2Re\alpha \quad \text{and} \quad \hat{D}^\dagger(\alpha)\hat{P}\hat{D}(\alpha) = \hat{P} + 2Im\alpha. \tag{2.63}$$

Using the expression $\hat{D}(\alpha) = \exp(-\mid\alpha\mid^2/2)\exp(\alpha\hat{a}^\dagger)\exp(-\alpha^*\hat{a})$; [2], it is simple to find an expression to connect the coherent states to the Fock states,

$$|\alpha\rangle = \sum_{n=0}^{\infty} e^{-|\alpha|^2/2}\frac{\alpha^n}{\sqrt{n!}}\,|n\rangle\,. \tag{2.64}$$

Note that only for $\alpha = 0$, coherent states have a well defined number of excitations and for other value of α coherent states the number of *quanta* is distributed according to a Poisson probability

[2] Using the general formula $\exp(\hat{A}+\hat{B}) = \exp(-[\hat{A},\hat{B}]/2)\exp(\hat{A})\exp(\hat{B})$, valid for operators $[\hat{A},[\hat{A},\hat{B}]] = [\hat{B},[\hat{A},\hat{B}]] = 0$.

distribution

$$P_n(\alpha) = |\langle n|\alpha\rangle|^2 = e^{-|\alpha|^2}\frac{|\alpha|^{2n}}{n!}, \tag{2.65}$$

with mean photon number $\langle\hat{N}\rangle = |\alpha^2|$ and uncertainty $\Delta N = |\alpha|$.

We see that the state of a quantum harmonic oscillator is not well localized as a point in phase space as it is in classical mechanics. Similarly, coherent-state expectation of quadratures; $\langle\hat{X}\rangle_\alpha = \mathit{Re}[\alpha]$ and $\langle\hat{P}\rangle_\alpha = \mathit{Im}[\alpha]$, indicates that complex α-plane plays the role of phase space where the real and imaginary parts of α are position and momentum variables, respectively. Thus, a coherent state $|\alpha\rangle$ with $\alpha = |\alpha|e^{i\phi}$ can be represented by a circle with its center located at distance $|\alpha| = \langle\hat{n}\rangle^{1/2}$ and at angle $\phi = \arctan\langle\hat{Y}\rangle/\langle\hat{X}\rangle$ with respect to the origin. The area of the circle represents the *uncertainty area* of the coherent state. The phase-space representation of coherent states allows us to understand $\Delta\phi$ as phase uncertainty which diminishes by increasing $|\alpha|$ and it is maximum, i.e. $\Delta\phi = 2\pi$, for vacuum state(where $|\alpha| = 0$).

2.3.2 Squeezed states

Another class of minimum-uncertainty states are known as *squeezed states*. Differently from the coherent states, for which both quadratures have equal fluctuations $\Delta\hat{X} = \Delta\hat{P}$, for squeezed states, the uncertainty in one quadrature is increased.

The squeezed states may be generated using the unitary squeeze operator

$$\hat{S}(z) = \exp(\frac{z^*}{2}\hat{a}^2 - \frac{z}{2}\hat{a}^{\dagger 2}) \quad z \in \mathbb{C}, \tag{2.66}$$

where $z = re^{2i\phi}$ and $r = |z|$ is known as *squeezing parameter* and determines the the degree of squeezing, with $r \in [0, \infty]$ and $\theta \in [0, 2\pi]$. Note that $\hat{S}^{-1}(z) = \hat{S}^\dagger(z) = \hat{S}(-z)$. If we define rotated complex amplitude at an angle $\theta/2$

$$\hat{X}^{\theta/2} + i\hat{P}^{\theta/2} = (\hat{X} + i\hat{P})e^{-i\theta/2}, \tag{2.67}$$

in terms of quadratures, these expressions are easily rewritten as

$$\hat{S}^\dagger(z)\hat{X}^{\theta/2}\hat{S}(z) = e^{-r}\hat{X}^{\theta/2} \quad \text{and} \quad \hat{S}^\dagger(z)\hat{P}^{\theta/2}\hat{S}(z) = e^{r}\hat{P}^{\theta/2}. \tag{2.68}$$

It is worthwhile to mention that, a squeezed coherent state $|\alpha, \xi\rangle$ can be obtained by first squeezing the vacuum followed by displacing it , i.e.,

$$|\alpha, \xi\rangle = \hat{D}(\alpha)\hat{S}(\xi)\,|0\rangle\,. \tag{2.69}$$

One of the important applications of harmonic oscillators is sensing where the oscillator is put in contact with the signal that we want to examine. This signal leads to a very tiny force on the laboratory instrument. We see that when the system is in a coherent state, the uncertainty relation implies a limitation on the exact values that on can get from amplitude and phase measurements. In the case of quantum sensing, the signal under study is extremely weak and it can even be hidden by quantum noise, so that it might not be sensed at all. Squeezed state is a possible solution for this problem; one can retrieve information from one quadrature with an arbitrary accuracy, while the other quadrature has increased uncertainty so that their product is kept bounded by $\Delta X.\Delta P \geqslant 1$.

2.3.3 Thermal States

Thermal states are another important class of states and unlike those we have introduced so far, these states are considered as mixed states. Often in a real experiment, the system is correlated with another inaccessible system, say environment, hence we do not have enough information to describe completely the state of a system. In this case, the state of a system with Hamiltonian $\hat{H}$ is described as a mixed state determined by a density matrix $\hat{\rho}$;

$$\bar{\rho}_{th}(\bar{n}) = \frac{\exp(-\beta\hat{H})}{Tr\{\exp(-\beta\hat{H})\}}, \tag{2.70}$$

where $\beta = 1/(k_B T)$, being absolute temperature and $k_B = 1.381 \times 10^{-23} m^2 kg s^{-1} K^{-1}$ is Boltzmann's constant. the expectation value of the photon number $\bar{n}$ (also known as mean photon number) is given by

$$\begin{aligned} \bar{n} = \langle \hat{n} \rangle &= Tr(\hat{\rho}\hat{n}) \\ &= [\exp(\beta\hbar\omega) - 1]^{-1}. \end{aligned} \tag{2.71}$$

Alternatively, $\hat{\rho}_{th}$ is diagonal in the Fock basis $|n\rangle$;

$$\bar{\rho}_{th}(\bar{n}) = \sum_{n=0}^{\infty} \frac{\bar{n}^n}{(1+\bar{n})^{1+n}} |n\rangle \langle n| . \tag{2.72}$$

At thermal equilibrium the occupancy probability $p(n)$ follow Bose-Einstein statistics for both photons and phonons,

$$p(n) = \exp\big(-\frac{\hbar\omega n}{k_B T}\big)[1 - \exp(-\frac{\hbar\omega n}{k_B T})]. \tag{2.73}$$

At room temperature and for a typical micro- or nano-classical oscillator, where frequency is in the range $\omega = 1 - 1000$ MHz and $k_B T/\hbar\omega = 10^4 - 10^7$, hence Eq. (**??** simplifies to

$$\bar{n}_{k_B T \gg \hbar\omega} = \frac{k_B T}{\hbar\omega}. \tag{2.74}$$

In the other side, for visible light ($\omega \sim 10$ GHz) and at room temperature, Eq. (2.71) leads to $\bar{n} \sim 10^{-35}$. As a result, optical fields in thermal equilibrium can be considered in their ground state.

In summary;

$$\bar{n} \approx \begin{cases} \frac{k_B T}{\hbar\omega} & (k_B T \gg \hbar\omega) \\ \exp(-\hbar\omega/k_B T) & (k_B T \ll \hbar\omega) \end{cases}. \tag{2.75}$$

By referring to the corresponding Wigner distribution, it can be appreciated that thermal states are similar to a vacuum state (rotationally symmetric), but with $\sqrt{2\bar{n}+1}$ times more noise. The vacuum state, for example, can be seen as a thermal state with zero mean photon number.

2.4 Detection: power spectral density

We have explored the most important properties of the harmonic oscillators, and now, we are interested to know how these states are measured(-or detected) in the real experiments. In fact, we have to consider a realistic model that is coupled to the environments, providing a channel to perform measurements. In addition, this coupling introduces a damping channel and also adds environment noises perturbing the system. In experiments, the mechanical motion is often not analysed in real time but instead it is more convenient to evaluate the noise spectrum in the frequency domain where the spectrum can be easily transferred to the electronic signal.

Before describing power spectral noise expressions in a quantum context, it is worthwhile to briefly explain the classical relationship. For a classical system in thermal equilibrium with its environment at temperature T , the fluctuation–dissipation theorem provides a formal link between the energy decay rate of the oscillator γ and the power spectral density $S_{FF}(\omega)$ of the thermal force $F(t)$ exerted on it by the environment [39]

$$S_{FF}(\omega) = 2\gamma m k_B T. \tag{2.76}$$

Classically, the power spectral density $S_{ff}(\omega)$ of a complex classical variable $f(t)$ is defined as

$$S_{ff}(\omega) = \lim_{\tau\to\infty} \frac{1}{\tau} \langle f_\tau^*(\omega) f_\tau(\omega) \rangle. \tag{2.77}$$

where $f_\tau(\omega)$ is the Fourier transform of $f(t)$ sampled over the time interval $-\tau/2 < t < \tau/2$. Throughout this text the Fourier transform and its inverse are defined as

$$f(\omega) = \mathcal{F}[f(t)] = \int_{-\infty}^{\infty} f(t)e^{i\omega t}dt, \tag{2.78}$$

$$f(t) = \mathcal{F}^{-1}[f(\omega)] = \frac{1}{2\pi}\int_{-\infty}^{\infty} f(\omega)e^{-i\omega t}d\omega. \tag{2.79}$$

The Wiener-Khinchin theorem establishes a link between the power spectral density of a variable(with stationary statistics) and its time autocorrelation function

$$S_{ff}(\omega) = \int_{-\infty}^{\infty} d\tau e^{i\omega\tau}\langle f^*(t+\tau)f(t)\rangle_{t=0} = \int_{\infty}^{\infty} d\omega'\langle f^*(-\omega)f(\omega')\rangle. \tag{2.80}$$

Note that in this text we use the standard convention that $f^*(\omega) = \mathcal{F}\{f(t)\}^*$, and the same convention for operators.

2.4.0.1 Quantum power spectral density

In quantum context, the power spectral density of a general operator $\hat{\mathcal{O}}$ is defined as [40]

$$S_{\mathcal{O}\mathcal{O}}(\omega) \equiv \lim_{\tau\to\infty}\frac{1}{\tau}\big\langle\hat{\mathcal{O}}_\tau^\dagger(\omega)\hat{\mathcal{O}}_\tau(\omega)\big\rangle, \tag{2.81}$$

and using Wiener–Khinchin theorem for an operator with a stationary statistics

$$S_{\mathcal{O}\mathcal{O}}(\omega) = \int_{-\infty}^{\infty} d\tau e^{i\omega\tau}\big\langle\hat{\mathcal{O}}^\dagger(t+\tau)\hat{\mathcal{O}}(t)\big\rangle_{t=0} = \int_{-\infty}^{\infty} d\omega'\big\langle\hat{\mathcal{O}}^\dagger(-\omega)\hat{\mathcal{O}}(\omega')\big\rangle, \tag{2.82}$$

for the conjugate operator $\hat{\mathcal{O}}^\dagger$

$$S_{\mathcal{O}^\dagger\mathcal{O}^\dagger}(\omega) = \int_{-\infty}^{\infty} d\tau e^{i\omega\tau}\big\langle\hat{\mathcal{O}}(t+\tau)\hat{\mathcal{O}}^\dagger(t)\big\rangle_{t=0} = \int_{-\infty}^{\infty} d\omega'\big\langle\hat{\mathcal{O}}(\omega)\hat{\mathcal{O}}^\dagger(\omega')\big\rangle. \tag{2.83}$$

Note that spectral power density is real both in classical or quantum formalism. However, as a remarkable difference, the quantum spectral density, generally can be asymmetric in frequency. The reason is that, despite a classical variable, the quantum observables do not necessarily commute at different time i.e. $p[\hat{\mathcal{O}}(t), \hat{\mathcal{O}}(t')] \neq 0$, which leads to non-symmetric power spectral density: $S_{\mathcal{O}\mathcal{O}}(\omega) \neq S_{\mathcal{O}\mathcal{O}}(-\omega)$.

This difference between the positive and negative parts of the power spectral density of a quantum observable has important consequences for our understanding of fluctuation and dissipation in quantum systems and is particularly useful in defining their temperature.

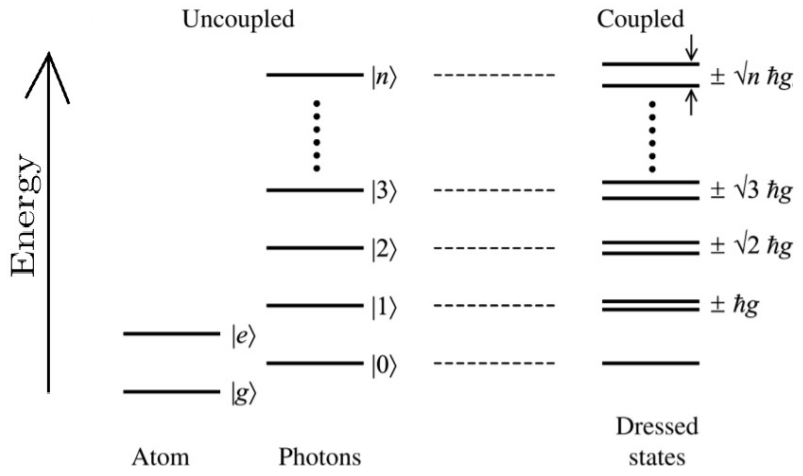

Figure 2.4: Energy spectrum of a two-level atom(left) and a cavity(middle) and energy level of composite cavity-atom system (right) with coupling strength g.

2.5 Quantized field-atom interaction: Jaynes Cummings model

The most basic interesting quantum system is described by considering a field mode and two-level atom as interacting quantum oscillator and qubit. The quantum oscillator can be manifested by a single mode cavity. On the other hand, a two-level atom is a nonlinear quantum element which only absorbs and emits single photons at a time. In order to benefit from this nonlinearity, a strong interaction between the atom and field is needed which it is, however, very difficult to achieve in free space. One solution is to put the atom inside a cavity where the photon interacts with the atom several times and therefore the coupling efficiency is enhanced. The interaction of atom and cavity mode is described by the Jaynes Cummings (JC) model [41]. In this model both atom and field are quantized and the energy difference of the atom is ω_a, while that of the cavity mode is ω.

Let us first consider the atom-field interaction

$$\hat{H}_I = -\hat{d}.\hat{E}(t), \tag{2.84}$$

where $\hat{d}$ is the dipole moment operator that is non-diagonal in the atomic Hilbert space;

$$\begin{aligned} \hat{d} &= e\hat{r} \\ &= \sum_{i,j} |i\rangle \langle i| \hat{d} |j\rangle \langle j| \\ &= \hat{d}_{ge}(\hat{\sigma}_+ + \hat{\sigma}_-), \end{aligned} \tag{2.85}$$

where the complete basis $(i, j) \in \{|g\rangle, |e\rangle\}$ denote atomic ground and excited states, $\hat{\sigma}_- = |g\rangle \langle e|$

and $\hat{\sigma}_+ = |e\rangle\langle g|$ are Pauli operators that link atomic states. In the above equation, due to parity, only off diagonal terms $d_{ge} = \langle g|\hat{d}|e\rangle$ are non zero (without loss of generality we assumed that d_{ge} is real).

Using Eq. (2.44) (in the Schroedinger picture) for single mode and considering the atom fixed at the origin ($\mathbf{r} = 0$), Eq. (2.85) turns to

$$\hat{H}_I = \hbar g(\hat{a} + \hat{a}^\dagger)(\hat{\sigma}_- + \hat{\sigma}_+), \tag{2.86}$$

where $g = \sqrt{\frac{\omega}{2\hbar\epsilon_0 V}}\hat{d}_{ge}.\vec{\epsilon}$ is the field-atom coupling constant.

The expansion of Eq. (2.85) involves four terms. The terms proportional to $\hat{\sigma}^\dagger\hat{a}^\dagger$ and $\hat{\sigma}\hat{a}$ correspond to create or destroy two quanta simultaneously: the first one corresponds to *emission* of photon by cavity together with atom transition from ground state $|g\rangle$ to excited state $|e\rangle$, the later, on the other hand, describes reverse process; *absorption* of photon together with atom excitation. When the atomic transition and cavity frequency, ω_a and ω_c, are close, these terms correspond to strongly *nonresonant* processes,and they play a minor role compared to resonant terms proportional to $\hat{\sigma}_+\hat{a}$ and $\hat{\sigma_-}\hat{a}^\dagger$. Neglecting nonresonant (or anti-resonant) terms is the so-called rotating wave approximation (RWA) [42] in classical electrodynamics and simplifies Eq. (2.85) to arrive to the JC interaction Hamiltonian

$$\hat{H}_I = \hbar g_k(\hat{a}\hat{\sigma}_+ + \hat{a}^\dagger\hat{\sigma}_-), \tag{2.87}$$

where in this case $g_k = \sqrt{\frac{\omega_k}{2\hbar\epsilon_0 V}}\hat{d}_{ge}.\vec{\epsilon}_k$. As illustrated in Fig. (2.4), the corresponding eigenvalues of the field-atom system is nonlinear which leading to the so-called *JC Ladder*.

It is possible to show that the JC Hamiltonian Eq. (4.15) involves two main processes: absorption and emission. The eigenstates of these Hamiltonian can be written in the basis states defined as $|n_k, i\rangle$ which actually is tensor product of radiation field basis and atomic basis, e.g., $|n_k\rangle \otimes |i\rangle$. So any states can be expanded in the complete basis form by $\{|n_k, g\rangle, |n_k, e\rangle\}$. The non zero matrices elements are as follow

$$\langle n_k - 1, e|\hat{H}|n_k, g\rangle = \hbar g_k\sqrt{n_k} \quad \textit{(Absorption)}, \tag{2.88}$$

$$\langle n_k + 1, g|\hat{H}|n_k, e\rangle = \hbar g_k\sqrt{n_k + 1} \quad \textit{(Emission)}, \tag{2.89}$$

implying that the transition rates depend on the number of photons and it is stronger if we have already a number of photons in the mode and this is called bosonic enhancement of the transition rates. Moreover, in the emission process there is an additional plus one in the square. While this is not very important for large photon number, when there is no photon, e.g. $n_k = 0$, this expression predicts coupling between excited state to the vacuum field. In the other words, vacuum fluctuation triggers spontaneous emission.

CHAPTER 3

Cavity Optomechanics

In this chapter we discuss the basic theory used to describe optomechanical systems, which in general are characterized by the transfer of momentum between light and (mechanical) motion. This field aims to study dynamic effects that can occur when the cavity properties are modified by the radiation pressure and the motion, or alternatively the mechanical motion is engineered by the optical dynamics. Studies on cavity optomechanics have a wide application on high-precision measurements such as sensing and enable testing fundamental quantum properties like quantum fluctuation on the macroscopic level.

This chapter provides a brief basic introduction to the theory used to describe cavity-optomechanical systems. We first review the Hamiltonian and show how it can be approximately brought into quadratic form. Then we discuss the classical dynamics both in the linear regime (featuring optomechanical damping, optical spring, and strong coupling) and in the nonlinear regime. Finally, we discuss briefly the single-coupling regime which enables us to understand some pure quantum effects such as the photon blockade effect.

3.1 The optomechanical Hamiltonian

A generic simple model to explore optomechanics is a Fabry Perot cavity consisting of two mirrors separated at distance L, one of the mirrors is fixed and the other is suspended on a spring allowing it to oscillate in the direction of the cavity axis, Fig. (3.1). The cavity supports resonance frequencies $\omega_{c,m} = m\pi c/L$. Here $m \in \mathbb{N}$ and c is the speed of light. In the following we always consider a single cavity mode with frequency denoted by ω_c. The radiation pressure coupling is a dispersive coupling, where the cavity resonance frequency (or equivalently the detuning, Δ) is modified under mechanical displacement.

A cavity optomechanical system is typically described by the Hamiltonian (in term of dimen-

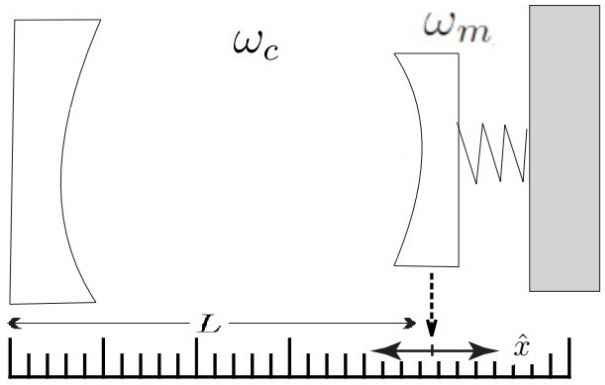

Figure 3.1: A typical Fabry Perot cavity with a movable mirror. The movable mirror can oscillate around its equilibrium position ($x = 0$).

sionless quadratures $\hat{x}$ and $\hat{p}$)

$$\hat{H} = \hbar\omega_{cav}(x)\hat{a}^\dagger\hat{a} + \underbrace{\frac{m_{eff}\omega_m^2\hat{x}^2}{2} + \frac{\hat{p}^2}{2m_{eff}}}_{\mathrm{H}_m}, \tag{3.1}$$

where $\hat{H}_m$, denotes the Hamiltonian of the mechanical oscillator with effective mass m_{eff} and resonance frequency ω_m, and $\omega_{cav}(x)$ denotes the optical mode frequency which depends on the mirror displacement (due to its dependence on the cavity length). The frequency $\omega_{cav}(x)$ can be expanded around some equilibrium position x_0 as $\omega_{cav}(x) = \omega_c(x_0) + (x - x_0)\dfrac{\partial\omega_{cav}(x_0)}{\partial x} + ...$, for small displacement compared to the cavity length L. For the majority of experiments it is sufficient to keep only the linear terms in the expansion as

$$\omega_{cav}(\hat{x}) \approx \omega_c - G\hat{x}, \tag{3.2}$$

where ω_c is frequency for the bare cavity and $G = -\partial\omega_{cav}/\partial x$ denotes the optical frequency shift per displacement. In the case of a Fabry-Perot cavity one finds $G = \omega_c/L$, which evidently relates to the cavity geometry.

By introducing the creation and annihilation operators for mechanical excitations ($\hat{x} = x_{zpf}(\hat{b} + \hat{b}^\dagger)$ and $\hat{p} = i(\hat{b}^\dagger - \hat{b})p_{zpf}$) and using Eq. (3.2), one can rewrite Eq. (3.1) as

$$\begin{aligned}\hat{H} &= \hbar(\omega_c - G\hat{x})\hat{a}^\dagger\hat{a} + \hbar\omega_m\hat{b}^\dagger\hat{b} \\ &= \hbar\omega_c\hat{a}^\dagger\hat{a} + \hbar\omega_m\hat{b}^\dagger\hat{b} - \hbar g_{cm}\hat{a}^\dagger\hat{a}(\hat{b} + \hat{b}^\dagger),\end{aligned} \tag{3.3}$$

where $g_{cm} = Gx_{zpf}$ is the vacuum optomechanical coupling strength, with frequency units [rad s^{-1}], which quantifies the coupling to single photon level. Note, the position and the momentum

are, respectively, normalized to $x_{zpf} = \sqrt{\hbar/2m\omega_m}$ and $p_{zpf} = \sqrt{\hbar m\omega_m/2}$.

Alternately, one can rewrite Eq. (3.3) based on the position and momentum quadratures ($\hat{X} = x/x_{zpf}$ and $\hat{P} = p/p_{zpf}$), hence we have

$$\hat{H} = \hbar\omega_c \hat{a}^\dagger \hat{a} + \frac{\hbar\omega_m}{4}\left(\hat{X}^2 + \hat{P}^2\right) - \hbar x_{zpf} G \hat{X} \hat{a}^\dagger \hat{a}. \tag{3.4}$$

Typically, the coupling strength g_{cm} is much smaller than optical and mechanical frequencies and depends upon the cavity geometry and the mechanical parameters (mass and frequency). The coupling strength g_{cm} displays the linear dispersive shift in the optical resonance frequency induced by the mechanical displacement. It is evident that the Hamiltonian of Eq. (3.3) consists of two free Hamiltonians for the optical field and the mechanical oscillator, and also an interaction Hamiltonian $\hat{H}_{int}$ capturing the coupling between them. The interaction Hamiltonian $\hat{H}_m$ can give rise to non-linear processes.

The motion of mechanical field is modulated by radiation pressure. In fact, this radiation pressure lies at the core of cavity optomechanics. The radiation pressure force is given by

$$\hat{F}_{rad} = -\frac{d\hat{H}_{int}}{d\hat{x}} = \hbar G \hat{a}^\dagger \hat{a} = \hbar \frac{g_{cm}}{x_{zpf}} \hat{a}^\dagger \hat{a}. \tag{3.5}$$

The coupling that we considered here is known as *dispersive* coupling where the coupling strength G is independent of the cavity decay rate (while in the dissipative coupling case this quantity depends the decay rate). The expression Eq. (3.5) shows that the radiation pressure force depends upon to the number of photon $\hat{n} = \hat{a}^\dagger \hat{a}$ inside the cavity; by increasing the photon number, for instance by a strong laser driving, one increases the radiation pressure force.

3.2 Open system dynamics

So far we considered an isolated optomechanical system with perfect mirrors, however in reality the system is linked to its environment. Considering the system as an *open system* allows us to include laser driving as well as decay processes (photons or phonons decays). In this realistic case, the mirrors of the cavity are partially transmitting which enables us to inject a field inside it, and also measuring the light coming out of it.

In the next paragraphs we model an open system in the presence of a laser drive and then we model the environment as a thermal bath consisting of a large number of (independent) oscillators. To this aim we explore the evolution of system in both the Heisenberg and Schroedinger pictures.

3.2.0.1 Driving laser

Injecting a coherent laser field corresponds to add a driving term Hamiltonian given by $\hat{H}_{drive} = \hbar F_L[\hat{a}^\dagger \exp(-i\omega_L t) + \hat{a}\exp(i\omega_L t)]$, leads to a greater radiation pressure force and this may lead to an effective enhancement of the optomechanical coupling. To get rid of the time dependence of the Hamiltonian , it is convenient to switch to a frame rotating at the incident laser frequency ω_L. Using the unitary operator $\hat{U} = \exp(i\omega_L \hat{a}^\dagger \hat{a} t)$, the Hamiltonian undergoes a transformation as

$$\hat{H} \rightarrow \hat{U}(\hat{H} - i\hbar\frac{\partial}{\partial t})\hat{U}^\dagger. \tag{3.6}$$

Thus, the resulting optomechanical time-independent Hamiltonian in the rotating frame is

$$\hat{H}_{sys-drive} = -\hbar\Delta\hat{a}^\dagger\hat{a} + \hbar\omega_m\hat{b}^\dagger\hat{b} - \hbar g_{cm}\hat{a}^\dagger\hat{a}(\hat{b} + \hat{b}^\dagger) + i\hbar F_L(\hat{a}^\dagger + \hat{a}), \tag{3.7}$$

where the laser detuning is defined as

$$\Delta = \omega_L - \omega_c, \tag{3.8}$$

and the laser driving rate F_L is related to the laser power P such that $F_L = \sqrt{2P\kappa/\hbar\omega_L}$, where κ is the decay rate of photons through the input mirror and will be defined in the next subsection.

3.2.1 Coupling to the Environment

An open optomechanical cavity system interacts with its environment which means it receives and gives information to the exterior world. The exchange of information introduces some noises and causes new phenomena such as damping and dissipation. The environment consists of two different kinds of bath: On the one hand the cavity mode can loose or absorb a photon through coupling to the electromagnetic environment, on the other hand, the mechanical resonator interacts with a mechanical heat bath through the connection to its support or from motion in the surrounding fluid. At equilibrium, this damping can be described in terms of Brownian motion [43].

The main idea is to model both the mechanical and the optical baths as a large number of independent oscillators each linearly interacting with the corresponding system. As detailed in Ref [23], a system coupled to a bath with an infinite number of oscillators of environmental modes, can be modelled as a system under a fluctuating force $\hat{F}(t)$ exerted by the environment and undergoing a damping process with rate γ[1], see Fig. (3.2). Throughout this text we only take the case of constant damping which for our purpose is a good approximation. In the optical case the oscillators

[1] In our notation, instead, the damping associated with the optical bath and the mechanical bath denote by κ and γ_m, respectively

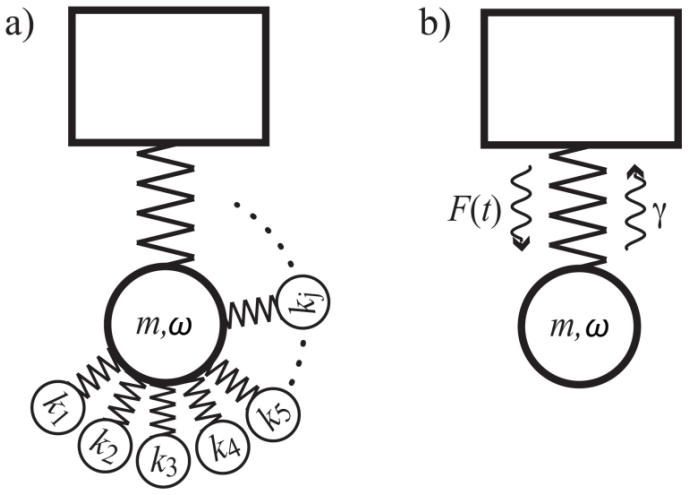

Figure 3.2: Quantum system interacting with its environment. (a) The quantum system (mass m, and frequency ω) is interacting with a large number of bath modes (k_j is spring constant for the jth bath oscillator with mass m_j). (b) Reduced model where the coupling to the environment is captured by a fluctuating force $\hat{F}(t)$ and damping γ. Figure adapted from [23].

describe just the optical modes of the vacuum outside the cavity in second quantization, for the mechanical case the oscillators describe fictitious environmental excitations, which in some cases coincide with the phonon modes of the frame where the mechanical resonator is clamped. From now onwards, we refer to the optomechanical system as "system", while we call the mechanical environment and the external electromagnetic radiation field "environment" or "bath".

The bath is supposed to be so large as the effect of the system on the bath modes is negligible, while the dynamics of the system can be severely affected by the presence of the bath. Note, even in the vacuum, the system is affected by vacuum noise and radiate a vacuum noise output.

The cavity mode is coupled to an optical bath whose mode q with frequency ω_q is characterized by bosonic operators $\hat{\alpha}_q$ and $\hat{\alpha}_q^\dagger$. Furthermore, the thermal bath formed by "N" oscillators, with k-th oscillator mode is described by $\tilde{\omega}_k$, $\hat{\beta}_k^\dagger$, and $\hat{\beta}_k$, being the resonance frequency, mechanical creation and annihilation operator, respectively. Thus, the full Hamiltonian for an open optomechanical system can be written as

$$\hat{H}_{tot} = \hat{H}_{sys-drive} + \hat{H}_O^{bath} + \hat{H}_M^{bath}, \tag{3.9}$$

where the $\hat{H}_O^{bath}$ describes optical bath and its interaction with the cavity mode

$$\hat{H}_O^{bath} = \int_q dq \Big[\hbar\omega_q \hat{\alpha}_q^\dagger \hat{\alpha}_q + i\sqrt{\kappa_q}(\hat{\alpha}_q \hat{a}^\dagger - \hat{\alpha}_q^\dagger \hat{a})\Big], \tag{3.10}$$

and $\hat{H}_M^{bath}$ represents the mechanical bath

$$\hat{H}_M^{bath} = \int_k dk \Big[\hbar\tilde{\omega}_k \hat{\beta}_k^\dagger \hat{\beta}_k + i\sqrt{\tilde{\kappa}_q}(\hat{\beta}_k \hat{b}^\dagger - \hat{\beta}_k^\dagger \hat{b})\Big]. \tag{3.11}$$

In general, the summation of these two individual baths, i.e., $\hat{H}_{sys-bath} = \hat{H}_O^{bath} + \hat{H}_M^{bath}$, quantifies the interaction of the system with its environment. In the following we study the evolution equations for the system both in Schroedinger picture (states) and Heisenberg picture (at the level of operators) using the full Hamiltonian of Eq. (3.15).

3.2.1.1 Schrödinger approach: The master equation

In general, the dynamics of the density matrix of the full system is governed by the Schrödinger equation

$$\dot{\hat{\rho}}_{tot}(t) = -\frac{i}{\hbar}[\hat{H}_{tot}, \hat{\rho}_{tot}(t)]. \tag{3.12}$$

This equation describes the dynamics of *system + environment*, which, however, is too general for our purpose. We are only interested in the system dynamics and we have to eliminate the environment from the equations of motion. Under appropriate conditions which we specify below, the evolution of the system can be described using the *Lindblad master equation*

$$\dot{\hat{\rho}}(t) = -\frac{i}{\hbar}[\hat{H}(t), \hat{\rho}(t)] + \sum_n \frac{1}{2}\big[2\hat{C}_n \hat{\rho}(t) \hat{C}_n^\dagger - \hat{\rho}(t)\hat{C}_n^\dagger \hat{C}_n - \hat{C}_n^\dagger \hat{C}_n \hat{\rho}(t)\big], \tag{3.13}$$

where, $\hat{\rho} = Tr_{env}[\hat{\rho}_{tot}]$ represents the reduced density operator of the system, $\hat{C}_n = \hat{E}_n\sqrt{\gamma_n}$ are usually referred to as *jump (or collapse) operators*, with γ_n are the corresponding decay rates, and $\hat{E}_n$ are the operators through which the bath couples to the system. The details of the derivation of Eq. (3.13) is described in several references [44, 45].

In order to derive the master equation in the form of Eq. (3.13), various approximations are made:

- **Born approximation:** The environment bath is considered much larger than the system. This assumption means: (1) The interaction between the system and the environment is weak, so the interaction of the system and the environment does not change the environment states; (2) the system and its environment are non-correlated throughout the entire time of evolution. Therefore, $\hat{\rho}_{tot}(t) \approx \hat{\rho}(t) \otimes \hat{\rho}_{env}$.

- **Separability:** There are no correlations between the system and its environment at initial time $t = 0$, so the total density operator have a separable state in the form of tensor product $\hat{\rho}_{tot}(0) = \hat{\rho}(0) \otimes \hat{\rho}_{env}(0)$.

- **Rotating wave approximation:** All fast rotating terms in the interaction picture can be neglected.

- **Markov approximation:** The time scale of decay for the system dynamics (τ_{sys}) is much longer than the time scales of decay (τ_{env}) and the correlation (τ_{corr}) of the environment. This approximation implies the environmental correlation functions decay on a time-scale fast compared to the system.

3.2.1.2 Heisenberg approach: The Langevin equations

As an alternative to the Schrödinger approach, the system dynamics can also be described in the Heisenberg approach; operators are time varying and the states are time-independent. According to our assumption, the presence of the bath modifies the equation of motions of the system while the states of the bath almost remain unchanged, so it is possible to derive equations describing the system behaviour, without necessarily worrying about the bath dynamics. In the classical realm, this idea was introduced by Langevin to study the statistical mechanics of Brownian motion of a particle in a heat bath [46]. More recently this approach has been extended to the quantum domain. Due to its classical origin, Langevin approach is typically more intuitive than the Master equation (for an introduction to the Langevin approach see [47]).

In this model, tit is assumed that a particle is subject to a systematic force, i.e. a viscous drag, and a rapidly fluctuating force, which comes from the surrounding particles randomly impacting on the system under investigation, such that the net force is zero on average. In general, the Langevin equations for an arbitrary operator $\mathcal{O}$ is given by

$$\frac{\partial \hat{\mathcal{O}}}{\partial t} = \frac{i}{\hbar}[\hat{H}, \hat{\mathcal{O}}] + \hat{\mathcal{N}}, \tag{3.14}$$

where $\hat{\mathcal{N}}$ represents noise operator of $\hat{\mathcal{O}}$.

3.3 Application to cavity optomechanics

Let us here model an optomechanical cavity coupled to the environment. A Fabry-Perot cavity is a most common representative experimental model which implements the optomechanical interactions. In this system, the moving end-mirror is subjected to the radiation pressure forces, and the time-evolution of the system operators are given using Eq. (3.14). As an assumption, we model the environment as mechanical bath + optical bath and the system interacts with an infinite number of optical and a mechanical harmonic oscillators:

Optical bath: The coupling to the optical bath is modelled via Eq. (3.14). In this model, the processes $\hat{\alpha}_m\hat{a}^\dagger$ and $\hat{\alpha}_q^\dagger\hat{a}$ are responsible for photon creation and annihilation, respectively. In this case, the interaction of the system-bath is simplified using the RWA, since ω_c is very large compared to the other frequencies. Moreover, since $\hbar\omega_c \gg k_bT$, the mean photon number is almost zero; $\bar{n}_{th}(\omega_c) \simeq 0$.

Mechanical bath:

As stated before, the thermal interaction of the system with its environment yields zero-mean, stochastic force $\hat{F}(t)$ and rate γ. Therefore the system interaction is described in terms of Brownian Motion, affecting the moving mirror.

The total Hamiltonian for our optomechanical cavity system reads as

$$\begin{aligned}\hat{H}_{tot} &= \hbar\omega_c\big(\hat{a}^\dagger\hat{a} + \frac{1}{2}\big) + \hbar\omega_m\big(\hat{b}^\dagger\hat{b} + \frac{1}{2}\big) - \hbar g_{cm}\hat{a}^\dagger\hat{a}(\hat{b}^\dagger + \hat{b}) \\ &+ iF_L(\hat{a}^\dagger e^{-i\omega_L t} - \hat{a}e^{i\omega_L t}) \\ &+ \int_q dq\Big[\hbar\omega_q\hat{\alpha}_q\hat{\alpha}_q^\dagger + i\sqrt{\kappa_q}(\hat{\alpha}_q\hat{a}^\dagger - \hat{\alpha}_q\hat{a})\Big] \\ &+ \int_k dk\Big[\hbar\tilde{\omega}_k\hat{\beta}_k^\dagger\hat{\beta}_k + i\sqrt{\tilde{\kappa}_q}(\hat{\beta}_k\hat{a}^\dagger - \hat{\beta}_k^\dagger\hat{a})\Big].\end{aligned} \tag{3.15}$$

We can obtain the time evolution of the system observables using Langevin equation of Eq. (3.14). In a frame rotating with laser frequency ω_p [2] we have,

$$\begin{aligned}\dot{\hat{a}} &= i\Delta\hat{a} + ig_{cm}\hat{a}(\hat{b} + \hat{b}^\dagger) + iF_L + \int_q dq\sqrt{\kappa_q}\hat{\alpha}_q, \\ \dot{\hat{b}} &= -i\omega_m\hat{b} + ig_{cm}\hat{a}^\dagger\hat{a} + \int_k dk\sqrt{\kappa_k}\hat{\beta}_k.\end{aligned} \tag{3.16}$$

Here $\Delta = \omega_L - \omega_c$ is the frequency detuning of the driving laser with respect to the cavity frequency. The set of Eqs. (3.16) shows the time evolution of the whole system, e.g., the optomechanical cavity and its environment.

By integrating the equations on the environment's operators and using first Markov approximation; $\gamma_j(t) = \gamma_j\delta(t)$, the stochastic differential Eqs. 3.16 can be rewritten as

$$\begin{aligned}\dot{\hat{a}} &= i\Delta\hat{a} - \kappa\hat{a} + ig_{cm}\hat{a}(\hat{b} + \hat{b}^\dagger) + F_L + \hat{\xi}_c(t), \\ \dot{\hat{b}} &= -i\omega_m\hat{b} - \gamma_m\hat{b} + ig_{cm}\hat{a}^\dagger\hat{a} + \hat{\xi}_m(t),\end{aligned} \tag{3.17}$$

where γ_c and γ_m are, respectively, the cavity and mechanical damping rates arising due to the coupling to the environment. The operators $\xi_j(t)$ refer to the noise introduced by the environment

[2] Moving to the rotating frame is done by unitary transformation $\hat{H} \to \hat{U}(\hat{H} - i\hbar\frac{\partial}{\partial t})\hat{U}^\dagger$, where $\hat{U} = e^{i\omega_c t\hat{a}^\dagger\hat{a}}$.

on the system, they possess zero mean value, obey the following two relations

$$\langle[\hat{\xi}_i(t), \hat{\xi}_j^\dagger(t')]\rangle = \gamma_j \delta_{ij} \delta(t - t'), \tag{3.18}$$

$$\langle\hat{\xi}_j^\dagger(t)\hat{\xi}_j(t')\rangle = 2\gamma_j \frac{1}{\exp(\hbar\omega_j/kT) - 1}\delta(t - t'). \tag{3.19}$$

The right hand of Eq. (3.19) contains a factor related to the average thermal occupation. In the case of optical frequency ($\omega_j = \omega_c$), where $\hbar\omega_c \gg kT$, the average thermal occupation can be almost approximated to zero. On the contrary, for the mechanical resonator ($\omega_j = \omega_m$) the thermal occupation number can be also very large for example for MHz resonators at room temperature.

3.3.1 Input-output formalism and semi-classical dynamics

Related to the description of an open system is *input-output theory*, which allows to relate the cavity, the drive and the field emitted by the cavity, see Ref. [40]. In this formalism, $\hat{a}_{in}$ obeys the canonical commutation relation; $[\hat{a}_{in}(t), \hat{a}_{in}^\dagger(t')] = \delta(t - t')$, and describes an input noise operator entering the cavity through the lossy channel. In the presence of monochromatic coherent driving, the input noise has an average value $F_L e^{-i\omega_L t}$. Hence, $\hat{n}_{in}(t) = \hat{a}_{in}^\dagger(t)\hat{a}_{in}(t)$ is the flux of incident photons or phonons on the system from the environment. In the following, we always lump the effect of driving into the input noise $\hat{a}_{in}$. The reflected field from a single-sided optical cavity is given by [48]

$$\hat{a}_{out}(t) = \hat{a}_{in}(t) - \sqrt{\kappa}\hat{a}(t), \tag{3.20}$$

The input noise $\hat{a}_{in}$ is what we defined earlier as ξ_j, therefore it obeys same correlation relation as Eq. (3.19). Particularly, for thermal occupancy at the cavity frequency, one has

$$\langle\hat{a}_{in}(t)\hat{a}_{in}^\dagger(t')\rangle = [1 + \bar{n}_{th}(\omega_c)]\delta(t - t'), \tag{3.21}$$

$$\langle\hat{a}_{in}^\dagger(t)\hat{a}_{in}(t')\rangle = \bar{n}_{th}(\omega_c)\delta(t - t'). \tag{3.22}$$

with $\bar{n}_{th}(\omega_c) = [\exp(\hbar\omega_c/k_B T) - 1]^{-1}$ as the averaged thermal occupation at the cavity frequency and for the cavity thermal bath. While, at the optical frequency, $\hbar\omega_c \ll 1$, this parameter is almost neglected, but for microwave frequencies, i.e., $\omega \sim 10GHz$, the thermal occupancy is non trivial and might have a considerable role.

Using the input-output notations, the equation of motions Eqs. (3.17) rewrite as

$$\begin{aligned}\dot{\hat{a}} &= \frac{i}{\hbar}[\hat{H}, \hat{a}] - \frac{\kappa}{2}\hat{a} + \sqrt{\kappa}\hat{a}_{in} \\ &= (i\Delta - \frac{\kappa}{2})\hat{a} + ig_{cm}(\hat{b} + \hat{b}^\dagger)\hat{a} + \sqrt{\kappa}\hat{a}_{in}\end{aligned} \tag{3.23}$$

$$\begin{aligned}\dot{\hat{b}} &= \frac{i}{\hbar}[\hat{H},\hat{b}] - \frac{\gamma_m}{2}\hat{b} + \sqrt{\gamma_m}\hat{b}_{in} \\ &= (i\omega_m - \frac{\gamma_m}{2})\hat{b} + ig_{cm}\hat{a}^\dagger\hat{a} + \sqrt{\gamma_m}\hat{b}_{in}.\end{aligned} \tag{3.24}$$

The set of Langevin equations Eq. (3.23) and (3.24) are nonlinear, so, it is not possible to easily solve these equations. In the following, we focus on the standard optomechanical Hamiltonian and discuss different regimes of optomechanics.

3.3.1.1 Nonlinear-classical regime

In this part, in order to get physical insight and to describe some of general phenomena in the optomechanical systems, we study the system in the nonlinear classical regime. In this regime, however, the dynamics of the system is also affected by noises but by considering large intracavity field and investigating the system in stationary regime, one is able to drop all the noises. To this end, let us first write the equation of motions for a driven system in the rotating frame, Eq. (3.7). Using the Langevin Eqs. (3.23) and (3.24) one obtains

$$\begin{aligned}\dot{\hat{a}} &= (i\Delta - \frac{\kappa}{2})\hat{a} + ig_{cm}\hat{a}(\hat{b} + \hat{b}^\dagger) + F_L, \\ \dot{\hat{b}} &= (i\omega_m - \frac{\gamma_m}{2})\hat{b} + ig_{cm}\hat{a}^\dagger\hat{a}.\end{aligned} \tag{3.25}$$

Here, these expressions are obtained by dropping all noise terms. It is useful to separate the classical dynamics from the behaviour which arises because of noise terms. To do this, we define the following change of variables

$$\hat{a} \to \tilde{a} + \alpha, \qquad \hat{b} \to \tilde{b} + \beta \quad (\alpha, \beta \in \mathbb{C}), \tag{3.26}$$

To understand the physical interpretation of α and β, let us first assume that they are constant parameters, so, using Eq. (3.25) one yields

$$0 = (i\Delta - \frac{\kappa}{2})\alpha + ig_{cm}\alpha(\beta + \beta^*) + F_L, \tag{3.27}$$

$$0 = (i\omega_m - \frac{\gamma_m}{2})\beta + ig_{cm}|\alpha|^2. \tag{3.28}$$

Now, one can easily find the solutions of α and β, particularly, for small g_{cm}, the Eq. (3.27) implies that

$$|\alpha|^2 \approx \frac{F_L^2}{\Delta^2 + \kappa^2/4}, \tag{3.29}$$

This is an important result, since it shows that in near resonance and for small coupling, the absolute value of α is proportional to the laser drive, which means that for a strong driving or highly

populated cavity, the number of photons can be approximated as $\langle \hat{a}^\dagger \hat{a} \rangle \simeq |\alpha|^2$.

Thus, in this regime, the equation of motion can be rewritten based on classical quantities as

$$\begin{aligned} \dot{\alpha} &= i\alpha\big(\Delta + \frac{g_{cm}}{x_{zpf}} x\big) - \frac{\kappa}{2}\alpha - iF_L, \\ \ddot{x} &= -x\omega_m^2 + \frac{\hbar g_{cm}}{m x_{zpf}} |\alpha|^2 - \gamma_m \dot{x}. \end{aligned} \tag{3.30}$$

Here, to obtain these equations, we have used the expression $\hat{x} = x_{zpf}(\hat{b} + \hat{b}^\dagger)$ and $\hat{p} = p_{zpf}(\hat{b}^\dagger - \hat{b})i$[3].

The above set of equations of motion are fully classical as they have not any dependence on the quantum quantities[4]. These equations describe the system in the nonlinear classical regime. In this regime the quantum operators are replaced by their classical counterparts: the cavity mode $\hat{a}$ and the mechanical resonator position operator $\hat{x}$ are replaced with classical field α and the classical position x. The first relation Eq. (3.30) represents a driven optical cavity whose detuning is a function of the mechanical position x. On the other hand, the second relation describes a harmonic oscillator in which the restoring force is given by the radiation pressure force $F_{rad} = \hbar g_{cm}|\alpha|^2/m x_{zpf}$.

Even though, these equations of motion obtained by replacing quantum operators by classical quantities, one can already understand many of optomechanical features such as optomechanical bistability, optical spring effect, cooling and heating of mechanical motion.

3.3.1.2 Static bistability

One can describe bistability for optomechanical system using the nonlinear-classical Hamiltonian. Let us consider the Eq. (3.30) in the steady state, by setting the time derivatives to zero. Thus, the field amplitude and mechanical displacement are

$$\begin{aligned} \alpha &= \frac{F_L}{i[\Delta + g_{cm}x/x_{zpf}] - \kappa/2}, \\ \beta &= \frac{i g_{cm}|\alpha|^2}{i\omega_m - \gamma_m/2} \quad \text{or} \quad x = \frac{\hbar g_{cm}}{m\omega_m^2 x_{zpf}} |\alpha|^2. \end{aligned} \tag{3.31}$$

The first expression shows the cavity amplitude in the steady state. This amplitude, apparently, displays a Lorentzian behaviour and is a function of mechanical displacement. The second expression describes the equilibrium position of mechanical resonator which happens when the restoring force of Harmonic oscillator $F_{HO} = m\omega_m^2 x$ sets equal to the radiation pressure force

[3]Note, in the classical frame $\langle x \rangle \simeq (\beta + \beta^*)$ and $m\dot{x} \simeq i(\beta^* - \beta)$.

[4]Even though $\hbar$ appears in these relations, but it can be shown that the equations of motion are independent of $\hbar$.

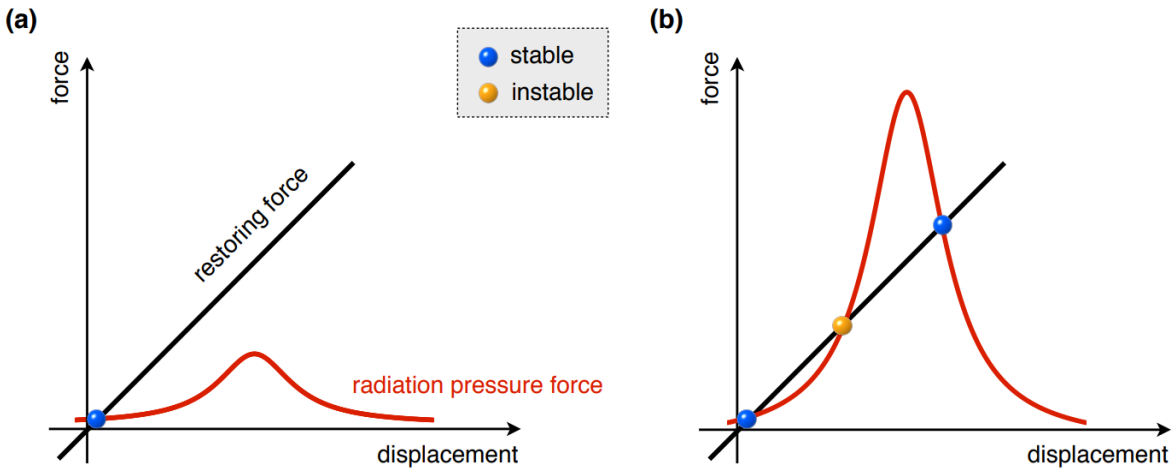

Figure 3.3: Bistability in the optomechanical system. The equilibrium positions are achieved when the restoring harmonics oscillator force F_{HO} equals the radiation pressure force F_{rad}. (a) For typical weak laser drive only one equilibrium displacement exists. (b) By increasing the laser power, these curves have three intersections where two (blue marks) of them represent stable equilibrium position.

$F_{rad} = \hbar g_{cm}|\alpha|^2/x_{zpf}$. From these relations, one can see the light field amplitude α is a nonlinear function of mechanical displacement x, which can lead to what we know as *bistability*. To see this phenomena, in Fig. (3.3), we show both the restoring harmonic oscillator F_{HO} and the radiation pressure force F_{rad} as a function of mechanical movement. The equilibrium positions correspond to the intersections of these two curves. As it is shown in Fig. (3.3.a) for a typical laser intensity, only one equilibrium displacement exists. By increasing the laser power, Fig. (3.3b), three equilibrium points are given by the curve intersections, where two of them represent the equilibrium positions.

The bistable behaviour is lost when $\Delta > -\sqrt{3}\kappa$, which means, the different driving rate proportional to F_L, leading to only one solution for circulating photon number $n_c = |\alpha^2|$ inside the cavity [49].

Alternatively, considering the effective potential for mechanical resonator, is another way to understand optical bistability in the optomechanical system. Let us here deal with the case of bad cavity limit, i.e. $\kappa \gg \omega_m$, where the light field amplitude α reacts instantaneously to any displacement of the mechanical motion. Hence, using Eq. (3.30), the position dependent radiation pressure force is given by

$$F_{rad}(x) = \hbar G \frac{F_L^2}{(\Delta + g_{cm}x/x_{zpf})^2 + \kappa^2/4}. \tag{3.32}$$

where, we have substituted α from Eq. (3.31).

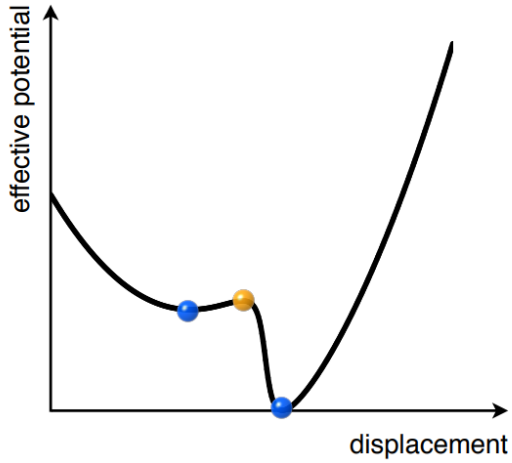

Figure 3.4: Effective potential for an optomechanical system $V_{eff} = V_{HO} + V_{rad}$. The V_{eff} is plotted as a function of displacement. This potential exhibits two minima as two stable displacements of mechanical resonator. The maximum point corresponds to an unstable position.

Therefore, the corresponding radiation potential is

$$V_{rad}(x) = -2\hbar(F_L^2/\kappa)\arctan\left[\frac{2}{\kappa}(\Delta + Gx)\right]. \tag{3.33}$$

Thus, the mechanical motion is affected by an effective potential given by

$$V_{eff}(x) = \frac{1}{2}m\omega_m^2 x^2 + V_{rad}(x). \tag{3.34}$$

Note that the overall force acting on the mechanical resonator is given by $F(x) = -\partial V_{eff}(x)/\partial x$. In the bistable regime, one can see that the effective potential shows two minima(corresponding to the two stable equilibriums) for a strong enough laser power, see Fig. (3.4). The bistability of the optomechanical system has been first reported experimentally by [49] and [50]. The bistability can be used for detection of very weak forces, as demonstrated in [51].

3.3.1.3 Optical spring effect and Optomechanical damping

The optomechanical interaction can also modify the effective mechanical spring constant, what is know as optical spring effect. Considering Eq. (3.34), the second derivative at a minimum (x_0) gives the effective spring constant

$$k_{eff} = V''(x_0) = m_{eff}\omega_m^2 + V''_{rad}(x_0), \tag{3.35}$$

where this reveals that the optomechanical interaction modifies the effective spring constant compared to the bare mechanical resonator spring constant. To demonstrate bistability we assumed bad cavity limit $\kappa \gg \omega_m$, by contrast, to understand spring effect let us here assume $\kappa \ll \omega_m$, which means that photons remain for $\tau \sim \kappa^{-1}$ before leaking out the cavity and thus the cavity does not react instantaneously to the mechanical motion. In this situation, the radiation pressure force has a time delay τ, i.e. $F_{rad}(x(t-\tau))$ relative to the actual position of mechanical resonator, $x(t)$. In general, expanding this force for small τ, we can decompose it into radiation pressure force plus a term that depends on mechanical oscillator velocity;

$$F_{rad}(x(t-\tau)) \approx F_{rad}(x(t)) - F'_{rad}(x(t))\dot{x}(t)\tau. \tag{3.36}$$

The second term can be considered as a friction force $-\gamma_{opt}\dot{x}$, where $\gamma_{opt} = F'_{rad}(x)\tau/m$ is the optomechanical damping rate. As a result, light-mechanical interaction induces (anti-)damping rate for mechanical resonator. These induced damping can be positive (damping) or negative (anti-damping) depending on the sign of $F'_{rad}(x)$; this can be associated with cooling or heating: $\gamma_{opt} > 0$ occurs for the left side of cavity resonance, and one has cooling while $\gamma_{opt} < 0$ occurs on the right side of the cavity resonance, and one has excitation and heating through the decrease of damping caused by the retarded radiation force.

3.4 Linearised regime

As mentioned before, the equations of motion can be simplified if we consider large amount of incident field drive. This enables one to use *linearized* treatment to describe the fundamentally nonlinear Hamiltonian $\hat{H}_{int} = -\hbar g_{cm}\hat{a}^\dagger\hat{a}(\hat{b}^\dagger + \hat{b})$. To this end, one can split the field operator into a steady classical state part plus a quantum fluctuations

$$\hat{a} \to \alpha_s + \delta\hat{a}, \tag{3.37}$$

where the fluctuation operator $\delta\hat{a}$ is small compared with the respective mean value $\langle\hat{a}\rangle = \alpha_s$. Using this approximation, we end up to the linearized optomechanical interaction

$$\hat{H}^{lin}_{int} = -\hbar g_{cm}\sqrt{\bar{n}_c}(\delta\hat{a}^\dagger + \delta\hat{a})(\hat{b}^\dagger + \hat{b}), \tag{3.38}$$

here, $\alpha_s = \sqrt{\bar{n}_c}$ is the mean photon number and the cavity mode phase can always, without loss of generality, be chosen so that it is real. Note, the effect of the laser drive is absorbed into the steady value as $\alpha \propto F_L$ and it does not affect the dynamics of the fluctuations. Moreover, the term $g_{cm}|\alpha|^2(\hat{b} + \hat{b}^\dagger)$ can be omitted by performing an appropriate shift in the displacement's origin as

this term describes a constant force acting on the mechanical resonator. Also, the term proportional to $\delta\hat{a}^\dagger\delta\hat{a}$ is neglected since it is of third order in the fluctuations.

One thus can rewrite the Hamiltonian (3.7) into a linearized Hamiltonian

$$\hat{H}_{lin} = -\hbar\Delta\delta\hat{a}^\dagger\delta\hat{a} + \hbar\omega_m\hat{b}^\dagger\hat{b} - \hbar g_{cm}\sqrt{\bar{n}_c}(\delta\hat{a}^\dagger + \delta\hat{a})(\hat{b}^\dagger + \hat{b}). \tag{3.39}$$

In fact, the Hamiltonian (3.7) turns to a Hamiltonian quadratic in the operators, resulting in linearized equation of motions. The interaction term shows that the optomechanical interactions coupling g_{cm}, which quantifies the single photon-phonon coupling, is enhanced by a factor equal to the intracavity amplitude α_s

$$G = g_{cm}\alpha_s = \frac{\omega_c}{L}\sqrt{\frac{\kappa P_{in}}{m\omega_m\omega_c(\kappa^2 + \Delta^2)}}. \tag{3.40}$$

Let us now, turn back to the Hamiltonian of Eq. (3.39) and treat it more classically. To this end, one may replace noise operator $\delta\hat{a}$ by a complex value α and phonon operator $\hat{b}$ by a complex value b in the equations of motion. As a result, the real part of b is proportional to the mechanical motion, thus $Re[b] = x/x_{zpf}$ and its imaginary part is proportional to the mechanical momentum, i.e., $Im[b] = p/p_{zpf}$.

We assume different scenarios based on the detuning in the resolved sideband regime, i.e. $\kappa \ll \omega_m$. First, for red-detuned regime ($\Delta < 0$), by moving to the interaction picture and neglecting counter-rotating terms one has the effective Hamiltonian $\hat{H}_{int} = -\hbar G(\hat{b}^\dagger\delta\hat{a} + \hat{b}\delta\hat{a}^\dagger)$ describing the optomechanical interactions. This interaction converts phonons to photons and vice-versa, it is also known as beam splitter Hamiltonian. In this regime, the classical-linearized equation of motions are

$$\delta\dot{\alpha} = (i\Delta' - \kappa/2)\delta\alpha + iGb, \tag{3.41}$$

$$\dot{b} = (-i\omega_m - \gamma_m/2)b + iG\delta\alpha. \tag{3.42}$$

The bright light inside the cavity displays mechanical resonator to a new equilibrium position, thus the resonance frequency of the cavity shifts. Here Δ' is the detuning of the cavity including radiation pressure effect

$$\Delta' = \Delta + \frac{g_{cm}^2|\alpha_s|^2}{\omega_m}. \tag{3.43}$$

Although these Eqs. (3.41) and (3.42) are obtained in the quantum regime, most of the interesting features of the optomechanical regime can be already understood in the classical domain. For the optical spring effect, the assumption is that the light field $\delta\alpha$ reacts instantaneously to the

mechanical displacement b, i.e,

$$\delta\alpha = \frac{iGb}{\kappa/2 - i\Delta'}. \tag{3.44}$$

By eliminating the light field $\delta\alpha$ in the equation of motion, the time evolution of the mechanical resonator is given by

$$\dot{b} = -ib(\omega_m + \delta\omega) - \frac{b}{2}(\gamma_m + \gamma_{opt}). \tag{3.45}$$

From the above equation we are able to identify the optomechanically induced damping rate γ_{opt} and mechanical frequency shift $\delta\omega_{opt}$ as

$$\gamma_{opt} = \frac{\kappa G^2}{\Delta'^2 + \kappa^2/4}, \tag{3.46}$$

$$\delta\omega = \frac{\Delta G^2}{\Delta'^2 + \kappa^2/4}. \tag{3.47}$$

The damping rate γ_{opt} can be understood also in terms of Stokes and anti-Stokes Raman scattering. For $\Delta < 0$ this process leads to an optical damping which also is known as the spring effect, as stated before. At the same time, the mechanical resonator is spring softened ($\delta\omega < 0$) for red detuning.

In the blue detuned regime $\Delta > 0$ (Stokes process), again when $G \ll \omega_m$ and that the good cavity condition $\omega_m \gg \kappa$ is fulfilled, the dominant interaction is given by $\hat{H}_{int} = \hbar G(\hat{b}^\dagger \delta\hat{a}^\dagger + \hat{b}\delta\hat{a})$ which can be seen again in the interacting picture and eliminating counter-rotating terms. The dynamics of this interaction leads to create photons and phonons in pairs (known as *two-mode squeezed states*), this means that the photon number and the phonon number states are highly correlated, corresponding to quantum entanglement. In this case, the Stokes process leads to an anti-damping $\gamma_{opt} < 0$. Likewise, the mechanical spring constant is stiffened as $\delta\omega > 0$.

The effective damping is described by $\gamma_{eff} = \gamma_m + \gamma_{opt}$ which can be either positive or negative. When $\gamma_{opt} > 0$ the effective damping is increased and one has cooling because one equilibrates at an effective temperature given by $T_{eff} = T\frac{\gamma_m}{\gamma_{eff}}$. Correspondingly when $\gamma_{opt} < 0$ one has heating and a larger effective temperature. In this regime, when $\gamma_{eff} = 0$, one enters a parametric instability and the oscillator sets itself into a self-oscillation regime where the linearization treatment is no longer valid.

Finally, for a resonantly driven optical cavity, $\Delta \approx 0$, the interaction Hamiltonian reads $\hat{H}_{int} = \hbar G(\delta\hat{a}^\dagger + \delta\hat{a})(\hat{b}^\dagger + \hat{b})$. In this process, the mechanical displacement $\hat{x} = x_{zpf}(\hat{b}^\dagger + \hat{b})$ leads to a phase shift of the light field reflected from the cavity. Hence, the detection of this phase shift can be used to measure the mechanical displacement.

3.4.1 Linearized and non linearized case

It is interesting to briefly study two optomechanical regimes, referred as "*strong coupling regime*" and "*single-photon strong coupling regime*". For the strong coupling regime the linearized coupling $G = g_{cm}\alpha_s$ becomes comparable or greater than the damping rate κ, i.e., $G/\kappa \gtrsim 1$. In this regime the cavity mode $\hat{a}$ and mechanical mode $\hat{b}$ start to hybridize, forming normal modes called *polaritons*. One can realize strong coupling by observing the normal splitting in the cavity output spectrum. Strong coupling between optical and mechanical modes has been first experimentally reported by S. Gröblacher et al [52].

For the case of single-photon strong coupling regime, the strength of the bare optomechanical coupling becomes comparable or greater than the mechanical cavity decay rate, $g_{cm} \gtrsim \kappa$. In this regime, the influence of the nonlinear interaction term becomes even more significant, so the aforementioned linearized approach can not be used to describe many new quantum effects such as *photon blockade effect*. This purely quantum behaviour has been first theoretically predicted and analysed for optomechanical systems by P.Rabl [53] and A. Nunnenkamp, K. Børkje & Girvin [54].

One can explain how strong coupling causes photon blockade effect for the resolved sideband regime $\omega_m > \kappa$, . To do so, we take the standard Hamiltonian

$$\hat{H} = \hbar\omega_c(x_0)\hat{a}^\dagger\hat{a} + \hbar\omega_m\hat{b}^\dagger\hat{b} + \hbar g_{cm}\hat{a}^\dagger\hat{a}(\hat{b}^\dagger + \hat{b}). \tag{3.48}$$

In this case the interaction of a photon with the mechanical resonator leads to a shift in the equilibrium position of the mechanical element, hence the frequency of the optical cavity shifts by $\delta\omega = -2g_{cm}^2/\omega_m$. If the frequency shift is larger than the cavity decay rate κ, a second photon would be out of resonant of the cavity and hence, the cavity blocks the transmission for a second photon and the system is capable to transmit single photons at a time (anti-bouncing). The energy levels of the system is depicted in Fig. (3.5). The states of the system $|n, m\rangle$ denotes a state with n photon and m phonons. If the system is driven resonantly with the laser $|0, 0\rangle \rightarrow |1, 0\rangle$, then the second photon is off-resonant with the transition $|1, 0\rangle \rightarrow |2, 0\rangle$ by $-2g_{cm}^2/\omega_m$, and therefore one can observe only one photon.

Alternatively, one can analyse the two-photon correlation function $g^{(2)}(\tau)$ in order to verify behaviours such as photon bunching and anti- bunching. The correlation function in the steady state reads

$$g^{(2)}(\tau) = \frac{\langle\hat{a}^\dagger(0)\hat{a}^\dagger(\tau)\hat{a}(\tau)\hat{a}(0)\rangle}{\langle\hat{a}^\dagger(0)\hat{a}(0)\rangle}^2. \tag{3.49}$$

In the case of $g^{(2)}(\tau) > 1$, a group of photon would be detected so this refers to photon bunching. However, in the case of anti-bunching, $g^{(2)}(\tau) < 1$, this implies that transmitted photons tend to

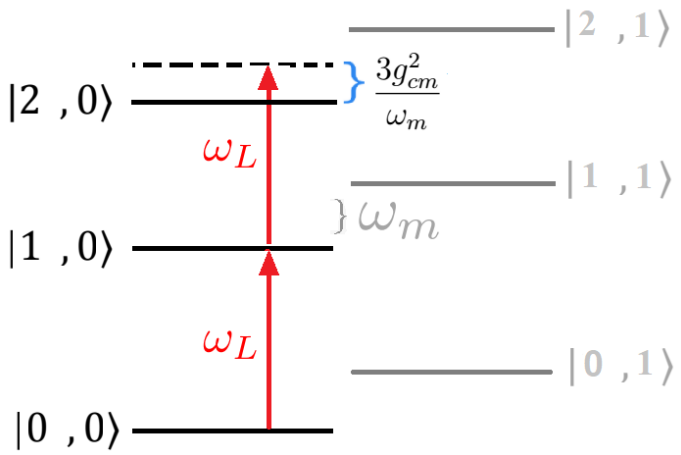

Figure 3.5: Photon blockade effect. Energy levels $|n, m\rangle$ of the optomechanical system Eq. (3.48) is depicted, where n and m corresponds to photons and phonons, respectively. A laser drive with resonance frequency ω_L leads transition $|0, 0\rangle \rightarrow |1, 0\rangle$, while it cannot excite a second photon to $|2, 0\rangle$, since the corresponding energy level is shifted by $2g_{cm}^2/\omega_m$ due to optomechanical interactions at strong coupling regime. The gray lines show states when $m = 1$.

avoid each other.

This highly exciting effect is purely a quantum behaviour and one can investigate such phenomena by adding a two-level atom to an optomechanical system and such configuration is considered in the subsequent chapters.

CHAPTER 4

Tripartite Hybrid Optomechanical System: Spectrum

In this chapter, we investigate a full coupling quantum system which is the mixing of quantum electrodynamics and optomechanics. The system under study involves a tripartite system consisting of an optical cavity, an atom and a mechanical resonator which all are mutually coupled. Such configuration can be realized experimentally in a wide range of quantum systems, for example, the atomic cavity quantum electrodynamics (QED) and superconducting QED systems [56].

In order to study this system, let us first begin by describing the interaction of a two-level atom (qubit) with a radiation mode (one-dimension harmonic oscillator), which is known as the Rabi model [57].

4.1 Rabi Model

The Rabi model is a paradigmatic model describing the dipolar interaction of a qubit with an electromagnetic field. Even though this model has been introduced in 1936, there have been controversial opinions on its exact analytical solution [58, 59]. Its quantum version describes the interaction between a single-spin with a quantized single-mode radiation field, yielding the so-called quantum Rabi model (QRM)[60]. This model successfully describes many physical situations, ranging from quantum optics [61] to quantum computation and quantum information theory [62]. Therefore, the QRM plays an important role both in theoretical and experimental physics.

The Hamiltonian of the QRM is ($\hbar = 1$)

$$\hat{H}_R = \omega \hat{a}^\dagger \hat{a} + g\hat{\sigma}_x(\hat{a} + \hat{a}^\dagger) + \frac{\Omega}{2}\hat{\sigma}_z, \tag{4.1}$$

here $\hat{\sigma}_j$ (where $j = x, y, z$) are the Pauli matrices for a two-level atom with level splitting Ω. The operators $\hat{a}^\dagger$ and $\hat{a}$ are respectively the creation and annihilation operators of the cavity with resonant frequency ω. The light-matter interaction is quantified by the vacuum-Rabi frequency g.

The physical interpretation of the coupling constant depends on the particular experimental model and the two interacting subsystems.

A generalized form of Eq. (4.1) is known as generalized quantum Rabi model (GQRM) and is given by

$$\hat{H}_{GR} = \omega \hat{a}^\dagger \hat{a} + g\hat{\sigma}_x(\hat{a} + \hat{a}^\dagger) + \epsilon\hat{\sigma}_x + \Omega\hat{\sigma}_z. \tag{4.2}$$

The additional term $\epsilon\hat{\sigma}_x$ corresponds, physically, to the transition between the two levels, which is not driven by the radiation field [63].

In term of the spin raising and lowering operators, $\hat{\sigma}_\pm = (\hat{\sigma}_x \pm i\hat{\sigma}_y)/2$, the second term in the Eq. (4.1) can be written as the sum of a rotating term and a counter-rotating term; $g\hat{\sigma}_x(\hat{a}^\dagger + \hat{a}) = g(\hat{\sigma}_-\hat{a}^\dagger + \hat{\sigma}_+\hat{a}) + g(\hat{\sigma}_+\hat{a}^\dagger + \hat{\sigma}_-\hat{a})$. Typically, in most cavity QED experiments, coupling strengths are much smaller than the natural frequencies of the system; therefore, the contribution of the counter-rotating term can be neglected using the RWA. Hence, in this case, the Hamiltonian can be simplified to the standard Jaynes-Cummings (JC)[41] model, which in most experimental studies, gives acceptable results. The JC model is a good approximation when one studies QED systems in weak and not too strong coupling regimes. In particular it successfully describes the interaction between a two-level atom, and a single electromagnetic mode confined to a cavity. Even though the JC model is analytically solvable with exact solutions, this model is valid only in the cases of near resonance and weak coupling regimes, where the coupling strength (g) is small compared to the system frequencies.

Since the last decade, substantially large coupling values have become accessible, turning out that the approximate methods such as JC lead to the wrong predictions [64, 65]. However, at weak coupling regime, it is safe to ignore counter-rotating terms, but in the realm of ultra-strong coupling regime (USC) regime, where the coupling strength becomes comparable or even larger than the system frequencies, taking into account the counter-rotating term is crucial for explaining the variety of quantum novel phenomena such as single photon emission [66] and vacuum radiation [67]. In the superconducting circuits, for instance, it is possible to reach USC [68] or the deep strong coupling regime (DSC), which means that the RWA is not an adequate approximation for such experiments. In general, the breakdown of the RWA has significant consequences on almost every aspect of the theory, both in closed or open systems.

From a theoretical standpoint, the achievement of the ultra strong coupling regime makes it reasonable to reconsider the approximation methods for QRM, such as a method based on series expansion [69], a method called generalized RWA[42], and variational approaches[70]. In this chapter, we will apply the generalized RWA and also a variational technique, called the Bloch-Siegert (BS) method [71, 72] to approximate the system Hamiltonian. As explained in Sec. (4.2.3), in most cases, counter-rotating terms can be considered as perturbative terms hence it is possible to approximate QRM by the BS Hamiltonian. In the next chapter, another variational approach,

formulated by Schrieffer-Wolf [73] is used to approximate the system Hamiltonian in the USC regime.

Apart from approximation methods, difficulties in finding the exact solution of QRM have led to the idea that this model is not integrable [74, 75], but eventually, an important progress appeared in the literature in 2011 by Braak [63]. Braak also derived necessary conditions for obtaining eigenenergies for the quantum Rabi model. Yet, obtaining the exact eigenstates remains as a significant challenge.

In the following sections, we pursue a combination of analytical and approximation approaches to study our tripartite coupled system. In the first approach, the light-matter interaction is approximated by the JC model, and the resulted Hamiltonian is diagonalized using the idea of polariton number conservation. For a fixed photon number the problem simplified to phonon-polaritons interaction. Then we can write it in the generalized Rabi form, for which according to the Braak methods, its analytical solutions are accessible. As a second approach, we consider a more general Hamiltonian when the counter-rotating term is taken into account too. In this approach, the Hamiltonian is approximated using the BS method, where two sequences of unitary transformations are applied to the light-matter parts. This is followed by calculating the energy levels using both JC approximation and the exact Rabi approach, and then we compare the results in the resonance case. While there is a good agreement between the two models at small g, at the larger g the JC approximation deviates considerably relative to the exact Rabi solutions. Finally, In the last part, we study energy levels for different detunings in the system.

4.2 The system under consideration

The system under study is comprised of a single cavity mode, a mechanical resonator, and a two-level atom (or equivalently a qubit), with frequencies ω_c, ω_m, ω_a all mutually coupled to each other through coupling factors g_{ac}, g_{cm} and g_{am}. A schematic configuration of the system is shown in Fig. (4.1).

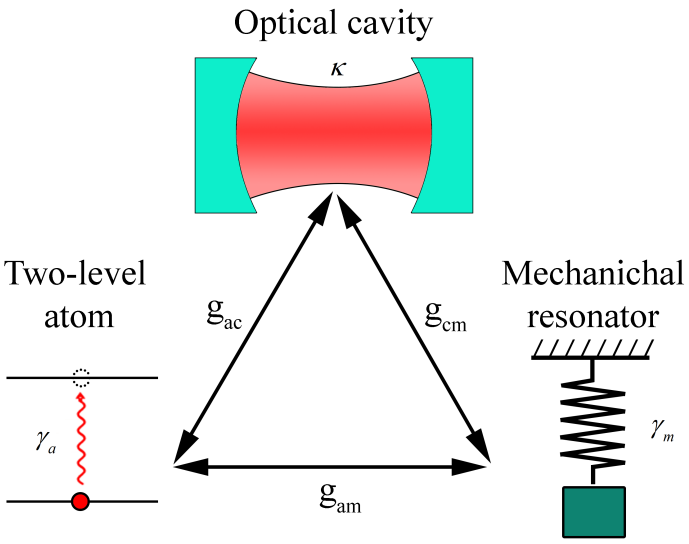

Figure 4.1: Sketch of a fully coupled tripartite system. A single mode cavity with frequency ω_c, an artificial two-level atom with transition frequency ω_a, and a mechanical resonator with frequency ω_m, all are coupled mutually. The parameters g_{ac}, g_{am} and g_{cm}, represent the atom-cavity, atom-mechanical and cavity-mechanical coupling strength, respectively.

The total Hamiltonian describing the full closed system is (here, for convenience the vacuum field energy is set to zero and we also take $\hbar = 1$),

$$\hat{H}_t = \hat{H}_0 + \hat{H}_1 + \hat{H}_2 + \hat{H}_{am} + \hat{H}_{cm}, \tag{4.3}$$

where $\hat{H}_0$ represents the Hamiltonian of the cavity and of the artificial atom, when there is no interaction between them, that is

$$\hat{H}_0 = \omega_c \hat{a}^\dagger \hat{a} + \frac{1}{2}\omega_a \hat{\sigma}_z, \tag{4.4}$$

$\hat{H}_1$ and $\hat{H}_2$ are, respectively, the rotating and counter-rotating terms

$$\hat{H}_1 = i g_{ac}(\hat{\sigma}_+ \hat{a} - \hat{\sigma}_- \hat{a}^\dagger), \quad \hat{H}_2 = i g_{ac}(\hat{\sigma}_- \hat{a} - \hat{\sigma}_+ \hat{a}^\dagger), \tag{4.5}$$

and the terms $\hat{H}_{cm}$ and $\hat{H}_{am}$ are cavity-resonator and atom-resonator interactions, respectively

$$\hat{H}_{cm} = -g_{cm}\hat{a}^\dagger \hat{a}(\hat{b} + \hat{b}^\dagger), \quad \hat{H}_{am} = -g_{am}\hat{\sigma}_z(\hat{b} + \hat{b}^\dagger) + \omega_m \hat{b}^\dagger \hat{b}, \tag{4.6}$$

where we have also included the free mechanical Hamiltonian in $\hat{H}_{am}$.

In the above expressions, $\hat{a}$ and $\hat{a}^\dagger$ are annihilation and creation operators of the cavity mode with frequency ω_c. $\hat{b}$ and $\hat{b}^\dagger$ are annihilation and creation operators of a phonon with frequency ω_m. The operators $\hat{\sigma}_{x,y,z}$ denote the Pauli matrices, and ω_a is the atomic transition frequency.

Note that, $\hat{H}_0 + \hat{H}_1 + \hat{H}_2$ models the interaction between the cavity mode and the atom in the form of Rabi model. In the JC model, the counter-rotating term $\hat{H}_2$ can be ignored under RWA.

In the subsequent sections, we focus on the solutions of the Hamiltonian Eq. (4.3) using various of approximation methods.

4.2.1 RWA and Generalized QRM

As pointed out above, the RWA is typically a valid approximation when the coupling strength is much smaller than the atom and the cavity frequencies, i.e. $g_{ac} \ll \omega_a, \omega_c$. Using this approximation, the total Hamiltonian $\hat{H}_t$ is simplified to the following form:

$$\hat{H}_0 = \omega_c \hat{a}^\dagger \hat{a} + \frac{\omega_a}{2}\hat{\sigma}_z + i g_{ac}(\hat{\sigma}_+ \hat{a} - \hat{\sigma}_- \hat{a}^\dagger) - g_{cm}\hat{a}^\dagger \hat{a}(\hat{b} + \hat{b}^\dagger) - g_{am}\hat{\sigma}_z(\hat{b} + \hat{b}^\dagger) + \omega_m \hat{b}^\dagger \hat{b}. \quad (4.7)$$

The uncoupled Hamiltonian ($g_{ac} = g_{cm} = g_{am} = 0$) possesses a complete basis of eigenvectors labelled as :$\{|g, e\rangle \otimes |k\rangle \otimes |l\rangle\}_{k,l\in\mathbb{N}}$. Here, $|g\rangle$ ($|e\rangle$) is the ground (excited) state in the two-level system, $|k\rangle$ corresponds to the cavity state with k photons, and $|l\rangle$ is the state with l phonons in the mechanical resonator. We can readily see that the model has an additional conserved operator called polariton number operator $\hat{N}_{Polariton} = \hat{a}^\dagger \hat{a} + \hat{\sigma}_+ \hat{\sigma}_-$, counting the sum of the number of photons and atomic excitations inside the cavity. It is easy to show the $\hat{H}_0$ commutes with the polariton number operator $\hat{N}_{Polariton}$: $[\hat{H}_0, \hat{N}_{Polariton}] = 0$, so that the two operators share a common basis in each subspace containing n polaritons and is a block-diagonal matrix in this basis.

$$\hat{H}_0 = \begin{pmatrix} \boxed{H_{JC}^{(0)}} & & & \\ & \boxed{H_{JC}^{(1)}} & 0 & \\ & & \ddots & \\ & 0 & & \boxed{H_{JC}^{(n)}} \\ & & & & \ddots \end{pmatrix}.$$

In order to understand better the situation, we neglect for the moment the mechanical resonator terms and we reduce $\hat{H}_0$ of Eq. (4.7) to

$$\hat{H}_{JC} = \omega_c \hat{a}^\dagger \hat{a} + \frac{\omega_a}{2}\hat{\sigma}_z + i g_{ac}(\hat{\sigma}_+ \hat{a} - \hat{\sigma}_- \hat{a}^\dagger). \quad (4.8)$$

The JC Hamiltonian can exactly diagonalized, with eigenstates

$$\begin{aligned} &n=0: \\ &\qquad |G\rangle = |g\rangle \otimes |k=0\rangle \\ &\forall n \geq 1: \\ &\qquad |+^{(n)}\rangle = \cos(\frac{\phi^{(n)}}{2})\,|g,n\rangle - i\sin(\frac{\phi^{(n)}}{2})\,|e,n-1\rangle \\ &\qquad |-^{(n)}\rangle = \sin(\frac{\phi^{(n)}}{2})\,|g,n\rangle + i\cos(\frac{\phi^{(n)}}{2})\,|e,n-1\rangle\,. \end{aligned} \tag{4.9}$$

These states are known "*dressed states*" of the atom-photon system. Here $\phi^{(n)} \in [-\pi/2, \pi/2]$ is defined through the relation $\tan(\phi^{(n)}) = (2g_{ac}\sqrt{n})/\Delta_{ac}$, where $\Delta_{ac} = \omega_a - \omega_c$ is the atom-cavity detuning.

Now, in the polariton basis with fixed polaritons n, the problem is simplified to diagonalize a 2×2 JC matrix

Thus, in the basis $(|g,n\rangle\,, |e,n-1\rangle\,, \forall n \geq 1)$

$$\hat{H}_{JC} \doteq \begin{pmatrix} \langle g,n|\, H_{JC}\, |g,n\rangle & \langle g,n|\, H_{JC}\, |e,n-1\rangle \\ \langle e,n-1|\, H_{JC}\, |g,n\rangle & \langle e,n-1|\, H_{JC}\, |e,n-1\rangle \end{pmatrix}. \tag{4.10}$$

Using the Pauli matrices $\hat{\sigma}_z \doteq \left(\begin{smallmatrix} -1 & 0 \\ 0 & 1 \end{smallmatrix}\right)$, $\hat{\sigma}_y \doteq \left(\begin{smallmatrix} 0 & i \\ -i & 0 \end{smallmatrix}\right)$, $\hat{\sigma}_x \doteq \left(\begin{smallmatrix} 0 & 1 \\ 1 & 0 \end{smallmatrix}\right)$, the 2×2 matrix takes the following form

$$\hat{H}_{JC} \doteq \begin{pmatrix} \omega_c(n-\frac{1}{2}) - \frac{\Delta_{ac}}{2} & -ig_{ac}\sqrt{n} \\ ig_{ac}\sqrt{n} & \omega_c(n-\frac{1}{2}) + \frac{\Delta_{ac}}{2} \end{pmatrix} = (n-\frac{1}{2})\omega_c\mathbb{I} + \frac{\Delta_{ac}}{2}\hat{\sigma}_z - g_{ac}\sqrt{n}\hat{\sigma}_y,$$

Equipped with these new basis we can rewrite all of the terms of $\hat{H}_0$ based on $\{|\pm\rangle^n\}$. Let us start by $\hat{a}^\dagger\hat{a}$,

$$\hat{a}^\dagger\hat{a} \doteq \begin{pmatrix} \langle +^{(n)}|\, \hat{a}^\dagger\hat{a}\, |+^{(n)}\rangle & \langle +^{(n)}|\, \hat{a}^\dagger\hat{a}\, |-^{(n)}\rangle \\ \langle -^{(n)}|\, \hat{a}^\dagger\hat{a}\, |+^{(n)}\rangle & \langle -^{(n)}|\, \hat{a}^\dagger\hat{a}\, |-^{(n)}\rangle \end{pmatrix}, \tag{4.11}$$

thus

$$\begin{aligned} \hat{a}^\dagger\hat{a} &\doteq \begin{pmatrix} n - \sin^2\frac{\phi^{(n)}}{2} & \frac{1}{2}\sin\phi^{(n)} \\ \frac{1}{2}\sin\phi^{(n)} & n - \cos^2\frac{\phi^{(n)}}{2} \end{pmatrix} \\ &= n\mathbb{I} + \frac{1}{2}\sigma_x^{(n)} - \begin{pmatrix} \sin^2\frac{\phi^{(n)}}{2} & 0 \\ 0 & \cos^2\frac{\phi^{(n)}}{2} \end{pmatrix} \\ &= (n-\frac{1}{2})\omega_c\mathbb{I} + \frac{1}{2}\sin\phi^{(n)}\sigma_x^{(n)} + \frac{1}{2}\cos\phi^{(n)}\sigma_z^{(n)}. \end{aligned} \tag{4.12}$$

Similarly, in this the atomic operator $\hat{\sigma}_z = |e\rangle\langle e| - |g\rangle\langle g|$ is represented by

$$\begin{aligned}\hat{\sigma}_z &\doteq \begin{pmatrix} -\cos\phi^{(n)} & -\sin\phi^{(n)} \\ -\sin\phi^{(n)} & \cos\phi^{(n)} \end{pmatrix} \\ &= -\cos\phi^{(n)}{\sigma_z}^{(n)} - \sin\phi^{(n)}\sigma_x^{(n)}.\end{aligned} \tag{4.13}$$

Not that for the equations Eq. (4.12) and Eq. (4.13), we have used a new set of Pauli and raising-lowering operators for the polariton subspace. The corresponding Pauli operators in the basis $|\pm^{(n)}\rangle$ are represented by the following matrices

$$\begin{aligned}&{\sigma_z}^{(n)} \doteq \begin{pmatrix} 1 & 0 \\ 0 & -1 \end{pmatrix}, \quad \sigma_x^{(n)} \doteq \begin{pmatrix} 0 & 1 \\ 1 & 0 \end{pmatrix}, \quad \sigma_y^{(n)} \doteq \begin{pmatrix} 0 & -i \\ i & 0 \end{pmatrix}, \\ &\sigma_+^{(n)} = |+^{(n)}\rangle\langle -^{(n)}| \doteq \begin{pmatrix} 0 & 1 \\ 0 & 0 \end{pmatrix}, \quad \sigma_-^{(n)} = |-^{(n)}\rangle\langle +^{(n)}| \doteq \begin{pmatrix} 0 & 0 \\ 1 & 0 \end{pmatrix}.\end{aligned} \tag{4.14}$$

Therefore, in the basis $|\pm^{(n)}\rangle$, the $\hat{H}_{JC}$ can be written as

$$\hat{H}_{JC} \doteq \begin{pmatrix} \omega_c(n-\frac{1}{2}) - \frac{\Delta_{ac}}{2} & -ig_{ac}\sqrt{n} \\ ig_{ac}\sqrt{n} & \omega_c(n-\frac{1}{2}) + \frac{\Delta_{ac}}{2} \end{pmatrix} = (n-\frac{1}{2})\omega_c\mathbb{I} - \frac{\Delta_{ac}}{2}\hat{\sigma}_z^{(n)} + g_{ac}\sqrt{n}\hat{\sigma}_y^{(n)}. \tag{4.15}$$

To find the eigenvalues, we use the following expression which is valid for any 2D Hermitian matrix:

$$A_{2\times 2} = \frac{1}{2}m_0 + \frac{1}{2}\vec{m}.\hat{\vec{\sigma}} \quad \xrightarrow{Eigenvalues} \quad \frac{m_0 \pm |\vec{m}|}{2}, \tag{4.16}$$

here $\vec{m}$ is a vector with components $m_i, i = 1, 2, 3$. Accordingly, the eigenvalues corresponding to the eigenstates Eq. (4.9) are:

$$\begin{aligned}&\hat{H}_{JC}|G\rangle = -\frac{\omega_a}{2}|G\rangle = E_G|G\rangle, \\ &\hat{H}_{JC}|\pm^{(n)}\rangle = \left[(n-\frac{1}{2})\omega_c \pm \sqrt{\frac{\Delta_{ac}^2}{4} + ng_{ac}^2}\right]|\pm^{(n)}\rangle = E_\pm^{(n)}|\pm^{(n)}\rangle.\end{aligned} \tag{4.17}$$

The energy levels of JC Hamiltonian is shown in Fig. (4.2). For the sake of simplicity, we shift the origin of the energy values to $-\omega_a/2$, so that $E_G = 0$.

Consequently, in the basis $|\pm^{(n)}\rangle$, the Hamiltonian Eq. (4.7) in which we include optomechan-

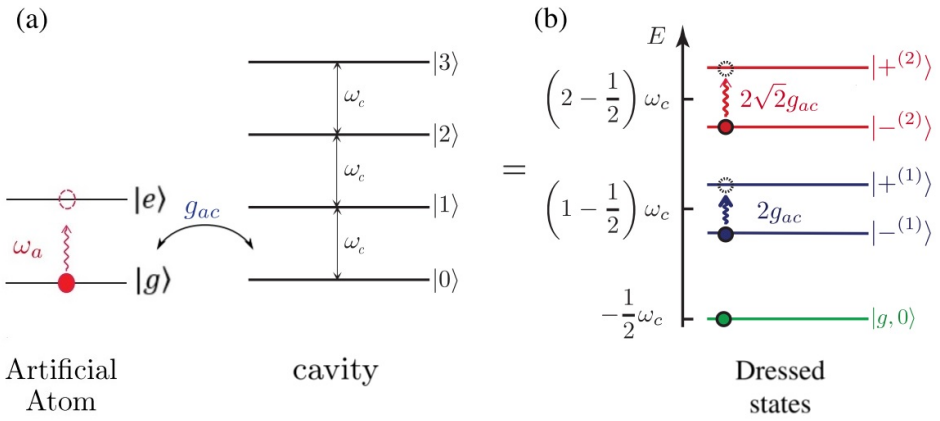

Figure 4.2: Energy levels of (a) uncoupled two-level atom and cavity, and (b) polariton energy levels of JC Hamiltonian for the coupled system.

ical mechanical part is rewritten as:

$$\begin{aligned}\hat{H}_n = (n-\frac{1}{2})\omega_c\mathbb{I} + \sqrt{\frac{\Delta_{ac}^2}{4} + n g_{ac}^2}\sigma_z^{(n)} - g_{cm}(n-\frac{1}{2})(\hat{b}+\hat{b}^\dagger) \\ - \frac{1}{2}\tilde{g}_{pm}\left[\sigma_x^{(n)}\sin(\phi^{(n)}) + \sigma_z^{(n)}\cos(\phi^{(n)})\right](\hat{b}+\hat{b}^\dagger) + \omega_m\hat{b}^\dagger\hat{b},\end{aligned} \tag{4.18}$$

where $\tilde{g}_{pm} = g_{cm} - 2g_{am}$ is the polariton-mechanics coupling. The third term in the $\hat{H}_n$ is originated from a constant force that applies on the mechanical resonator. In order to remove this term, we define two new operators as displaced creation and annihilation operators [76];

$$\hat{b}_n^\dagger = \hat{b}^\dagger - \frac{\alpha_0^{(n)}}{\sqrt{2}}, \quad \hat{b}_n = b^\dagger - \frac{\alpha_0^{(n)}}{\sqrt{2}}. \tag{4.19}$$

Therefore, the new equilibrium position of the mechanical resonator is $\alpha_0^{(n)} = \sqrt{2}(n-1/2)g_{cm}/\omega_m$. Hence, in the displaced frame the Hamiltonian $\hat{H}_n$ is rewritten as

$$\begin{aligned}\hat{H}_n = (n-1/2)\omega_c\mathbb{I} - \omega_m(n-1/2)^2\left(\frac{g_{cm}}{\omega_m}\right)^2 + \sqrt{\frac{\Delta_{ac}^2}{4} + n g_{ac}^2}\sigma_z^{(n)} \\ + \omega_m\hat{b}_n^\dagger\hat{b}_n - \frac{1}{2}\tilde{g}_{pm}\left[\hat{b}_n + \hat{b}_n^\dagger - \frac{2g_{cm}}{\omega_m}(n-1/2)\right]\left[\sigma_x^{(n)}\sin(\phi^{(n)}) + \sigma_z^{(n)}\cos(\phi^{(n)})\right].\end{aligned} \tag{4.20}$$

This Hamiltonian is written in the basis $\{|\pm^{(n)}\rangle, |m^{(n)}\rangle\}$ which $|m^{(n)}\rangle$ is the Fock state corresponding to m phonons in the displaced mechanical resonator.

Let us now, restrict to the small detuning case ($\Delta_{ac} << g_{ac}$) or more precisely when $\Delta_{ac} \simeq 0$. Using this assumption, $\sin(\phi) = 1$ and $\cos(\phi) = 0$, so the expression for H_n is considerably simplified. Moreover, in most experimental cases $g_{cm}/\omega_m << 1$, so we can neglect the perturbative

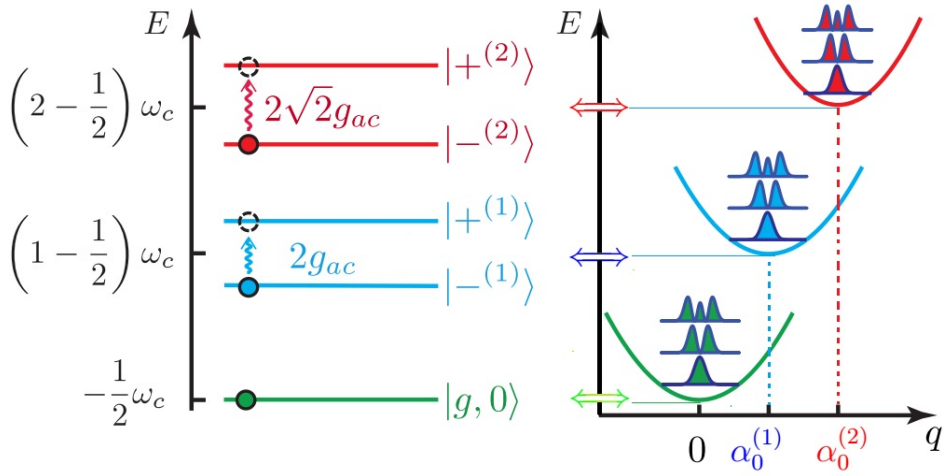

Figure 4.3: Structure of polaron eigenstates. Each polariton doublet coupled independently to a mechanical resonator with different displacements.

term $\propto \hat{\sigma}_x^n$ which actually is responsible for a Stark shift in the energy levels (in the next section we consider a general case and the Hamiltonian is studied without such restrictions). Based on these assumptions, the H_n turns to a Rabi like Hamiltonian;

$$\begin{aligned}\hat{H}_n \approx (n-1/2)\omega_c\mathbb{I} - \omega_m(n-1/2)^2\left(\frac{g_{cm}}{\omega_m}\right)^2 + \\ \omega_m\hat{b}_n^\dagger\hat{b}_n + \frac{\Omega_n}{2}\sigma_z^{(n)} - \frac{1}{2}\tilde{g}_{pm}(\hat{b}_n + \hat{b}_n^\dagger)\sigma_x^{(n)},\end{aligned} \tag{4.21}$$

where $\Omega_n = 2g_{ac}\sqrt{n}$. we can again implement RWA to the above Hamiltonian (this approximation is valid when $\tilde{g}_{pm} << \Omega_n, \omega_m$),

$$\begin{aligned}\hat{H}_n \approx (n-1/2)\omega_c\mathbb{I} - \omega_m(n-1/2)^2\left(\frac{g_{cm}}{\omega_m}\right)^2 + \\ \omega_m\hat{b}_n^\dagger\hat{b}_n + \frac{\Omega_n}{2}\sigma_z^{(n)} - \frac{1}{2}\tilde{g}_{pm}(\hat{b}_n\sigma_+^{(n)} + \hat{b}_n^\dagger\sigma_-^{(n)}).\end{aligned} \tag{4.22}$$

To find the energy levels we can use the same procedure that leads to the Eq. (4.17). Fig. (4.2) depicts coupling of polariton states with the mechanical resonator states. Note that here, the new "Polaron number" operator is defined as $\hat{N}_{Polaron} = \hat{b}_n^\dagger\hat{b}_n + \hat{\sigma}_+^{(n)}\hat{\sigma}_-^{(n)}$ which commutes with the Eq. (4.22). Finally, one can obtain the following polaron basis that diagonalizes Eq. (4.22):

$$
\begin{aligned}
&m=0: \\
&\qquad |G_n\rangle = |-^{(n)}\rangle \otimes |0^{(n)}\rangle\,, \\
&\forall m \geq 1: \\
&\qquad |+_{n,m}\rangle = \cos(\frac{\theta_{n,m}}{2})\,|+^{(n)}\rangle\,|(m-1)^{(n)}\rangle - i\sin(\frac{\theta_{n,m}}{2}))\,|-^{(n)}\rangle\,|m^{(n)}\rangle \\
&\qquad |-_{n,m}\rangle = \sin(\frac{\theta_{n,m}}{2})\,|+^{(n)}\rangle\,|(m-1)^{(n)}\rangle + i\cos(\frac{\theta_{n,m}}{2}))\,|-^{(n)}\rangle\,|m^{(n)}\rangle\,,
\end{aligned}
\tag{4.23}
$$

where $\theta_{n,m} \in [-\pi/2, \pi/2]$ defines via $\tan(\theta_{n,m}) = -(\tilde{g}_{pm}\sqrt{m})/(2g_{ac}\sqrt{m} - \omega_m)$. The corresponding eigenvalues for $m \geq 1$ and $n = 0$ are,

$$
\langle G_n|\,\hat{H}^{(n)}\,|G_n\rangle = n\omega_c - \omega_m(n-1/2)^2(\frac{g_{cm}}{\omega_m})^2 - g_{ac}\sqrt{n}, \tag{4.24}
$$

and the eigenvalues for $n, m \geq 1$ are,

$$
\begin{aligned}
\langle \pm_{n,m}|\,\hat{H}^{(n)}\,|\pm_{n,m}\rangle = n\omega_c - \omega_m(n-1/2)^2(\frac{g_{cm}}{\omega_m})^2 + \\
(m-\frac{1}{2})\omega_m \pm \sqrt{\frac{(2g_{ac}\sqrt{n}-\omega_m)^2}{4} + m\frac{\tilde{g}_{pm}^2}{4}}.
\end{aligned}
\tag{4.25}
$$

4.2.2 Solutions for $\hat{H}_n$ and Generalized Rabi model

In the previous section, we arrived to the Eq. (4.25) by making two important assumptions. First, we assumed that the artificial atom and the cavity mode are at resonance, e.g., $\Delta_{ac} \simeq 0$. As a second assumption, we neglect the term proportional to the $\hat{\sigma}_x^n$. In this section, however, we examine the Hamiltonian Eq. (4.20) more generally, without such restrictions. We use the analytical approach provided in [63], to express the Hamiltonian Eq. (4.20) in the form of a generalized QRM, Eq. (4.28), which is a non-integrable system but has analytical solutions.

To express Eq. (4.20) in the form of the generalized Rabi model, we just need to apply a rotation operator ($\hat{D}_a(\Theta) = \exp(-i\frac{\Theta}{2}\hat{e}_a.\hat{\sigma})$) on the Eq. (4.20), which rotates Pauli matrices around y axis by angle θ:

$$
\begin{aligned}
\hat{\sigma}_x' &\longrightarrow \hat{D}_y(\Theta)\hat{\sigma}_x\hat{D}_y(\Theta) = \hat{\sigma}_x\cos(\Theta) - \hat{\sigma}_z\sin(\Theta), \\
\hat{\sigma}_z' &\longrightarrow \hat{D}_y(\Theta)\hat{\sigma}_z\hat{D}_y(\Theta) = \hat{\sigma}_z\cos(\Theta) + \hat{\sigma}_x\sin(\Theta).
\end{aligned}
\tag{4.26}
$$

By substituting $\Theta = \phi - \pi/2$, we have

$$
\hat{\sigma}_x' = \hat{\sigma}_x\sin(\phi) + \hat{\sigma}_z\cos(\phi), \quad \hat{\sigma}_z' = \hat{\sigma}_z\sin(\phi) - \hat{\sigma}_x\cos(\phi), \tag{4.27}
$$

thus straightforwardly $\hat{\sigma}_z = \hat{\sigma}'_x \cos(\phi) - \hat{\sigma}'_z \sin(\phi)$.

Finally, the Hamiltonian Eq. (4.20), turns to the generalized quantum Rabi form:

$$\hat{H}_{GR} = \omega \hat{a}^\dagger \hat{a} + g\hat{\sigma}_x(\hat{a} + \hat{a}^\dagger) + \epsilon \hat{\sigma}_x + \Omega \hat{\sigma}_z, \tag{4.28}$$

using the following substitutions:

$$\begin{aligned} g &= -\frac{1}{2}\tilde{g}_{pm}, \\ \Omega &= \sqrt{\frac{\Delta_{ac}^2}{4} + n g_{ac}^2}\ \sin(\phi), \\ \epsilon &= \sqrt{\frac{\Delta_{ac}^2}{4} + n g_{ac}^2}\ \cos(\phi) + \frac{g_{cm} g_{pm}}{\omega_m}(n - \frac{1}{2}). \end{aligned} \tag{4.29}$$

Note that, in these relations we have used $\tilde{g}_{pm} = g_{cm} - 2g_{am}$.

4.2.3 Approximation based on Bloch-Siegert Hamiltonian

Let us now turn back to Eq. (4.3) and take it as our starting Hamiltonian. So far, the counter-rotating terms $\hat{H}_2$ has been neglected from the main Hamiltonian under the RWA. However, for the systems with ultra-strong coupling, when the coupling is comparable to ω_c and ω_a, the usual RWA is not valid, and the counter-rotating terms must be taken into account. Although the USC regime [68, 77] has been experimentally reached only recently, many of the approximation methods were proposed many years before the first USC experiments.

In the following, we discuss a scheme based on a perturbation scheme called Bloch–Siegert (BS) method, first introduced in 1940 [78]. Applying to the QRM Hamiltonian the BS correction gives rise to the correction in the energy spectrum known as BS shifts. This shift has been experimentally observed in a variety of systems with a driven superconducting qubit [79].

The system Hamiltonian is almost in the form proposed in Eq. (4.7), except that here we also include the counter-rotating term in the total Hamiltonian. The BS approximation is valid when the coupling strength g is small with respect to $\Sigma = \omega_a + \omega_c$, while the system is still in the USC regime. More precisely, according to the notation Eq. (4.4) and Eq. (4.5), the atom-cavity Hamiltonian has the QRM form, that is

$$\begin{aligned} \hat{H}_{ac} &= \hat{H}_0 + \hat{H}_1 + \hat{H}_2 \\ &= \omega_c \hat{a}^\dagger \hat{a} + \frac{\omega_a}{2}\hat{\sigma}_z + i g_{ac}(\hat{\sigma}_+ \hat{a} - \hat{\sigma}_- \hat{a}^\dagger) + i g_{ac}(\sigma_- \hat{a} - \sigma_+ \hat{a}^\dagger). \end{aligned} \tag{4.30}$$

According to the BS method, in order to eliminate counter-rotating term from this Hamiltonian,

two successive unitary transformations are performed, i.e., $V_2 V_1 H_{ac} V_1^\dagger V_2^\dagger$, where

$$\begin{aligned} V_1 &= \exp[i\epsilon A], \quad \text{with} \quad A = -(\hat{\sigma}_+ \hat{a}^\dagger + \hat{\sigma}_- \hat{a}), \\ V_2 &= \exp[\phi B], \quad \text{with} \quad B = \sigma_z (a^2 - a^{\dagger 2}), \quad \text{and} \quad \phi = \frac{\epsilon g}{2\omega_c} \backsim \epsilon^2. \end{aligned} \tag{4.31}$$

Where, $\epsilon = g_{ac}/\Sigma$ is a small real parameter. The first transformation, V_1, corresponds to a displacement in the cavity field, while the second one, V_2, generates squeezing of the field. We approximate these transformations up to second order in ϵ^2 using the Baker-Campbell-Hausdorff relation:

$$e^{i\epsilon \hat{D}} \hat{H} e^{-i\epsilon \hat{D}} \approx \hat{H} + i\epsilon[\hat{D}, \hat{H}] - \frac{\epsilon^2}{2}[\hat{D}, [\hat{D}, \hat{H}]].$$

Here $\hat{D}$ is an arbitrary hermitian operator, i.e., $\hat{D}^\dagger = \hat{D}$.

These calculations accordingly lead to the Bloch-Siegert Hamiltonian

$$V_2 V_1 \hat{H}_{ac} V_1^\dagger V_2^\dagger \approx H_0 + \epsilon g_{ac}[\sigma_z(\hat{n} + \frac{1}{2}) - \frac{1}{2}] + \tilde{H}, \tag{4.32}$$

where,

$$\tilde{H} = i\sigma_+ \hat{a} g^{(\hat{n})} - i g^{(\hat{n})} a, \quad g^{(\hat{n})} = g(1 - i\epsilon^2 \hat{n}),$$

and in the basis $(|g, n\rangle, |e, n-1\rangle, \forall n \geq 1)$, the resulting Hamiltonian takes the following form

$$\hat{H}_{ac} \doteq (n - \frac{1}{2})\omega_c \mathbb{I} - \frac{1}{2}\epsilon g^{(\hat{n})} + \frac{1}{2}(\Delta_{ac} + 2n\epsilon g_{ac})\hat{\sigma}_z - g_{ac}\sqrt{n}(1 + n\epsilon^2)\hat{\sigma}_y. \tag{4.33}$$

It is obvious that this expression is reduced to the JC Hamiltonian Eq. (4.15) at the limit of $\epsilon = 0$. Its eigenvalues can be immediately found using the expression Eq. (4.16). Note that, here $\tan(\phi^{(n)}) = (2g_{ac}\sqrt{n}(1 + n\epsilon^2))/(\Delta_{ac} + 2n\epsilon g_{ac})$ in this case.

In the subspace spanned by $\{|\pm^{(n)}\rangle, |m^{(n)}\rangle\}$, the total Hamiltonian Eq. (4.3) is expressed in the following form,

$$\begin{aligned} \hat{H}_{BS} =& (n - \frac{1}{2})\omega_c \mathbb{I} - \frac{1}{2}\epsilon g_{ac}\mathbb{I} + \omega_m \hat{b}^\dagger \hat{b} \\ &+ \left[\sqrt{\frac{\Delta_{ac}^2}{4} + n g_{ac}^2} + \omega_{BS}\right]\sigma_z^{(n)} - g_{cm}(n - \frac{1}{2})(\hat{b} + \hat{b}^\dagger) \\ &- \frac{1}{2}\tilde{g}_{pm}\left[\sin\phi^{(n)}\sigma_x^{(n)} + \cos\phi^{(n)}\sigma_z^{(n)}\right](\hat{b} + \hat{b}^\dagger), \end{aligned} \tag{4.34}$$

where the term $\omega_{BS} = \sqrt{(n\epsilon g_{ac})(1/2 + n\epsilon g_{ac})}$ is the Bloch-Siegert shift.

The Hamiltonian Eq. (4.34) is similar to the Hamiltonian Eq. (4.20), therefore one can rewrite it in the form of generalized QRM Hamiltonian Eq. (4.28). This is done by moving to a displaced

frame introduced by Eq. (4.19) together with a rotation around y axes according to the rotation operators, Eq. (4.26). The resulting Hamiltonian could be in the form of generalized QRM Eq. (4.28), if we consider the parameters same as Eq. (4.29), except that for both Ω and ϵ,

$$\begin{aligned}\Omega &= \left[\sqrt{\frac{\Delta_{ac}^2}{4} + n g_{ac}^2} + \omega_{BS}\right] \sin(\phi), \\ \epsilon &= \left[\sqrt{\frac{\Delta_{ac}^2}{4} + n g_{ac}^2} + \omega_{BS}\right] \cos(\phi) + \frac{g_{cm} g_{pm}}{\omega_m}(n - \frac{1}{2}),\end{aligned} \tag{4.35}$$

and we have an extra Bloch-Siegert shift ω_{BS}.

4.3 Eigenvalues and comparison of models

In this section, we focus on the Hamiltonian in the Rabi form as represented by Eq. (4.28) and explore its energy values as a function of coupling strength g. Here, unless otherwise stated, the following values for the parameters are considered: ω_c/ω_m=100, g_{ac}/ω_m=1/2, g_{cm}/ω_m=0.05, g_{am}/ω_m=-1/40 and $\omega_a = \omega_c + \Delta$.

It is not surprising that when $n = 0$, the levels of the mechanical resonator are independent of the coupling constant, and they do not depend on the cavity modes and the two-level atom.

However, when $n \neq 0$, the energy levels of the system depend on the coupling strength g and as g increases the spectrum changes drastically. To quantify the interaction, we introduce a dimensionless parameter η, known as normalized coupling parameter which is defined as the ratio between the coupling strengths and system frequencies. As long as $\eta << 1$ or in the weak coupling regime, RWA is a good approximation and works for a wide range of experiments. On the other hand, in the cases such as the superconducting qubits or microwave cavities (where $g \simeq$10 GHz), the system frequencies are of the order of coupling strength, i.e. $0.1 < \eta < 1$, which means the system is in the USC regime, so, the RWA is not applicable and leads to wrong results. The USC regime occurs when η = max(g/ω_c, g/ω_a) is in the range [0.1,1). Value of $\eta = 0.1$ has often been taken as a threshold for the USC regime [1].

For comparison, the energy spectrum of the system obtained by Rabi model Eq. (4.28) and the approximated JC model Eq. (4.22) are plotted in Fig. (4.4) as a function of coupling g and for zero detuning $\Delta_{ac} = 0$. Here, g ranges continuously from the JC limit, $0 < g \ll \omega_m$, into the USC regime, $g \sim 1.1$. While the Rabi model gives the exact solution for all η, the JC model correctly predicts the Rabi splitting between neighboring pairs of energy levels, but fails when g increases, around the Juddian points [80], in which pairs of energy levels begin to cross (see the gray region

[1]This definition does not involve system losses so it is possible in the USC regime, the system under study be in WC or SC regime too.

in Fig. (4.4)). This is expected since perturbation theory works well when η is small and for large values (strong coupling regime) the RWA breakdowns.

We can also notice from Fig. (4.4) that the accuracy of the JC model depends not only on η but also on the energy levels of the system [81]. In other words, as the spectrum becomes more energetic, the coincidence of the JC model happens for smaller ranges of η.

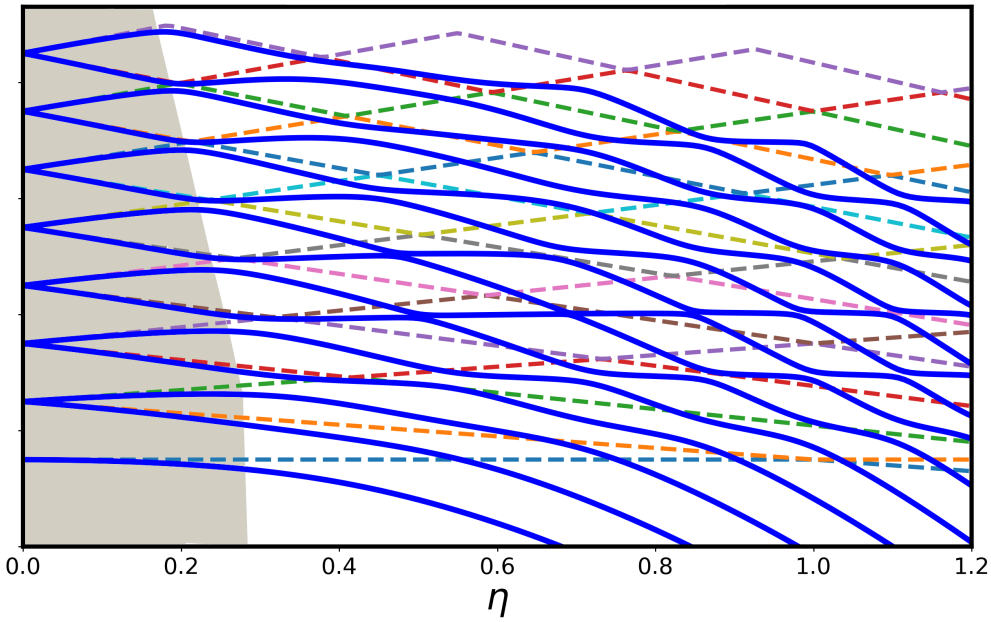

Figure 4.4: Comparison between the Rabi model Eq. (4.28) and the JC spectrum in the resonance case $\omega_a = \omega_c$ as a function of η. Solid (dashed) lines correspond to the Rabi (JC) spectrum. The JC model gives more accurate solutions in the shaded region when η is small. As η increases the RWA fails and deviation from exact solution appears.

In Fig. (4.5) the spectrum of the QRM Eq. (4.28) is compared with the results of BS approximation Eq. (4.34). The energy levels are shown as a function of the coupling constant for different detuning values Δ_{ac}. As it can be seen, these two results are in excellent agreement. This is an expected result since, in the BS approach, the Hamiltonian is expanded up to second order of ϵ, where ϵ is a very small quantity. In other words, since $\epsilon = \frac{g}{\omega_c+\omega_a} \sim 0.0025$, the higher orders of ϵ can be readily ignored without losing the accuracy. As it is clear in Fig. (4.5), for one-polariton subspace the coupling interaction depends strongly on the detuning Δ_{ac}. Particularly, for small detuning ($\Delta_{ac} \ll g_{ac}$) the hybridization between atomic and photonic excitations is more important.

In the following chapter, we investigate the dynamics of the tripartite system by taking into account damping and losses.

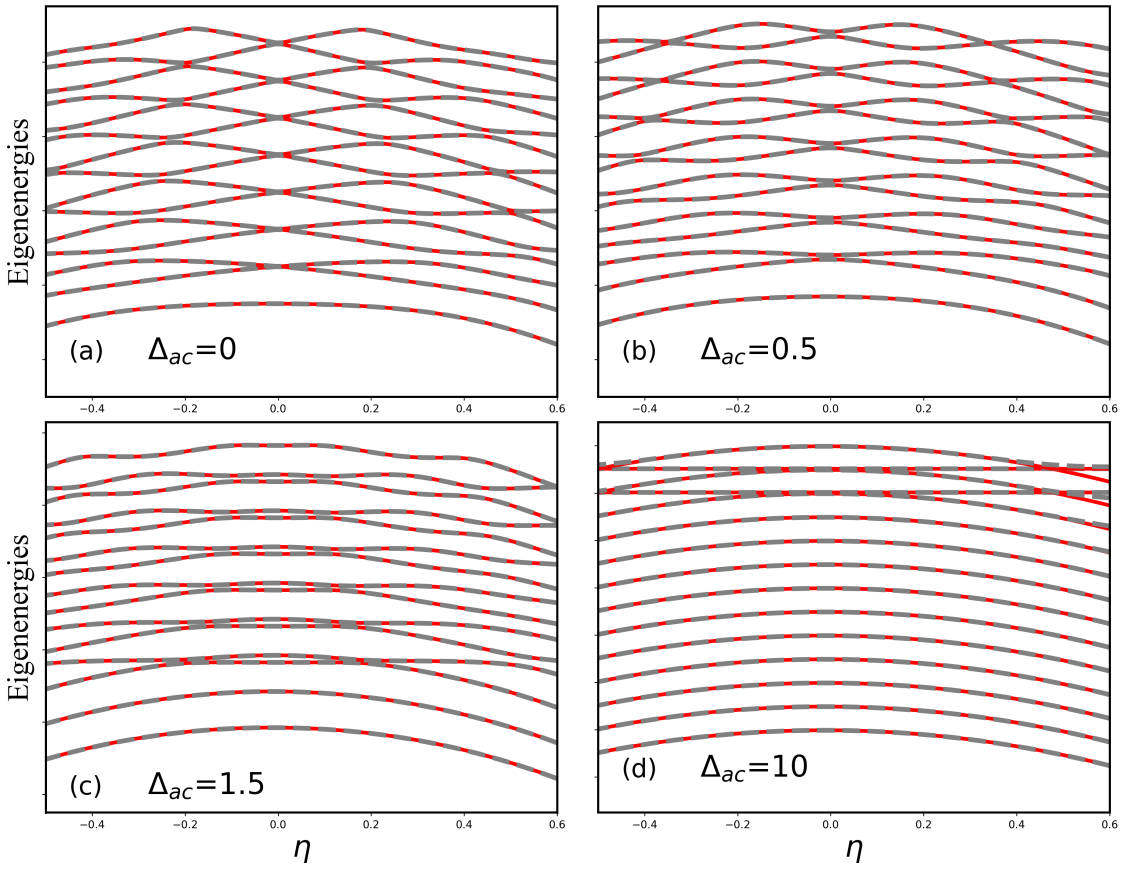

Figure 4.5: Rabi model(red full lines) vs. BS model(gray dashed lines) in the detuned case as a function of g. Energy levels strongly depend to Δ_{ac} values. The other parameters are: $\omega_c/\omega_m = 100$, $g_{ac}/\omega_m = 1/2$, $g_{cm}/\omega_m = 1/20$, and $g_{am}/\omega_m = -1/40$.

CHAPTER 5

Hybrid tripartite optomechanical system: single-photon strong coupling regime

In this chapter, we provide a general treatment of the hybrid tripartite system formed by the cavity mode, the mechanical resonator, and a generic qubit, in the dispersive regime of large detunings, determining the conditions under which the qubit can be adiabatically eliminated, and one can map the tripartite dynamics into that of an effective cavity optomechanical system in the strong coupling regime. The physics of this regime is very different from the one occurring when the qubit-cavity system is quasi-resonant (see for example, Reference [76] and references therein), and we will exploit the Schrieffer–Wolff method [82] in order to arrive at an effective optomechanical model Hamiltonian. We will provide the validity limits of this treatment and the expression of the effective optomechanical coupling rate. We will verify the results by investigating the stationary regime, and in particular, the cavity stationary photon number and the stationary mean phonon number in the low excitation regime, which are suitable for witnessing photon blockade [53] and other nonlinear optomechanical phenomena in the strong coupling regime [54, 55].

In this chapter, first, we briefly discuss the proposal for new platforms to achieve efficient optomechanical interaction, suitable for the lead to single-photon coupling regime. Next, we study a standard optomechanical set-up and using an analytical approach we calculate the cavity amplitude, in the weak driving regime. In the following part, we introduce the tripartite hybrid system and its relevant parameters. Then, we describe the Schrieffer–Wolff method through which we derive the effective optomechanical Hamiltonian, while in Section V, we describe the numerical results showing when the dynamics can be satisfactorily described in terms of a strongly coupled optomechanical system. The last section is for concluding remarks.

5.1 Introduction

Cavity optomechanics [83] has become an established platform for the implementation of quantum information processing in which one can manipulate electromagnetic (EM) fields and me-

chanical/phononic degrees of freedom for the realization of quantum interfaces [84, 85, 86], memories [83], and quantum gates [87, 88, 89, 90]. The optomechanical interaction is typically of parametric form; that is, the cavity frequency is modulated by the motion of the mechanical element, and therefore, it acts dispersively on the EM field. However, this interaction is very weak at the level of single quanta because the frequency shift due to a single phonon is typically much smaller than the cavity linewidth and the mechanical frequency. Therefore, as we explained in the previous chapter, one usually operates in the linearized regime where the cavity is intensely driven, and the effective coupling is enhanced by a large intracavity field amplitude [83]. In this latter regime, however, only a limited set of linear operations is possible, harnessing the design of efficient quantum gates within optomechanical platforms. For this reason, there is a growing interest in finding new schemes able to reach the regime where the optomechanical coupling rate g_{cm} is comparable or larger than the cavity decay rate κ and the mechanical frequency ω_m.

Recently, very promising results have been achieved with new platforms [91, 92], but it is typically very difficult to achieve simultaneously strong coupling $g_{cm} \geq \omega_m$ and the resolved sideband condition $\kappa < \omega_m$, which is important for enabling coherent control at the quantum level. These latter conditions are instead achievable by adopting a "hybrid" approach in which the interaction between the mechanical and the electromagnetic mode is mediated by a qubit simultaneously interacting with both modes [93, 94, 95, 96, 97, 98, 99].

A first experimental proof-of-principle demonstration of coupling enhancement has been achieved using an electromechanical system in a superconducting circuit, where a Cooper pair box [94] acted as the effective qubit. An alternative hybrid tripartite platform is represented by trapped atoms/ions in an optical cavity [98, 99], in which an internal Raman transition may act as an effective mediator between the cavity field and the atomic motional degree of freedom (see also References [100, 101, 102] for pioneering studies showing the ability to entangle light modes by means of these strongly coupled hybrid tripartite systems).

The physical mechanism at the basis of the enhancement of the optomechanical coupling, even by many orders of magnitude, is the following. In the dispersive regime in which the qubit is strongly detuned from the cavity (and any driving frequency), the qubit is never excited and remains in its effective ground state. In this case, the AC Stark shift caused by the qubit on the cavity frequency is modulated by the mechanical motion through the qubit-mechanics coupling, resulting in a very strong, effective dispersive optomechanical coupling g_{cm}^{eff}, which can reach the strong coupling regime $g_{cm}^{eff} \sim \omega_m$ (ω_m is the mechanical frequency), provided that the qubit-mechanics coupling rate g_{am} and the qubit-cavity coupling rate g_{ac} are large enough compared to ω_m.

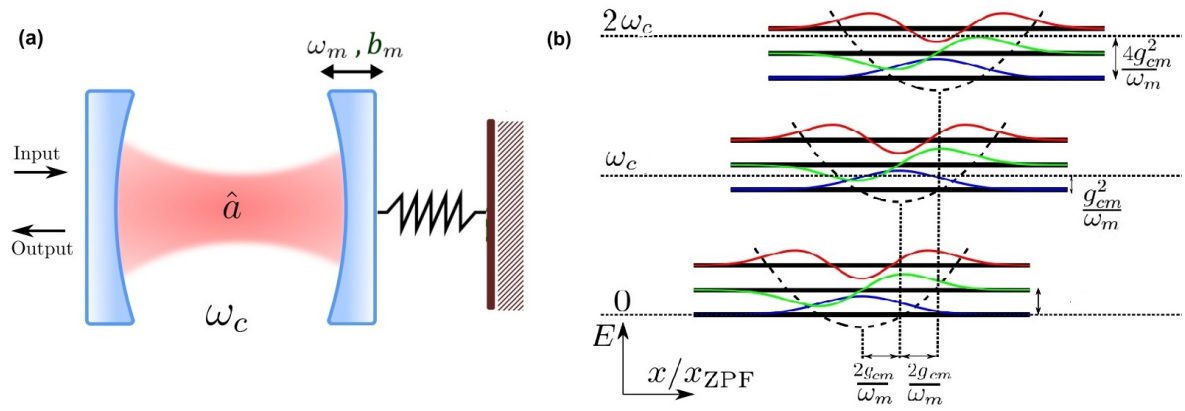

Figure 5.1: (a)Standard cavity optomechanical system. (b) Energy diagrams of Hamiltonian Eq. (5.1) adopted from [54]. For a photon number state $|n_c\rangle$, the radiation pressure force displaces the resonator to a new equilibrium position $\frac{2g_{cm}}{\omega_m}$ and the energy states are lowered by $n_c^2 g_{cm}^2/\omega_m$.

5.2 Standard model

Let us first, go back to the standard model of optomechanical system where a mechanical resonator is interacting with a single optical mode cavity, in the absence of losses and driving. The Hamiltonian is (by setting $\hbar = 1$) exactly same as Eq. (3.48), so

$$\hat{H}_0 = \omega_c \hat{a}^\dagger \hat{a} + \omega_m \hat{b}^\dagger \hat{b} + g_{cm} \hat{a}^\dagger \hat{a} (\hat{b} + \hat{b}^\dagger), \tag{5.1}$$

where $\hat{a}$ and b represent bosonic annihilation for the cavity mode and the mechanical resonator, respectively.

Straightforwardly, the eigenvalues and eigenvectors are obtained, by moving to a displaced resonator representation, i.e,. $\tilde{b} = \hat{b} + \frac{g_{cm}}{\omega_m} \hat{a}^\dagger \hat{a}$. The Hamiltonian now is

$$\hat{H}_0 = \omega_c \hat{a}^\dagger \hat{a} + \omega_m \hat{b}^\dagger \hat{b} - \frac{g_{cm}^2}{\omega_m} (\hat{a}^\dagger \hat{a})^2. \tag{5.2}$$

It is evident that the Hamiltonian conserves the photon number, that is, $[\hat{a}^\dagger \hat{a}, \hat{H}_0] = 0$, therefore $|n, \tilde{m}\rangle$ is the simultaneous eigenstates of photon number $\hat{n_a} = \hat{a}^\dagger \hat{a}$ and phonon number $\tilde{n}_b = \tilde{b}^\dagger \tilde{b}$. Alternatively, one can arrive to the same result by defining the unitary transformation $\hat{H}_0 \rightarrow \hat{U} \hat{H}_0 \hat{U}^\dagger$ with $\hat{U} = \exp\left[\frac{g_{cm}}{\omega_m} \hat{a}^\dagger \hat{a} (\hat{b}^\dagger - \hat{b})\right]$, which shifts the mechanical resonator $\hat{b} \rightarrow \hat{b} - \frac{g_{cm}}{\omega_m} \hat{a}^\dagger \hat{a}$.

Thus,

$$|n, \tilde{m}\rangle = \exp\left[\frac{g_{cm}}{\omega_m} \hat{a}^\dagger \hat{a} (\hat{b}^\dagger - \hat{b})\right] |n, m\rangle\,, \tag{5.3}$$

are the eigenvectors of Eq. (5.1), denoting the photon-number dependant displaced mechanical

Fock state. The corresponding eigenvalues are $E_{n,m} = n\omega_c + m\omega_m - g_{cm}^2 n^2/\omega_m$ and the energy levels of the system are shown in more detail in Fig (5.1).

5.2.1 Driven system with damping and losses

Including damping and losses, within the Heisenberg representation we get the quantum Langevin equations(QLE),

$$\begin{aligned}\dot{\hat{a}} &= i\Delta\hat{a} - \frac{\kappa}{2}\hat{a} - ig_{ac}(\hat{b}^\dagger + \hat{b})\hat{a} + \sqrt{\kappa}\hat{a}_{in},\\ \dot{\hat{b}} &= -i\omega_m\hat{b} - \frac{\gamma_m}{2}\hat{b} - ig_{ac}\hat{a}^\dagger\hat{a} + \sqrt{\gamma_m}\hat{b}_{in},\end{aligned} \tag{5.4}$$

where $\Delta = \omega_L - \omega_c$ is the detuning between laser frequency ω_L and the cavity mode ω_c, and κ and γ_m are the cavity and the mechanical damping rates. Note that, the cavity input is supposed to be the sum of driving and a vacuum noise operator $\hat{\xi}$, i.e., $\hat{a}_{in}(t) = \bar{a}_{in}e^{-i\omega_L t} + \hat{\xi}(t)$, where $\hat{\xi}$ satisfies $\langle\hat{\xi}(t)\hat{\xi}^\dagger(t')\rangle = \delta(t-t')$ and $\langle\hat{\xi}^\dagger(t)\hat{\xi}(t')\rangle = 0$

It is convenient to rewrite the QLE in the displaced basis for the oscillator which diagonalize the Hamiltonian. However, we first introduce the effect the mean value of the driving $\bar{a}_{in}e^{-i\omega_L t}$ into the Hamiltonian as an additional term, obtaining

$$\hat{H}_0 = \omega_c\hat{a}^\dagger\hat{a} + \omega_m\hat{b}^\dagger\hat{b} + g_{cm}\hat{a}^\dagger\hat{a}(\hat{b} + \hat{b}^\dagger) + i\sqrt{\kappa}\bar{a}_{in}\left[\hat{a}^\dagger e^{i\omega_L t} - \hat{a}e^{-i\omega_L t}\right]. \tag{5.5}$$

By moving to the displaced frame, which is equivalent to performing a unitary transformation $\hat{U} = e^{-i\hat{P}\hat{a}^\dagger\hat{a}}$ with $\hat{P} = \frac{g_{cm}}{\omega_m}i(\hat{b}^\dagger - \hat{b})$, the Hamiltonian rewrites as

$$\hat{H}_0 = \omega_c\hat{a}^\dagger\hat{a} + \omega_m\hat{b}^\dagger\hat{b} - \frac{g_{cm}^2}{\omega_m}(\hat{a}^\dagger\hat{a})^2 + i\sqrt{\kappa}\bar{a}_{in}\left[\hat{a}^\dagger e^{-i\hat{P}}e^{i\omega_L t} - \hat{a}e^{i\hat{P}}e^{-i\omega_L t}\right]. \tag{5.6}$$

Finally, in the frame rotating with the laser frequency, one obtains

$$\hat{H}_0 = -\Delta\hat{a}^\dagger\hat{a} + \omega_m\hat{b}^\dagger\hat{b} - \frac{g_{cm}^2}{\omega_m}(\hat{a}^\dagger\hat{a})^2 + i\sqrt{\kappa}\bar{a}_{in}\left[\hat{a}^\dagger e^{-i\hat{P}} - \hat{a}e^{i\hat{P}}\right]. \tag{5.7}$$

The corresponding QLE for the optical field becomes

$$\dot{\hat{a}}(t) = \left[i\Delta - \frac{\kappa}{2} + i\frac{g_{cm}^2}{\omega_m}(2\hat{a}^\dagger\hat{a} + 1)\right]\hat{a}(t) + \sqrt{\kappa}e^{-i\hat{P}(t)}[\bar{a}_{in} + \hat{\xi}(t)], \tag{5.8}$$

and for $\hat{b}(t)$

$$\dot{\hat{b}} = -\Big(i\omega_m - \frac{\gamma_m}{2}\Big)\hat{b} + \sqrt{\gamma_m}\hat{b}_{in}(t) + \sqrt{\kappa}\bar{a}_{in}\frac{g_{cm}}{\omega_m}\big[\hat{a}^\dagger e^{-i\hat{P}(t)} + \hat{a}e^{i\hat{P}(t)}\big]. \tag{5.9}$$

These equations are still nonlinear, therefore finding an exact solution is almost impossible, while one can solve these equations in the weak driving approximation. More precisely, we consider the problem in a regime where $n_0 = \dfrac{4|\bar{a}_{in}|^2}{\kappa} \ll 1$, which n_0 is the mean photon number for $g_{cm} = 0$, on resonance $\Delta = 0$. As a result, we can neglect the term $2\hat{a}^\dagger\hat{a}$ in the Eq. (5.8), hence the approximated formal solution is

$$\hat{a}(t) = \hat{a}(t_0)e^{-(\kappa/2 - i\tilde{\Delta})(t-t_0)} + \sqrt{\kappa}\int_{t_0}^{t} ds e^{-(\kappa/2 - i\tilde{\Delta})(t-s)}e^{-iP(s)}[\bar{a}_{in} + \hat{\xi}(s)], \tag{5.10}$$

where $\tilde{\Delta} = \Delta + \frac{g_{cm}^2}{\omega_m}$. Similarly, in this weak driving regime, the solution of Eq. (5.9) is given by the free motion of the mechanical resonator without the effect of the optomechanical coupling

$$\hat{b}(t) = \hat{b}(t_0)e^{-(\gamma_m/2 + i\omega_m)(t-t_0)} + \sqrt{\gamma_m}\int_{t_0}^{t} ds e^{-(\gamma_m/2 + i\omega_m)(t-s)}\hat{b}_{in}(s). \tag{5.11}$$

We are interested in the cavity spectrum in the stationary state, therefore we assume $t_0 \to -\infty$, neglect the transient term and get

$$\begin{aligned}
\hat{a}(t) &\simeq \sqrt{\kappa}\int_{-\infty}^{t} ds e^{-(\kappa/2 - i\tilde{\Delta})(t-s)}e^{-iP(s)}[\bar{a}_{in} + \hat{\xi}(s)], \\
\hat{b}(t) &\simeq \sqrt{\gamma_m}\int_{-\infty}^{t} ds e^{-(\gamma_m/2 + i\omega_m)(t-s)}\hat{b}_{in}(s).
\end{aligned} \tag{5.12}$$

The above expressions are in the displaced frame, therefore, we have to apply the reverse unitary transformation $\hat{a}(t) \to \hat{U}^\dagger\hat{a}(t)\hat{U}(t)$, which gives rise to

$$\hat{a}(t) = \sqrt{\kappa}\int_{0}^{+\infty} d\tau e^{-(\kappa/2 - i\tilde{\Delta})\tau}e^{iP(t)}e^{-iP(t-\tau)}[\bar{a}_{in} + \hat{\xi}(t-\tau)], \tag{5.13}$$

where $\tau = t - s$ is a change of variable, and $\hat{P}(t)$ is given by

$$\hat{P}(t) = -i\sqrt{\gamma_m}\frac{g_{cm}}{\omega_m}\int_{0}^{+\infty} d\tau e^{-\frac{\gamma_m}{2}\tau}\Big[e^{-i\omega_m\tau}\hat{b}_{in}(t-\tau) - e^{i\omega_m\tau}\hat{b}_{in}^\dagger(t-\tau)\Big] \tag{5.14}$$

Finally, the cavity amplitude is obtained

$$\begin{aligned}\langle \hat{a}(t)\rangle &= \sqrt{\kappa}\bar{a}_{in}\int_0^{+\infty} d\tau e^{-(\kappa/2-i\tilde{\Delta})\tau}\langle e^{iP(t)}e^{-iP(t-\tau)}\rangle \\ &= \sqrt{\kappa}\bar{a}_{in}\int_0^{+\infty} d\tau e^{-(\kappa/2-i\tilde{\Delta})\tau}e^{-\frac{g_{cm}^2}{\omega_m^2}(2\bar{n}_{th}+1)}\Big[1-\cos\omega_m\tau\cosh\frac{\gamma_m}{2}\tau+i\sin\omega_m\tau\sinh\frac{\gamma_m}{2}\tau\Big].\end{aligned} \tag{5.15}$$

Where we have assumed that the mechanical oscillator is in thermal equilibrium, so that $\bar{n}_{th} = (\exp(\hbar\omega_m/kT)-1)^{-1}$ is the mean phonon occupation number at temperature T.

5.3 The Hybrid Tripartite System

The tripartite hybrid system we shall study is shown in Fig. (5.2).a , where a driven single-mode EM cavity, a mechanical resonator, and a qubit are mutually coupled. The system Hamiltonian can be quite generally written as ($\hbar = 1$)

$$\begin{aligned}\hat{H}_t = \omega_c\hat{a}^\dagger\hat{a} + \frac{1}{2}\omega_a\sigma_z + ig_{ac}\sigma_x(\hat{a}-\hat{a}^\dagger) - g_{am}(\hat{\sigma}_z+1)(\hat{b}+\hat{b}^\dagger) \\ - g_{cm}\hat{a}^\dagger\hat{a}(\hat{b}+\hat{b}^\dagger) + \omega_m\hat{b}^\dagger\hat{b} + iF_L(\hat{a}^\dagger e^{-i\omega_L t} - \hat{a}e^{i\omega_L t}),\end{aligned} \tag{5.16}$$

where $\hat{a}$ and $\hat{a}^\dagger$ are the annihilation and creation operators of the cavity mode with frequency ω_c, and $\hat{b}$ and $\hat{b}^\dagger$ those of the mechanical resonator, with frequency ω_m. $\hat{\sigma}_x$, $\hat{\sigma}_y$, and $\hat{\sigma}_z$ are Pauli operators associated with the qubit, whose levels are separated by ω_a. The interaction between the cavity and the qubit with coupling rate g_{ac} is in the full Rabi form, while the qubit–mechanical resonator interaction is of a dispersive nature: the qubit shifts the equilibrium position of the resonator when it is in its (unperturbed) excited state with $\sigma_z = 1$. We also include a direct optomechanical radiation–pressure interaction with coupling rate g_{cm}, which is, however, typically much smaller than all the other coupling rates. The last term describes the cavity driving tone, with rate F_L and frequency ω_L; that is, the excitation of the cavity mode through an external classical source, which could be a laser in the optical case or a low noise narrow-band coherent source in the microwave case. The rate F_L is given by $F_L = \sqrt{P_L\eta_{in}\kappa/\hbar\omega_L}$, where P_L is the source power, κ is the cavity decay rate, $0 < \eta_{in} \leq 1$ is the mode matching factor between the input driving mode and the cavity mode.

We remark that Eq. (5.16) provides a simplified description of the physical scenario, and in particular, of the system mediating between the electromagnetic cavity and the mechanical resonator, which is here described by a two-level system. In general, one should start from the full electromagnetic interaction between the various subsystems, as for example, in References [103, 104],

and consider the whole space of states. However, when the qubit transition frequency ω_a is clearly separated from all the other transition frequencies of the mediating system, and the driving tone at frequency ω_L is tuned around ω_a and is very far from all the other transitions, the present model and the dipole-like interaction assumed in Eq. (5.16) provide a satisfactory description of a wide range of phenomena.

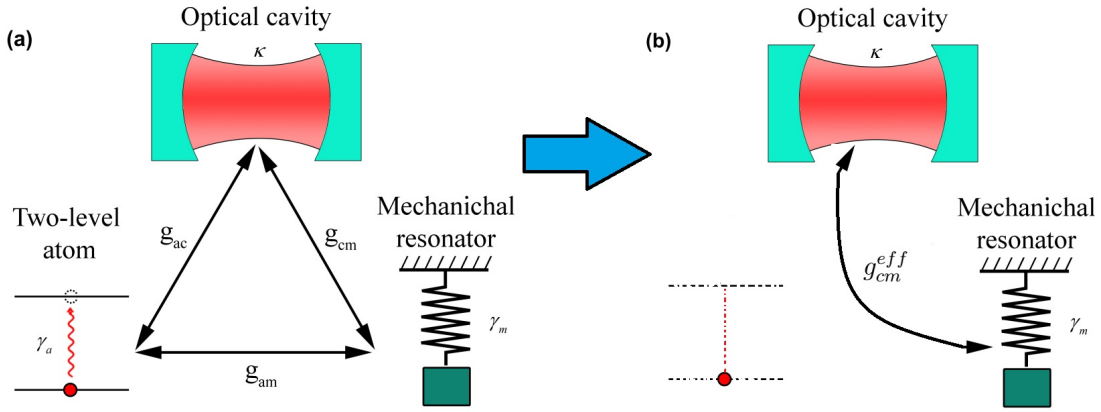

Figure 5.2: A tripartite hybrid system: (a) A single-mode EM cavity, a two-level atom and a mechanical resonator are coupled to each other via the coupling strengths g_{ac}, g_{cm}, and g_{am}. (b) An effective optomechanical system; when $\omega_a \gg g_j$ the qubit can be adiabatically eliminated and the dynamics of system can be treated as an effective optomechanical system Eq. (5.29) in the strong coupling regime with an effective coupling rate g_{cm}^{eff}, given by Eq. (5.30).

It is convenient to move to the interaction picture with respect to $H_0 = \omega_L(\hat{a}^\dagger\hat{a} + \sigma_z/2)$, that is, to move to a frame rotating at the driving tone frequency ω_L, which will represent from now on our frequency reference. In this rotating frame, the counter-rotating terms in the cavity–qubit interaction become $ig_{ac}\left(\sigma_-\hat{a}e^{-2i\omega_L t} - \sigma_+\hat{a}^\dagger e^{2i\omega_L t}\right)$, that is, they oscillate at $2\omega_L$, where we have used the usual definitions $\sigma_\pm = (\sigma_x \pm i\sigma_y)/2$. One can make the rotating wave approximation (RWA), i.e., neglect them since they average to zero in the timescales of interest. The resulting total Hamiltonian in this interaction picture therefore becomes

$$\begin{aligned}\hat{H}_{hyb} = &-\Delta\hat{a}^\dagger\hat{a} + \frac{1}{2}\Delta_{aL}\sigma_z + ig_{ac}(\sigma_+\hat{a} - \sigma_-\hat{a}^\dagger) - g_{am}(\hat{\sigma}_z + 1)(\hat{b} + \hat{b}^\dagger) \\ &- g_{cm}\hat{a}^\dagger\hat{a}(\hat{b} + \hat{b}^\dagger) + \omega_m\hat{b}^\dagger\hat{b} + iF_L(\hat{a}^\dagger - \hat{a}),\end{aligned} \tag{5.17}$$

where $\Delta = \omega_L - \omega_c$ is the cavity detuning and $\Delta_{aL} = \omega_a - \omega_L$ is the atomic detuning from the driving frequency.

A realistic description of the tripartite system must also include decay and noisy processes due to the coupling with the external reservoir. The full description of the dynamics is therefore

provided by the following master equation for the density matrix $\hat{\rho}_t$ of the whole tripartite system

$$\begin{aligned}\frac{d\hat{\rho}_t}{dt} &= -i\left[\hat{H}_{hyb}, \hat{\rho}_t\right] + \kappa\mathcal{D}[\hat{a}]\hat{\rho}_t + \gamma_a\mathcal{D}[\hat{\sigma}_-]\hat{\rho}_t \\ &\quad + \gamma_m(n_{th}+1)\mathcal{D}[\hat{b}]\hat{\rho}_t + \gamma_m n_{th}\mathcal{D}[\hat{b}^\dagger]\hat{\rho}_t,\end{aligned} \tag{5.18}$$

where $\mathcal{D}[\hat{c}]\hat{\rho}_t = \hat{c}\hat{\rho}_t\hat{c}^\dagger - (\hat{c}^\dagger\hat{c}\hat{\rho}_t + \hat{\rho}_t\hat{c}^\dagger\hat{c})/2$ is the standard dissipator in Lindblad form, κ is the cavity decay rate, γ_a the qubit decay rate from the excited to the ground state, γ_m is the mechanical damping rate, and $n_{th} = (e^{\hbar\omega_m/k_BT}-1)^{-1}$ is the mean thermal excitation number of the reservoir of the mechanical mode. We consider thermal equilibrium at temperature T, and thermal excitations (and the corresponding Lindblad terms) are negligible for the qubit and cavity subsystems because $\hbar\omega_c/k_BT \sim \hbar\omega_a/k_BT \gg 1$.

We notice that we have not included qubit dephasing in Eq. (5.18), corresponding to a Lindblad dissipator of the form $\mathcal{D}[\sigma_z]\rho_t$. In general this dephasing process is present together with the usual qubit decay, but in the regime we will consider of very large detuning, the qubit will remain unexcited in its ground state, and qubit dephasing has no effect on the dynamics of the system. Therefore this omission is well justified in our case.

Moreover, since we are considering the qubit coupled strongly to both the cavity and the mechanical resonator, one may wonder if the standard dissipative model adopted in Eq. (5.18), in which each system component has its own independent dissipative term, is appropriate. In fact, in these strong coupling cases it has been proposed to use a first-principle derivation of the master equation in which the various environments are eliminated altogether and that could lead to dissipative coupling terms in which quanta are exchanged simultaneously by the qubit cavity and mechanical resonator. However, in our case even though the couplings are quite large, the detunings and the unperturbed energy differences are still large enough and we expect that the standard dissipative model used here still provide a satisfactory description of the dynamics.

In the next section, we will show that when the qubit is far off resonance from the cavity and its driving, it is able to mediate an effective dispersive interaction between the cavity and the mechanical resonator, reproducing therefore an effective optomechanical system in the strong coupling regime.

5.4 The Schrieffer–Wolff Approximation and Effective Optomechanical System

In order to study a quantum system, one is often interested to get a precise description of its low-energy Hamiltonian. Using Schrieffer-Wolff (SW) approach one is able to focus on to the

low-energy system dynamics by integrating out high-energy degrees of freedom. In the standard SW approach, the system Hamiltonian represents by perturbed Hamiltonian $\hat{H}_0 + \epsilon\hat{V}$, in which $\hat{H}_0$ describes unperturbed system. The low-energy subspace invariant under $\hat{H}_0$, while, it does not preserve under perturbation $\epsilon\hat{V}$. In this method, the goal is to create an effective Hamiltonian $\hat{H}_{eff}$ acting on low-energy subspace and whose spectrum matches the low-energy spectrum of $\hat{H}_0 + \epsilon\hat{V}$ originating from low-energy subspace. The main assumption in SW is that the spectrum of unperturbed Hamiltonian has a sufficiently large gape [82].

In the following, we apply SW to our tripartite system providing that the qubit stays in its effective ground state such that the low-energy subspace is separated from high-energy subspace. Our goal is to construct an effective optomechanical Hamiltonian valid for system operating at dispersive regime for the qubit.

We first rewrite Eq. (5.16) by grouping together the terms involving the qubit operators,

$$\hat{H}_{hyb} = \hat{H}_{om} + \hat{H}_{qubit} + \hat{H}_{drv}, \tag{5.19}$$

where

$$\hat{H}_{om} = \omega_c\hat{a}^\dagger\hat{a} + +\omega_m\hat{b}^\dagger\hat{b} - (g_{am} + g_{cm}\hat{a}^\dagger\hat{a})(\hat{b} + \hat{b}^\dagger), \tag{5.20}$$

Note, the last Hamiltonian is related to the coherent drive, that is, $\hat{H}_{drv} = iF_L\left(\hat{a}^\dagger e^{-i\omega_L t} - \hat{a}e^{i\omega_L t}\right)$. $\hat{H}_{qubit}$ can be written as that of a magnetic dipole in an effective magnetic field

$$\hat{H}_{qubit} = \frac{1}{2}\left(\hat{B}_x\hat{\sigma}_x + \hat{B}_z\hat{\sigma}_z\right), \tag{5.21}$$

where $\hat{B}_x = -g_{ac}\hat{p}_c$, $\hat{B}_z = \Delta_{aL} - 2g_{am}\hat{x}_m$, with $p_c = -i(a - a^\dagger)$, and $x_m = b + b^\dagger$.

In a frame rotating with $\hat{H}_0$, one obtains

$$\tilde{H}_{hyb} = e^{iH_0 t}\hat{H}_{hyb}e^{-i\hat{H}_0 t} - \hat{H}_0 \tag{5.22}$$

Hence, in this rotating frame, the Eq. (5.19) turns to

$$\tilde{H}_{hyb} = \tilde{H}_{om} + \tilde{H}_{qubit} + \tilde{H}_{drv}, \tag{5.23}$$

with

$$\tilde{H}_{qubit} = ig_{ac}\left[\hat{a}\hat{\sigma}_+ - \hat{a}^\dagger\hat{\sigma}_- + \hat{a}\hat{\sigma}_- e^{-2i\omega_L t} - \hat{a}^\dagger\hat{\sigma}_+ e^{2i\omega_L t}\right] + \frac{\tilde{B}_z\hat{\sigma_z}}{2}. \tag{5.24}$$

Because, we are in the regime where $\omega_L \approx \omega_c \approx \omega_a \gg \omega_m, g_J$, thus the fast rotating term rotating

at $\pm 2\omega_L$ can be neglected under RWA. Hence, Eq. (5.24) can be rewritten as

$$\begin{aligned}\tilde{H}_{qubit} &\approx \frac{g_{ac}}{2}\big[-\hat{\sigma}_x\hat{p}_c - \hat{\sigma}_y\hat{x}_c\big] + \frac{\tilde{B}_z\hat{\sigma}_z}{2} \\ &= \frac{\tilde{B}_x\hat{\sigma}_x + \tilde{B}_y\hat{\sigma}_y + \tilde{B}_z\hat{\sigma}_z}{2}\end{aligned} \tag{5.25}$$

where $\hat{B}_y = -g_{ac}\hat{x}_c$, with $x_c = a + a^\dagger$.

Therefore, in the frame rotating at the laser frequency ω_L, and by applying the RWA, we have

$$\tilde{H}_{hyb} = \tilde{H}_{qubit} - \Delta\hat{a}^\dagger\hat{a} + iF_L(\hat{a}^\dagger - \hat{a}) + \omega_m\hat{b}^\dagger\hat{b} - (g_{am} + g_{cm}\hat{a}^\dagger\hat{a})(\hat{b} + \hat{b}^\dagger). \tag{5.26}$$

We now make the important assumption that Δ_{aL} is larger than the coupling rates of the qubit, g_{ac} and g_{am}, that is, the qubit is far off-resonance from the cavity and the mechanical resonator, and it is not excited by the cavity driving. In this dispersive limit, the qubit does not exchange energy with the other subsystems, and it remains in its effective ground state. We are in the condition to apply the Schrieffer–Wolff method because we have a lower energy subspace, corresponding to the effective qubit ground state, which is well separated from the high energy subspace. In this lower energy subspace, the effective qubit Hamiltonian is

$$\hat{H}^{eff}_{qubit} = -\frac{1}{2}\sqrt{\hat{B}_x^2 + \hat{B}_y^2 + \hat{B}_z^2} = -\frac{1}{2}\sqrt{4g_{ac}^2\left(\hat{a}^\dagger\hat{a} + \frac{1}{2}\right) + (\Delta_{aL} - 2g_{am}\hat{x}_m)^2}, \tag{5.27}$$

which is an effective operator acting on the Hilbert space of the optomechanical system. It is now consistent to expand this effective square-root operator as a power series in the small parameters g_j/Δ_{aL} ($g_j = g_{ac}, g_{am}$), using $\sqrt{1+\eta} \simeq 1 + \eta/2 - \eta^2/8 + \eta^3/16 - 5\eta^4/128 + O(\eta^5)$. In the parameters regime that we consider (see the parameters value in the caption of Fig. (5.5)), we truncate the expansion up to the third order. However, including higher order as such as fourth order, for example, leads to terms as $O(g_{am}^4/\omega_a^3)$ which are effectively negligible compared to those we have kept. Therefore, by keeping the terms up to the third order, one gets

$$\hat{H}^{eff}_{qubit} = -\frac{\Delta_{aL}}{2} + g_{am}(\hat{b} + \hat{b}^\dagger) - \frac{g_{ac}^2}{\Delta_{aL}}\left(\hat{a}^\dagger\hat{a} + \frac{1}{2}\right) - \frac{2g_{ac}^2 g_{am}}{\Delta_{aL}^2}\left(\hat{a}^\dagger\hat{a} + \frac{1}{2}\right)(\hat{b} + \hat{b}^\dagger), \tag{5.28}$$

which, inserted into Eq. (5.26) and neglecting constant energy terms, yields the following effective, low-energy, optomechanical Hamiltonian valid in the considered dispersive regime for the qubit,

$$\hat{H}^{eff}_{om} = -(\Delta + \tfrac{g_{ac}^2}{\Delta_{aL}})\hat{a}^\dagger\hat{a} - (\tfrac{g^{eff}_{cm} - g_{cm}}{2})(\hat{b} + \hat{b}^\dagger) - g^{eff}_{cm}\hat{a}^\dagger\hat{a}(\hat{b} + \hat{b}^\dagger) + \omega_m\hat{b}^\dagger\hat{b} + iF_L(\hat{a}^\dagger - \hat{a}), \tag{5.29}$$

where

$$g_{cm}^{eff} = g_{cm} + \frac{2g_{ac}^2 g_{am}}{\Delta_{aL}^2} \tag{5.30}$$

is the effective optomechanical radiation–pressure-like interaction rate, with the additional term at third order in g_j/Δ_{aL} representing the effective indirect interaction mediated by the qubit through the AC Stark shift. This latter term can be significantly larger than the direct optomechanical coupling g_{cm}, and under the condition $\Delta_{aL} \gg g_{ac}, g_{am} \gg \omega_m$, one expects to achieve the strong coupling regime $g_{cm}^{eff} \sim \omega_m$, see Fig. (5.2).b. In order to verify this fact, we have therefore to compare the dynamics of the full tripartite system associated with Eq. (5.18) to that of the effective optomechanical Hamiltonian described by the following master equation for the cavity-mechanics density operator ϱ

$$\frac{d\hat{\varrho}}{dt} = -i\left[\hat{H}_{om}^{eff}, \hat{\varrho}\right] + \kappa\mathcal{D}[\hat{a}]\hat{\varrho} + \gamma_m(n_{th}+1)\mathcal{D}[\hat{b}]\hat{\varrho} + \gamma_m n_{th}\mathcal{D}[\hat{b}^\dagger]\hat{\varrho}. \tag{5.31}$$

Also in this case we have taken a standard dissipative model in which the Lindblad dissipator is added independently to the cavity and to the mechanical resonator. We expect it provides a satisfactory description of the dynamics also in the strong coupling limit where the mechanical frequency is of the same order of the coupling considered here, even though there is no experimental confirmation of that at the moment.

5.5 Results for the Stationary State of the Optomechanical System

Here we focus on the stationary state of the system achieved at long times. We first consider the stationary cavity photon number $\langle\hat{a}^\dagger\hat{a}\rangle$, and the results for the two dynamics are compared in Figs. (5.3) and (5.4), where we study the behavior of $\langle\hat{a}^\dagger\hat{a}\rangle$ as a function of the cavity detuning. To plot the Figs. (5.3)-(5.6), we perform the numerical simulations using a toolbox in Python called QUTIP (Quantum Toolbox in Python) [105].

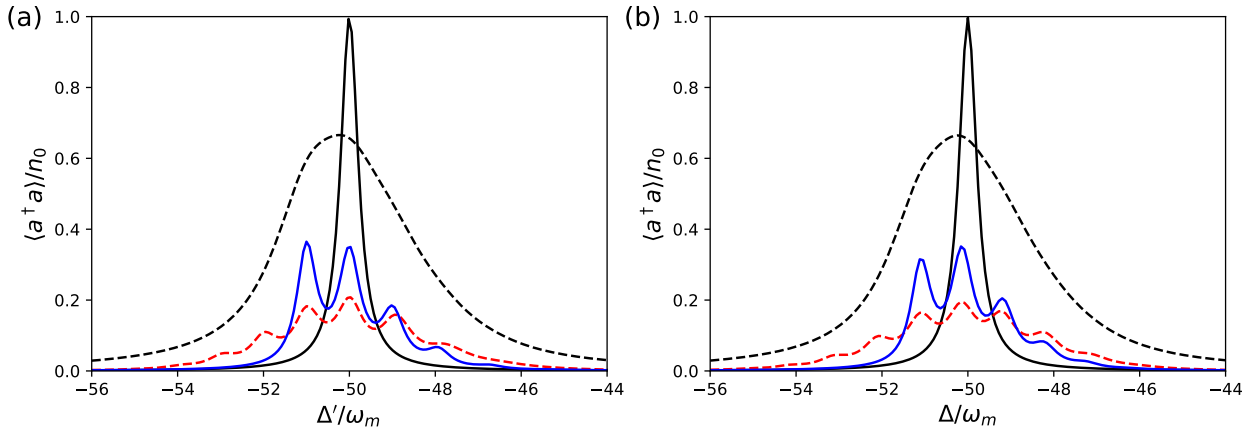

Figure 5.3: Stationary cavity photon number $\langle \hat{a}^\dagger \hat{a} \rangle$ versus the cavity detuning for the effective optomechanical model of Eq. (5.31) (**a**), and for the hybrid tripartite system with master equation Eq. (5.18) (**b**). We have chosen the following set of parameters: $\omega_a/\omega_m = 1.5\times10^4$, $\omega_L/\omega_m = 10^4$, $g_{am}/\omega_m = 50$, $g_{ac}/\omega_m = 500$, $g_{cm}/\omega_m = 10^{-3}$, so that the system is in the strong optomechanical coupling regime $g_{cm}^{eff} = \omega_m$. In (**a**), we use the effective detuning $\Delta' = \Delta + g_{cm}^{eff}(g_{cm}^{eff} - g_{cm})/\omega_m$, which takes into account the cavity frequency shift associated with the mechanical displacement in Eq. (5.29). The other parameters are $\omega_m/\kappa = 2$ and $n_{th} = 0$ for the blue solid line, $\omega_m/\kappa = 2$ and $n_{th} = 1$ for the red dashed line, $\omega_m/\kappa = 0.5$ and $n_{th} = 0$ for the black dashed line. The black solid line refers to the uncoupled cavity, i.e., $g_j = 0$ (where $j = am, ac$ and cm). All curves are normalized with respect to the value of the peak of this latter curve, $n_0 = 4F_L^2/\kappa^2$. In this parameter regime, the two models provide almost indistinguishable predictions. We have also taken $\gamma_m/\omega_m = \gamma_a/\omega_m = 1/20$, and $F_L = 10^{-2}\sqrt{\kappa}$.

In Fig. (5.3), we consider a set of parameters satisfying the dispersive regime described in the previous section, $\Delta_{aL} \gg g_{ac}, g_{am} \gg \omega_m$, where the tripartite hybrid system reproduces a strongly coupled optomechanical system well, that is, $\omega_a/\omega_m = 1.5 \times 10^4$, $\omega_L/\omega_m = 10^4$, $g_{am}/\omega_m = 50$, $g_{ac}/\omega_m = 500$, $g_{cm}/\omega_m = 10^{-3}$. In this case, in fact, $g_{cm}^{eff} = \omega_m$, and, as predicted, the two master equations, Eqs. (5.18) and (5.31), yield almost indistinguishable predictions. Moreover, the typical signatures of strong optomechanical coupling manifest themselves because we see that, in the weak excitation limit of small driving rate F_L, and in the resolved sideband regime $\kappa < \omega_m$ (the blue and red curves of Fig. (5.3)), the resonance peaks corresponding to the absorption of single mechanical quanta are clearly visible [54]. At a finite thermal phonon number n_{th} (see the red curves and the caption of Fig. (5.3)), additional peaks appear even though for increasing n_{th} they tend to blur into a broad thermal background [54]. The various resonances overlap and vanish as soon as we move to the unresolved sideband regime $\kappa > \omega_m$ (dashed black lines in Fig. (5.3)), and we get a broad peak, even larger than the standard Lorenztian response of the cavity, which tends to be reproduced at strong driving and not too strong coupling. We notice that thanks to the mediating action of the off-resonant qubit, the optomechanical coupling has been increased

by three orders of magnitude. We also notice that in Fig. (5.3a), we use the effective detuning $\Delta' = \Delta + g_{cm}^{eff}(g_{cm}^{eff} - g_{cm})/\omega_m$ rather than Δ, in order to take into account the cavity frequency shift associated with the mechanical displacement term, $-(\frac{g_{cm}^{eff} - g_{cm}}{2})(\hat{b} + \hat{b}^\dagger)$ in Eq. (5.29). All the other parameters are given in the figure caption.

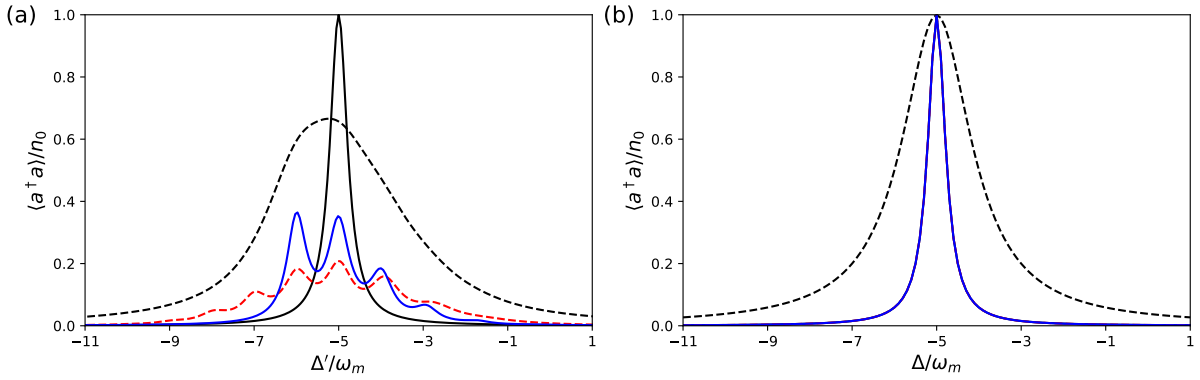

Figure 5.4: Stationary cavity photon number $\langle \hat{a}^\dagger \hat{a} \rangle$ versus the cavity detuning for the effective optomechanical model of Eq. (5.31) (**a**), and for the hybrid tripartite system with the master equation, Eq. (5.18) (**b**), for the following set of parameters, different from that of Fig. (5.3); $\omega_a/\omega_m = 1.5 \times 10^3$, $\omega_L/\omega_m = 10^3$, $g_{am}/\omega_m = g_{ac}/\omega_m = 50$, $g_{cm}/\omega_m = 10^{-3}$. Furthermore, with these different values, the strong optomechanical coupling regime condition, $g_{cm}^{eff} = \omega_m$, holds. The other parameters and styles of the curve are the same as in Fig. (5.3). In this parameter regime, the assumptions of the Schrieffer–Wolff method are only approximately valid, and the two models provide different predictions.

In Fig. (5.4), we consider a slightly different set of parameters, $\omega_a/\omega_m = 1.5 \times 10^3$, $\omega_L/\omega_m = 10^3$, $g_{am}/\omega_m = g_{ac}/\omega_m = 50$, $g_{cm}/\omega_m = 10^{-3}$, which again satisfies the strong optomechanical coupling regime condition, $g_{cm}^{eff} = \omega_m$, while all the other parameters are kept unchanged. This figure shows that the equivalence between the two models of Eqs. (5.18) and (5.31) is not easy to achieve, and it is valid in a quite limited parameter region. In fact, even though we apparently still satisfy the conditions for the Schrieffer–Wolff method because $g_j/\Delta_{aL} = 0.1$, we see that we have very different predictions for the cavity photon number versus detuning. The prediction of the effective optomechanical model of Eq. (5.31) is almost unchanged, while that of the full tripartite system is now very different, it shows no additional resonance peaks, and it does not differ significantly from the standard Lorenztian form. A closer inspection of the chosen parameters explains why in this latter case the two models significantly differ. In fact, the effective optomechanical Hamiltonian of Eq. (5.29) is valid up to *first* order in g_{am}/Δ_{aL}, and up to *second* order in g_{ac}/Δ_{aL}. Therefore, one needs to consider *smaller* values of g_{am} compared to g_{ac} due to the lower accuracy in the expansion parameter g_{am}/Δ_{aL}. This is verified for the set of parameters of Fig. (5.3), where $g_{am}/\Delta_{aL} = 0.01$ and $g_{ac}/\Delta_{aL} = 0.1$, and it is not satisfied for the choice of parameters

of Fig. (5.4), for which $g_{am}/\Delta_{aL} = g_{ac}/\Delta_{aL} = 0.1$. This higher value of the qubit–mechanics coupling alone is responsible for a very different behavior of the stationary state of the system.

These findings are confirmed by the behavior of another steady-state quantity, the mean phonon number of the mechanical resonator $\langle \hat{b}^\dagger \hat{b} \rangle$, which we study again as a function of detuning, and it is shown in Fig. (5.5) and (5.6).

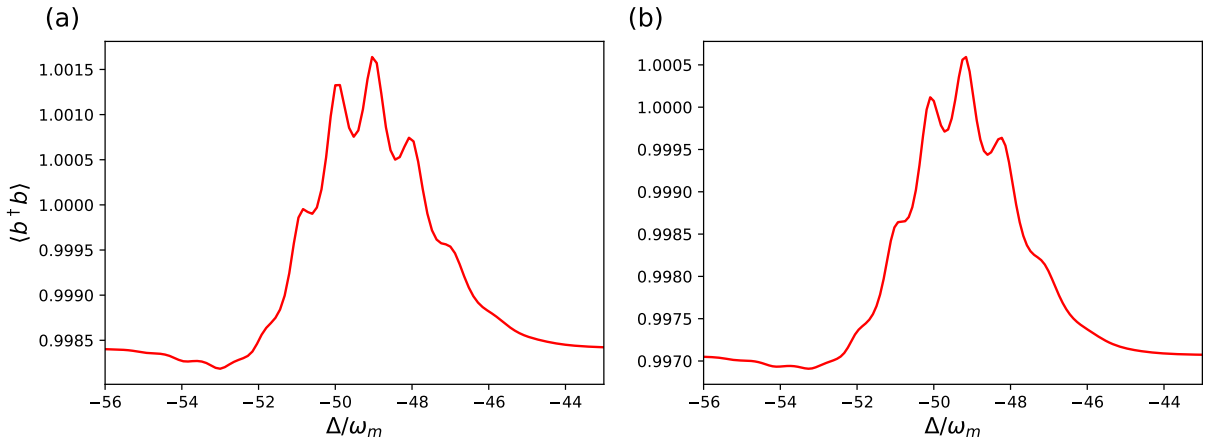

Figure 5.5: Stationary cavity phonon number $\langle \hat{b}^\dagger \hat{b} \rangle$ versus the cavity detuning for the effective optomechanical model of Equation (5.31) (**a**), and for the hybrid tripartite system with the master equation, Equation (5.18) (**b**). For this curve, we used the same parameters as in the red dashed line in Figure 5.3: $\omega_m/\kappa = 2$ and $n_{th} = 1$. We also choose the set of parameters as in Figure 5.3: $\omega_a/\omega_m = 1.5 \times 10^4$, $\omega_L/\omega_m = 10^4$, $g_{am}/\omega_m = 50$, $g_{ac}/\omega_m = 500$, $g_{cm}/\omega_m = 10^{-3}$, which is the parameter regime where the Schrieffer–Wolf approximation is valid. The other parameters are as in Fig. (5.3).

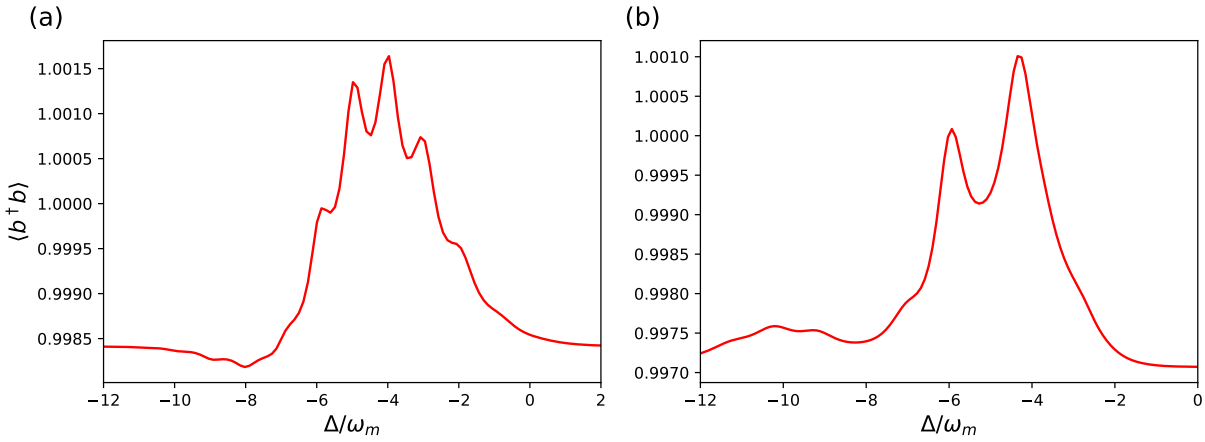

Figure 5.6: Stationary cavity phonon number $\langle \hat{b}^\dagger \hat{b} \rangle$ versus the cavity detuning for the effective optomechanical model of Equation (5.31) (**a**), and for the hybrid tripartite system with master equation Equation (5.18) (**b**). The parameters are the same as in Figure 5.4: $\omega_a/\omega_m = 1.5 \times 10^3$, $\omega_L/\omega_m = 10^3$, $g_{am}/\omega_m = g_{ac}/\omega_m = 50$, $g_{cm}/\omega_m = 10^{-3}$ where the predictions of the two models are different. The other parameters are as in Figure 5.5.

In Fig. (5.5), we consider the same parameters of Fig. (5.3) and focus on the case corresponding to the red dashed curve ($\omega_m/\kappa = 2$ and $n_{th} = 1$). At this low temperature, the stationary phonon number $\langle \hat{b}^\dagger \hat{b} \rangle$ is only weakly modified by the weak cavity driving, but the resonances corresponding to the various phonon transitions are clearly visible, and the two models provide very similar predictions. On the contrary, in Fig. (5.6), we consider the same parameters of Fig. (5.4), and also for the stationary mechanical excitation, in this different parameter regime in which g_{am}/ω_m is not small enough, the full hybrid tripartite system of Eq. (5.18) and the effective optomechanical model of Eq.(5.31) provide clearly distinct behavior.

5.6 Discussion

In this chapter, we have shown under which conditions a qubit can effectively mediate the interaction between a mechanical resonator and an electromagnetic cavity mode, enabling to reach the optomechanical strong-coupling limit, which is otherwise very difficult to achieve in conventional optomechanical systems [83, 91]. We have reconsidered in general this idea that was put forward within the context of superconducting electromechanical systems [93, 94, 95, 96, 97] and trapped atoms [98, 99]. We have seen that in the dispersive regime when the qubit is far off resonance so that the condition $\Delta_{aL} \gg g_{ac}, g_{am} \gg \omega_m$ is satisfied, there is a parameter regime where the qubit-cavity-mechanical resonator system behaves very similarly to an optomechanical system in the strong coupling regime, where the effective optomechanical coupling rate is comparable to the frequency. We have verified this fact by looking at the stationary properties of the cavity and

of the mechanical resonator. The parameter regime in which the dynamics driven by Eqs.(5.18) and (5.31) is equivalent is, however, quite limited because this is valid at first order in g_{am}/Δ_{aL} and at second order in g_{ac}/Δ_{aL}.

Despite the limited validity range of our treatment, the present optomechanical coupling enhancement could be designed and tested in the case of superconducting circuits coupled to driven microwave cavities. A proof-of-principle demonstration in these setups has already been given in Reference [94]. A more effective and clear demonstration could be given using circuits with a very large charging energy so that the qubit transition frequency ω_a is clearly separated from all the other transition frequencies of the circuit. Then, for example, the conditions of Fig. (5.3) could be realistically implemented taking achievable values such as $\omega_m = 1$ MHz, $\omega_a = 15$ GHz, $\omega_L = 10$ GHz, $g_{am} = 50$ MHz, $g_{ac} = 500$ MHz. Values of κ equal to 0.5 or 2 MHz are easy to achieve for a microwave cavity, and one should operate in a dilution fridge environment. Furthermore, weak driving with small intracavity photon number n_0 is achieved by using attenuators.

The present study can be extended in various directions. One can compare the two models in more detail by also looking at dynamical quantities such as spectra and optomechanical correlations, and also focus on the regime where other higher-order nonlinear phenomena, such as the cross–Kerr interaction, play a role due to the presence of the mediating qubit [94, 97]. Another interesting option for quantum information applications is to consider the case when the qubit mediates the interaction between two (or more) mechanical and electromagnetic modes in order to exploit the strong coupling (and also the resolved sideband) regime for the realization of quantum gates between photonic and phononic qubits [88].

CHAPTER 6

Conclusion

This thesis theoretically studies a full coupling quantum system which is a mix of quantum electrodynamics and optomechanics. To do this, we consider a generic cavity optomechanics scheme which involves a tripartite system consisting of a Fabry-Perot cavity, a qubit and a mechanical resonator with the three components mutually interacting.

One of the goals of this work was to study analytical solutions of the tripartite system, valid in strong coupling (SC) or even ultra-strong coupling (USC) regime. To do so, we implemented approximated methods for describing the Hamiltonian of the system, which is in the form of Quantum Rabi model. We also studied the system in the presence of decay and dissipation.

In chapter 4, we introduced the Hamiltonian of the closed system, which combines the Jaynes-Cummings (JC) coupling between the cavity mode and a two-level atom and radiation pressure coupling between the cavity mode and mechanical motion. We aimed to study the system with large coupling values when the system operates in higher coupling regimes, i.e., SC or USC regimes. To do this, we used a combination of analytical and approximation approaches to study our tripartite coupled system. For a fixed photon number the problem is simplified to phonon-polaritons interaction and then the Hamiltonian can be rewritten it in the generalized Rabi form, which can be analytically solved [63]. Moreover, we consider a more general Hamiltonian when the counter-rotating terms are taken into account too. In this approach, the Hamiltonian is approximated using a variational method called Bloch-Siegert (BS) methods.

The comparison of energy levels derived using the RWA and the exact Rabi model in the resonant case (zero detuning) revealed that the energy levels almost coincide at small coupling g. In contrast, at the larger g, the JC approximation deviates considerably from the exact Rabi solutions. Next, the spectrum of the QRM model is compared with the results of the BS approximation for different detuning values.

Chapter 5 explored the system dynamics in the presence of drive and losses. Introducing a two-level atom to the standard optomechanical system leads to the system being able to operate in the strong coupling regime and within the resolved sideband condition, which is important for enabling coherent control at the quantum level.

We studied the system Hamiltonian when the cavity mode and the mechanical mode interact via an off-resonant qubit, and as a consequence, new scenarios become possible. The system is driven with a weak laser drive, and the qubit is strongly detuned from the cavity; hence it is never excited and remains in its effective ground state.

We have observed that in the dispersive regime when the qubit is largely detuned, one can assume the tripartite dynamics as an effective optomechanical system where the qubit-cavity-mechanical resonator system behaves very similarly to a conventional optomechanical system in the strong coupling regime, where the effective optomechanical coupling rate is of the order of the frequency. In order to verify this, we investigated the stationary regime, particularly by looking at the static properties of the cavity and of the mechanical resonator. For a specific range of parameters, the cavity stationary photon number and the stationary mean phonon number are compared for two models.

However, this model operates under specific parameter conditions; the present optomechanical coupling scheme could be designed and tested in the case of superconducting circuits coupled to driven microwave cavities.

The present work can be extended to other exciting studies. It would be interesting to compare two models in more detail by investigating the dynamical quantities such as spectra and correlations and focusing on the regime where other higher-order nonlinear phenomena play a role due to the presence of the two-level atom. Another interesting scenario is possible applications in quantum information, for instance, considering a case when the qubit mediates the interaction between multi mechanical and electromagnetic modes to exploit the strong coupling regime for the realization of quantum gates between photonic and phononic qubits.

BIBLIOGRAPHY

[1] Ernest Fox Nichols and Gordon Ferrie Hull. A preliminary communication on the pressure of heat and light radiation. *Physical Review (Series I)*, 13(5):307, 1901.

[2] Peter Lebedew. Untersuchungen über die druckkräfte des lichtes. *Annalen der Physik*, 311(11):433–458, 1901.

[3] VB Braginski and AB Manukin. Ponderomotive effects of electromagnetic radiation. *Sov. Phys. JETP*, 25(4):653–655, 1967.

[4] Vladimir Borisovich Braginskii and Anatoliĭ Manukin. Measurement of weak forces in physics experiments.

[5] Nasa. https://solarsystem.nasa.gov/multimedia/gallery/Comet_Parts.jpg.

[6] Stefano Mancini and Paolo Tombesi. Quantum noise reduction by radiation pressure. *Physical Review A*, 49(5):4055, 1994.

[7] S Bose, K Jacobs, and PL Knight. Preparation of nonclassical states in cavities with a moving mirror. *Physical Review A*, 56(5):4175, 1997.

[8] Vladimir B Braginsky and Braginskiĭ. *Quantum measurement*.

[9] Stefano Mancini, David Vitali, and Paolo Tombesi. Optomechanical cooling of a macroscopic oscillator by homodyne feedback. *Physical Review Letters*, 80(4):688, 1998.

[10] Pierre-François Cohadon, Antoine Heidmann, and Michel Pinard. Cooling of a mirror by radiation pressure. *Physical Review Letters*, 83(16):3174, 1999.

[11] Arthur Ashkin. Acceleration and trapping of particles by radiation pressure. *Physical review letters*, 24(4):156, 1970.

[12] Arthur Ashkin. Trapping of atoms by resonance radiation pressure. *Physical Review Letters*, 40(12):729, 1978.

[13] Harold J Metcalf and Peter van der Straten. Laser cooling and trapping of atoms. *JOSA B*, 20(5):887–908, 2003.

[14] Hossein Rokhsari, Tobias J Kippenberg, Tal Carmon, and Kerry J Vahala. Radiation-pressure-driven micro-mechanical oscillator. *Optics Express*, 13(14):5293–5301, 2005.

[15] H Rokhsari, TJ Kippenberg, T Carmon, and KJ Vahala. Theoretical and experimental study of radiation pressure-induced mechanical oscillations (parametric instability) in optical microcavities. *IEEE journal of selected topics in Quantum Electronics*, 12(1):96–107, 2006.

[16] JD Thompson, BM Zwickl, AM Jayich, Florian Marquardt, SM Girvin, and JGE Harris. Strong dispersive coupling of a high-finesse cavity to a micromechanical membrane. *Nature*, 452(7183):72–75, 2008.

[17] Jordi Gomis-Bresco, Daniel Navarro-Urrios, Mourad Oudich, Said El-Jallal, Amadeu Griol, Daniel Puerto, Emiglio Chavez, Yan Pennec, Bahram Djafari-Rouhani, Franscesca Alzina, et al. A one-dimensional optomechanical crystal with a complete phononic band gap. *Nature communications*, 5(1):1–6, 2014.

[18] Olivier Arcizet, P-F Cohadon, Tristan Briant, Michel Pinard, and Antoine Heidmann. Radiation-pressure cooling and optomechanical instability of a micromirror. *Nature*, 444(7115):71–74, 2006.

[19] Kater W Murch, Kevin L Moore, Subhadeep Gupta, and Dan M Stamper-Kurn. Observation of quantum-measurement backaction with an ultracold atomic gas. *Nature Physics*, 4(7):561–564, 2008.

[20] CA Regal, JD Teufel, and KW Lehnert. Measuring nanomechanical motion with a microwave cavity interferometer. *Nature Physics*, 4(7):555–560, 2008.

[21] Yuxiang Liu, Marcelo Davanço, Vladimir Aksyuk, and Kartik Srinivasan. Electromagnetically induced transparency and wideband wavelength conversion in silicon nitride microdisk optomechanical resonators. *Physical review letters*, 110(22):223603, 2013.

[22] John D Teufel, Dale Li, MS Allman, K Cicak, AJ Sirois, JD Whittaker, and RW Simmonds. Circuit cavity electromechanics in the strong-coupling regime. *Nature*, 471(7337):204–208, 2011.

[23] Warwick P Bowen and Gerard J Milburn. *Quantum optomechanics*. CRC press, 2015.

[24] Ferdinand Brennecke, Stephan Ritter, Tobias Donner, and Tilman Esslinger. Cavity optomechanics with a bose-einstein condensate. *Science*, 322(5899):235–238, 2008.

[25] Markus Aspelmeyer, Tobias J Kippenberg, and Florian Marquardt. Cavity optomechanics. *Reviews of Modern Physics*, 86(4):1391, 2014.

[26] AG Kuhn, M Bahriz, O Ducloux, Claude Chartier, O Le Traon, T Briant, P-F Cohadon, A Heidmann, Christine Michel, L Pinard, et al. A micropillar for cavity optomechanics. *Applied Physics Letters*, 99(12):121103, 2011.

[27] Constanze Höhberger Metzger and Khaled Karrai. Cavity cooling of a microlever. *Nature*, 432(7020):1002–1005, 2004.

[28] Garrett D Cole, Simon Gröblacher, Katharina Gugler, Sylvain Gigan, and Markus Aspelmeyer. Monocrystalline al x ga 1- x as heterostructures for high-reflectivity high-q micromechanical resonators in the megahertz regime. *Applied Physics Letters*, 92(26):261108, 2008.

[29] Xuefeng Jiang, Min Wang, Mark C Kuzyk, Thein Oo, Gui-Lu Long, and Hailin Wang. Chip-based silica microspheres for cavity optomechanics. *Optics express*, 23(21):27260–27265, 2015.

[30] Lu Ding, Christophe Baker, Pascale Senellart, Aristide Lemaitre, Sara Ducci, Giuseppe Leo, and Ivan Favero. High frequency gaas nano-optomechanical disk resonator. *Physical review letters*, 105(26):263903, 2010.

[31] Ivan Favero, Sebastian Stapfner, David Hunger, Philipp Paulitschke, Jakob Reichel, Heribert Lorenz, Eva M Weig, and Khaled Karrai. Fluctuating nanomechanical system in a high finesse optical microcavity. *Optics express*, 17(15):12813–12820, 2009.

[32] Jasper Chan, Amir H Safavi-Naeini, Jeff T Hill, Seán Meenehan, and Oskar Painter. Optimized optomechanical crystal cavity with acoustic radiation shield. *Applied Physics Letters*, 101(8):081115, 2012.

[33] John D Teufel, Tobias Donner, Dale Li, Jennifer W Harlow, MS Allman, Katarina Cicak, Adam J Sirois, Jed D Whittaker, Konrad W Lehnert, and Raymond W Simmonds. Sideband cooling of micromechanical motion to the quantum ground state. *Nature*, 475(7356):359–363, 2011.

[34] Paul Adrien Maurice Dirac. The fundamental equations of quantum mechanics. *Proceedings of the Royal Society of London. Series A, Containing Papers of a Mathematical and Physical Character*, 109(752):642–653, 1925.

[35] Yoshihisa Yamamoto, Francesco Tassone, and Hui Cao. *Semiconductor cavity quantum electrodynamics*, volume 169. Springer, 2003.

[36] Roy J Glauber. The quantum theory of optical coherence. *Physical Review*, 130(6):2529, 1963.

[37] Kôdi Husimi. Some formal properties of the density matrix. *Proceedings of the Physico-Mathematical Society of Japan. 3rd Series*, 22(4):264–314, 1940.

[38] Wolfgang P Schleich. *Quantum optics in phase space*. John Wiley & Sons, 2011.

[39] Rep Kubo. The fluctuation-dissipation theorem. *Reports on progress in physics*, 29(1):255, 1966.

[40] Aashish A Clerk, Michel H Devoret, Steven M Girvin, Florian Marquardt, and Robert J Schoelkopf. Introduction to quantum noise, measurement, and amplification. *Reviews of Modern Physics*, 82(2):1155, 2010.

[41] Edwin T Jaynes and Frederick W Cummings. Comparison of quantum and semiclassical radiation theories with application to the beam maser. *Proceedings of the IEEE*, 51(1):89–109, 1963.

[42] Yu-Yu Zhang and Qing-Hu Chen. Generalized rotating-wave approximation for the two-qubit quantum rabi model. *Physical Review A*, 91(1):013814, 2015.

[43] Paul Langevin. *On the theory of Brownian motion*. 1908.

[44] Carlos Alexandre Brasil, Felipe Fernandes Fanchini, and Reginaldo de Jesus Napolitano. A simple derivation of the lindblad equation. *Revista Brasileira de Ensino de Física*, 35:01–09, 2013.

[45] Howard M Wiseman and Gerard J Milburn. *Quantum measurement and control*. Cambridge university press, 2009.

[46] D Lemons, A Gythiel, and Paul Langevin's. Sur la théorie du mouvement brownien [on the theory of brownian motion]. *CR Acad. Sci. Paris*, 146:530–533, 1908.

[47] WT Coffey. Kalmykov yu. p., waldron jt the langevin equation. *World Scientific Series in Contemporary Chemical Physics*, 10:704, 2004.

[48] Crispin W Gardiner and Matthew J Collett. Input and output in damped quantum systems: Quantum stochastic differential equations and the master equation. *Physical Review A*, 31(6):3761, 1985.

[49] A Dorsel, John D McCullen, Pierre Meystre, E Vignes, and H Walther. Optical bistability and mirror confinement induced by radiation pressure. *Physical Review Letters*, 51(17):1550, 1983.

[50] A Gozzini, Francesco Maccarrone, F Mango, I Longo, and S Barbarino. Light-pressure bistability at microwave frequencies. *JOSA B*, 2(11):1841–1845, 1985.

[51] Samuel Aldana, Christoph Bruder, and Andreas Nunnenkamp. Detection of weak forces based on noise-activated switching in bistable optomechanical systems. *Physical Review A*, 90(6):063810, 2014.

[52] Simon Gröblacher, Klemens Hammerer, Michael R Vanner, and Markus Aspelmeyer. Observation of strong coupling between a micromechanical resonator and an optical cavity field. *Nature*, 460(7256):724–727, 2009.

[53] Peter Rabl. Photon blockade effect in optomechanical systems. *Physical review letters*, 107(6):063601, 2011.

[54] Andreas Nunnenkamp, Kjetil Børkje, and Steven M Girvin. Single-photon optomechanics. *Physical review letters*, 107(6):063602, 2011.

[55] Jie-Qiao Liao, HK Cheung, CK Law, et al. Spectrum of single-photon emission and scattering in cavity optomechanics. *Physical Review A*, 85(2):025803, 2012.

[56] Xiu Gu, Anton Frisk Kockum, Adam Miranowicz, Yu-xi Liu, and Franco Nori. Microwave photonics with superconducting quantum circuits. *Physics Reports*, 718:1–102, 2017.

[57] II Rabi. On the process of space quantization. *Physical Review*, 49(4):324, 1936.

[58] R Graham and M Höhnerbach. Quantum chaos of the two-level atom. *Physics Letters A*, 101(2):61–65, 1984.

[59] Luigi Amico, Holger Frahm, Andreas Osterloh, and Tobias Wirth. Separation of variables for integrable spin–boson models. *Nuclear Physics B*, 839(3):604–626, 2010.

[60] Enrique Solano. The dialogue between quantum light and matter. *Physics*, 4:68, 2011.

[61] Leong Chuan Kwek et al. *Strong light-matter coupling: from atoms to solid-state systems*. World Scientific, 2013.

[62] Michael A Nielsen and Isaac Chuang. Quantum computation and quantum information, 2002.

[63] Daniel Braak. Integrability of the rabi model. *Physical Review Letters*, 107(10):100401, 2011.

[64] Bruce J West and Katja Lindenberg. On the rotating wave approximation. *Physics Letters A*, 102(4):189–193, 1984.

[65] G.W. Ford and R.F. O'Connell. Inconsistency of the rotating wave approximation with the ehrenfest theorem. *Physics Letters A*, 215(5):245 – 246, 1996.

[66] Alexandre Le Boité, Myung-Joong Hwang, Hyunchul Nha, and Martin B Plenio. Fate of photon blockade in the deep strong-coupling regime. *Physical Review A*, 94(3):033827, 2016.

[67] Eduardo Sánchez-Burillo, Luis Martín-Moreno, Juan José García-Ripoll, and David Zueco. Single photons by quenching the vacuum. *Physical review letters*, 123(1):013601, 2019.

[68] Anton Frisk Kockum, Adam Miranowicz, Simone De Liberato, Salvatore Savasta, and Franco Nori. Ultrastrong coupling between light and matter. *Nature Reviews Physics*, 1(1):19–40, 2019.

[69] Mang Feng, Xiwen Zhu, Ximing Fang, Min Yan, and Lei Shi. Exact solution of a trapped ultracold ion interacting with a standing wave laser without rotating wave approximation. *Journal of Physics B: Atomic, Molecular and Optical Physics*, 32(3):701, 1999.

[70] Yuanwei Zhang, Gang Chen, Lixian Yu, Qifeng Liang, J-Q Liang, and Suotang Jia. Analytical ground state for the jaynes-cummings model with ultrastrong coupling. *Physical Review A*, 83(6):065802, 2011.

[71] Andrei B Klimov and Sergei M Chumakov. *A group-theoretical approach to quantum optics: models of atom-field interactions*. John Wiley & Sons, 2009.

[72] Pol Forn-Díaz, Jürgen Lisenfeld, David Marcos, Juan José Garcia-Ripoll, Enrique Solano, CJPM Harmans, and JE Mooij. Observation of the bloch-siegert shift in a qubit-oscillator system in the ultrastrong coupling regime. *Physical review letters*, 105(23):237001, 2010.

[73] John R Schrieffer and Peter A Wolff. Relation between the anderson and kondo hamiltonians. *Physical Review*, 149(2):491, 1966.

[74] PW Milonni, JR Ackerhalt, and HW Galbraith. Chaos in the semiclassical n-atom jaynes-cummings model: Failure of the rotating-wave approximation. *Physical Review Letters*, 50(13):966, 1983.

[75] Clive Emary and Tobias Brandes. Quantum chaos triggered by precursors of a quantum phase transition: the dicke model. *Physical review letters*, 90(4):044101, 2003.

[76] Juan Restrepo, Ivan Favero, and Cristiano Ciuti. Fully coupled hybrid cavity optomechanics: quantum interferences and correlations. *Physical Review A*, 95(2):023832, 2017.

[77] P Forn-Díaz, L Lamata, E Rico, J Kono, and E Solano. Ultrastrong coupling regimes of light-matter interaction. *Reviews of Modern Physics*, 91(2):025005, 2019.

[78] F Bloch and A Siegert. Magnetic resonance for nonrotating fields. *Physical Review*, 57(6):522, 1940.

[79] Jani Tuorila, Matti Silveri, Mika Sillanpää, Erkki Thuneberg, Yuriy Makhlin, and Pertti Hakonen. Stark effect and generalized bloch-siegert shift in a strongly driven two-level system. *Physical review letters*, 105(25):257003, 2010.

[80] BR Judd. Exact solutions to a class of jahn-teller systems. *Journal of Physics C: Solid State Physics*, 12(9):1685, 1979.

[81] Daniel Z Rossatto, Celso J Villas-Bôas, Mikel Sanz, and Enrique Solano. Spectral classification of coupling regimes in the quantum rabi model. *Physical Review A*, 96(1):013849, 2017.

[82] Sergey Bravyi, David P DiVincenzo, and Daniel Loss. Schrieffer–wolff transformation for quantum many-body systems. *Annals of physics*, 326(10):2793–2826, 2011.

[83] David P Lake, Matthew Mitchell, Denis D Sukachev, and Paul E Barclay. Processing light with an optically tunable mechanical memory. *Nature communications*, 12(1):1–9, 2021.

[84] Sh Barzanjeh, Mehdi Abdi, Gerard J Milburn, Paolo Tombesi, and David Vitali. Reversible optical-to-microwave quantum interface. *Physical Review Letters*, 109(13):130503, 2012.

[85] Leonardo Midolo, Albert Schliesser, and Andrea Fiore. Nano-opto-electro-mechanical systems. *Nature nanotechnology*, 13(1):11–18, 2018.

[86] Rodrigo A Thomas, Michał Parniak, Christoffer Østfeldt, Christoffer B Møller, Christian Bærentsen, Yeghishe Tsaturyan, Albert Schliesser, Jürgen Appel, Emil Zeuthen, and Eugene S Polzik. Entanglement between distant macroscopic mechanical and spin systems. *Nature Physics*, 17(2):228–233, 2021.

[87] Max Ludwig, Amir H Safavi-Naeini, Oskar Painter, and Florian Marquardt. Enhanced quantum nonlinearities in a two-mode optomechanical system. *Physical review letters*, 109(6):063601, 2012.

[88] K Stannigel, Peter Komar, SJM Habraken, SD Bennett, Mikhail D Lukin, P Zoller, and P Rabl. Optomechanical quantum information processing with photons and phonons. *Physical review letters*, 109(1):013603, 2012.

[89] Wen-Zhao Zhang, Jiong Cheng, and Ling Zhou. Quantum control gate in cavity optomechanical system. *Journal of Physics B: Atomic, Molecular and Optical Physics*, 48(1):015502, 2014.

[90] Muhammad Asjad, Paolo Tombesi, and David Vitali. Quantum phase gate for optical qubits with cavity quantum optomechanics. *Optics express*, 23(6):7786–7794, 2015.

[91] Francesco Fogliano, Benjamin Besga, Antoine Reigue, Philip Heringlake, Laure Mercier de Lépinay, Cyril Vaneph, Jakob Reichel, Benjamin Pigeau, and Olivier Arcizet. Mapping the cavity optomechanical interaction with subwavelength-sized ultrasensitive nanomechanical force sensors. *Physical Review X*, 11(2):021009, 2021.

[92] Florian Vigneau, Juliette Monsel, Jorge Tabanera, Léa Bresque, Federico Fedele, GA D Briggs, Janet Anders, Juan MR Parrondo, Alexia Auffèves, and Natalia Ares. Ultrastrong coupling between electron tunneling and mechanical motion. *arXiv preprint arXiv:2103.15219*, 2021.

[93] Tero T Heikkilä, Francesco Massel, Jani Tuorila, Raphaël Khan, and Mika A Sillanpää. Enhancing optomechanical coupling via the josephson effect. *Physical Review Letters*, 112(20):203603, 2014.

[94] J-M Pirkkalainen, SU Cho, Francesco Massel, J Tuorila, TT Heikkilä, PJ Hakonen, and MA Sillanpää. Cavity optomechanics mediated by a quantum two-level system. *Nature communications*, 6(1):1–6, 2015.

[95] AJ Rimberg, MP Blencowe, AD Armour, and PD Nation. A cavity-cooper pair transistor scheme for investigating quantum optomechanics in the ultra-strong coupling regime. *New Journal of Physics*, 16(5):055008, 2014.

[96] Marios Kounalakis, Yaroslav M Blanter, and Gary A Steele. Flux-mediated optomechanics with a transmon qubit in the single-photon ultrastrong-coupling regime. *Physical Review Research*, 2(2):023335, 2020.

[97] Mohammad Tasnimul Haque, Juuso Manninen, David Vitali, and Pertti Hakonen. Enhancement of the optomechanical coupling and kerr nonlinearity using the josephson capacitance of cooper-pair box. *arXiv preprint arXiv:2010.13493*, 2020.

[98] Lukas Neumeier and Darrick E Chang. Exploring unresolved sideband, optomechanical strong coupling using a single atom coupled to a cavity. *New Journal of Physics*, 20(8):083004, 2018.

[99] Lukas Neumeier, Tracy E Northup, and Darrick E Chang. Reaching the optomechanical strong-coupling regime with a single atom in a cavity. *Physical Review A*, 97(6):063857, 2018.

[100] Giovanna Morigi, Jürgen Eschner, Stefano Mancini, and David Vitali. Entangled light pulses from single cold atoms. *Physical review letters*, 96(2):023601, 2006.

[101] David Vitali, Priscilla Cañizares, Jürgen Eschner, and Giovanna Morigi. Time-separated entangled light pulses from a single-atom emitter. *New Journal of Physics*, 10(3):033025, 2008.

[102] David Vitali, Giovanna Morigi, and Jürgen Eschner. Single cold atom as efficient stationary source of epr-entangled light. *Physical Review A*, 74(5):053814, 2006.

[103] Vidar Gudmundsson, Olafur Jonasson, Chi-Shung Tang, Hsi-Sheng Goan, and Andrei Manolescu. Time-dependent transport of electrons through a photon cavity. *Physical Review B*, 85(7):075306, 2012.

[104] Vidar Gudmundsson, Olafur Jonasson, Th Arnold, C-S Tang, H-S Goan, and Andrei Manolescu. Stepwise introduction of model complexity in a generalized master equation approach to time-dependent transport. *Fortschritte der Physik*, 61(2-3):305–316, 2013.

[105] J Robert Johansson, Paul D Nation, and Franco Nori. Qutip: An open-source python framework for the dynamics of open quantum systems. *Computer Physics Communications*, 183(8):1760–1772, 2012.